Supplementary Information

Contents:

Supplementary Information section 1:
Details of the Shum Laka site and skeletons

Location of the site

Shum Laka is located close to the northern border of the equatorial forest in north-western Cameroon, close to Bamenda (lat. 5°51'31 "N, long. 10°04'40"E, altitude 1650m asl) (Figure S1a, b, c). This large rockshelter, measuring 1181 m^2, is part of a series of escarpments originating from ancient volcanic massifs in the "Grassfields" region (de Maret *et al* 1993). It was probably formed initially from a small recess in the tertiary basaltic tuff of a waterfall cliff, and then widened through the seepage of water along the shelter walls (Moeyersons 1996a/b, Moeyersons *et al* 1996).

This site is unique for West-Central Africa, as human remains are generally poorly preserved in tropical environments and acidic soils. Most of the comparable sites that have yielded burials have also been rockshelters, such as Mbi Crater in Cameroon (date on human bone: 7,790±80 bp[1]; Asombang 1988); Ntadi Yomba in Congo (date on charcoal associated with burial: 7,090±140 bp and 1,990±90 bp; Van Neer & Lanfranchi 1985); and Iwo Eleru in Nigeria (radiocarbon date on charcoal associated with burial: 11,200±200 bp: Brothwell & Shaw 1971; U-series date on human bone: 11,700-16,300 BP: Harvati *et al* 2011). Mbi Crater is geographically and chronologically closest to Shum Laka, but, in contrast to the latter, it revealed only one very fragmentary skeleton, as did the other two sites.

Excavations

After a number of surveys and test pits in the Grassfields region of Cameroon (de Maret 1980, Warnier 1984, de Maret *et al* 1987, Asombang 1988), two main archaeological excavations took place at Shum Laka rockshelter between 1991/1992 and 1993/1994 (Asombang & de Maret 1992, Ribot *et al* 2001). A total surface area of 82m^2 was excavated, ranging in depth from 30cm at the back to 3.3m at the entrance. Nine burials or so-called burial units (corresponding to a single structure or pit, but sometimes to more than one skeleton) were found at the site (Table S1). The strategy for excavating the burials was to record the maximum amount of data in the field (e.g., anatomical position of bones, measurements if the bone was fragile) in order to have preliminary data (both funerary and osteological) as recommended by Duday *et al* (1990) and Duday (2005, 2006). Once exposed, the skeletons, whose state of preservation was very fragile, were delicately excavated, and the deposits were all dry-sieved using 0.5mm mesh.

Whilst excavating the burials, a screen was erected to prevent the bones from drying too quickly due to the intense ultra-violet light, and during the night, the burial was covered with a plastic sheet to protect it from temperature variations and fauna predation. As the excavation was done in the 1990s before the era of 3D-photogrammetry, the site was photographed and mapped on a two dimensional grid (xy coordinates) at various scales

[1] Radiocarbon dates are reported here as either uncalibrated (bp) or calibrated (calBP) years before present.

(1/15th, 1/10th, 1/20th). Each bone was recorded with a number, which corresponded to a precise location (using a theodolite) on a scale drawing (square and depth). In addition, its anatomical view (e.g. anterior, posterior, medial, lateral) and degree of articulation were also noted.

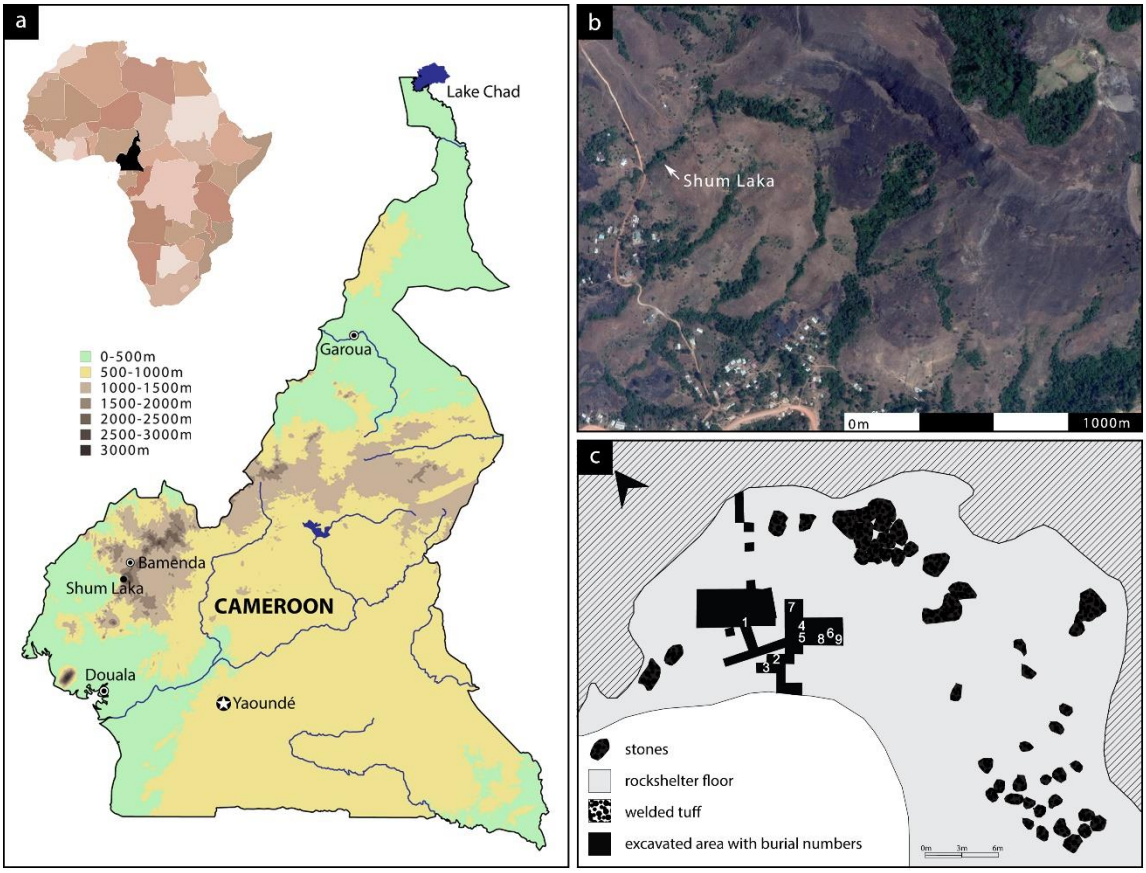

Figure S1: Geographical location of Shum Laka on (a) continental level; (b) regional level (Map data ©2018 Google Earth, 5°52'07"N, 10°03'37"E, date accessed: 2 November 2018); and (c) the rockshelter's excavation map (Figure from Ribot *et al* 2001 and modified by O. Graf).

Charcoal and bone samples for ^{14}C dating were systematically collected *in situ*, as well as soil samples for each square. During the second archaeological season (1993-1994), as the pelvic and long bones from Burial Unit 6 appeared to be extremely fragile, they were selectively stabilized *in situ* with a consolidant (Mowilith — polyvinyl acetate resin diluted to 10-30% with acetone) as recommended by Johnson (1994). The remaining skeletal elements were not treated with consolidant, in order to keep them for future analysis (e.g., ancient DNA, isotopes). Finally, each skeletal element was carefully packed and sent to the Institut Royal des Sciences Naturelles de Belgique (Brussels) for analysis (according to an agreement with the University of Yaounde and R. Asombang).

Table S1: Bioarchaeological analysis of human remains from Shum Laka.

Burial unit #	Excavation date	Burial type[1]	N[2]	API[3]	Estimated age-at-death[4]	Estimated Sex[5]
Early Holocene phase (7,882-7,635 calBP)[6]						
1	1984	single primary	1	-	(adult)	(♂)
2	1994	double primary	2	SEI: 56%	4±1years	♂? (aDNA: ♂)
				SEII: 48%	15±3 years	? (aDNA: ♂)
3	1993	secondary	1	26%	adult	♂ ?
Late Holocene phase (3,370-3,030 calBP)[6]						
4	1993	single primary	1	A: 69%	8±2 years	♀? (aDNA:♂)
5	1993	single primary	1	B: 28%	4±1 years	♀? (aDNA:♀)
6	1994	double primary	2	SE III: 68%	20-30 years	♀*
				SE IV:51%	>40 years	♀*
7	1993	collective secondary & primary	7	1% to 47%	from ±1 to ±12 years	3 ♂, 1♀? & 3?
8 (within 6)	1994	secondary (partly burnt and ochre)	2	2 to 4%	adult	1♂? &1?
Undated						
9 (below 6)	1994	secondary (cremation)	1	<50%	adult	?

[1] Primary burial corresponds to articulated skeleton (one funerary event) and secondary to disarticulated remains (more than one event) as defined by Duday *et al* (1990) and Duday (2005, 2006);
[2]N: number of identified individuals;
[3] API: Anatomical Preservation Index as defined by Dutour (1989) and Bello & Andrews (2006);
[4] Various methods for age-at-death estimations were used for non-adults (Scheuer *et al* 2010, Moorees *et al* 1963a/b, Scheuer & MacLaughlin-Black 1994, Steyn & Henneberg 1996) and adults (Buikstra & Ubelaker 1994;
[5] Sex was evaluated using various methods for the adults (Buikstra & Ubelaker 1994) and attempted for the juveniles (Schutkowski 1993). The results obtained here from aDNA confirmed or provided more resolution on the skeletal estimates.
[6] Dates were calibrated using a mixed curve, detailed in Figure S3 a & b (see also the Radiocarbon dates section of main paper).
*The ancient DNA analysis failed.

Stratigraphy and archaeological and paleoenvironmental context

The site's stratigraphy consists at its base of a bedrock composed of volcanic breccia, followed by overlying Pleistocene (P, S and Si) and Holocene (T and A) deposits, the oldest ones dating to 32,000 BP (de Maret et *al* 1993, 1995) (Extended Data Figure 1). The Holocene A layers correspond to anthropogenic ash of two kinds (Ao: ochre ash layer; Ag: grey ash layer) (Moeyersons 1996a/b, Moeyersons et al 1996). These deposits were dated to between ~9,000 bp and 3,000 bp and contained all the associated burial material. According to lithic analysis (Cornelissen 1996, Lavachery 1996, Lavachery *et al* 1996), each Holocene layer (Ao and Ag) was distinct. First, the Ao layer, dated around 9,000-6,000 bp (from 10,490 calBP to 6,210 calBP), contained mainly a Late Stone Age (LSA)

quartz microlithic tools assemblage, which was already present throughout the Pleistocene deposits, but it also included macrolithic tools made from basalt and tuff (Lavachery 2001). The lowest Holocene Ag layers, dated around 4,000-3,000BP (from 4,410 calBP to 1,870 calBP), provided lithic artefacts very similar to the underlying layer, but with an increasing number of macrolithic *versus* microlithic tools (Lavachery 2001). Finally, the upper levels of Ag were characterized by the presence of Early Iron Age (EIA) artefacts, such as pottery that progressively became more decorated with time.

According to paleoenvironmental results (e.g., charcoal, phytoliths, fauna), the deposits were associated with a mixed savannah and forest environment (de Maret *et al* 1987; H. Doutrelepont *pers. comm*.). This was confirmed by previous paleoclimatic data that showed only slight variations of temperature in the Grassfields, a region influenced by the Guinean Gulf that remained hot and humid throughout the Holocene and for the past 32,000 years (Giresse *et al* 1994). However, a recent study showed that between 4,500 calBP and 4,000 calBP, the Central African rainforest underwent an important climate-induced contraction at its periphery with the emergence of forest-savannah mosaics (Ngomanda *et al* 2009). Pollen profiles from lake sediments in Cameroon and Congo indicated an increase in grasses and/or pioneers (e.g. *Elaeis guineensis, Canarium schweinfurthii*) and a decrease of forest taxa. In fact, although there was probably long-term continuity in hunting strategies into the Holocene, these climatic changes seem to coincide with changes in ceramic use and lithic technology (de Maret *et al* 1987) and may have favoured various new economic strategies (e.g., arboriculture) and demographic growth in the region of the Grassfields from the mid-Holocene.

The burial finds and re-calibrated dates

In 1982, one human skeleton (Burial Unit 1) was discovered during a test pit excavation (Asombang 1988). In 1991/1992, ten skeletons were discovered in the uppermost Holocene deposits (Ag) and in 1993/1994 seven more were found in the earliest A-layers (Ao) (N=18) (Figure S2). The burials were located mostly in the south-eastern part of the rockshelter (Burial Units: 4, 5, 6, 7, 8 and 9), with a few in the western (Burial Units 2 and 3) and north-western parts (Burial Unit 1) (Figure S1c). Only one burial found in the Holocene Ag layer (Burial Unit 6) cut into the earlier Holocene layer (Ao).

The two Holocene burial periods, stratigraphically identified, were confirmed by ^{14}C dating of the human bones (Figure S3a, b). Fourteen dates were produced from Burial Units 1, 2, 3, 4, 5, 6 and 7. The dates were recently re-calibrated using Oxcal.version 4.3.2 and probability distributions (95.4%) were produced for all age ranges (see also Radiocarbon dates section of the main paper) (Figure S3a). A mixed calibration curve (IntCal13/SHCal13 with the "U" function allowing for uncertainty in mixture ratio) was also used as recommended for the tropics where ^{14}C variations are not well understood (Figure S3 a & b). We note that using the IntCal13 curve alone results in only very minor differences.

The early phase was dated between 7,150±70 bp and 6,870±80 bp and after calibration with the mixed curve between 7,882 calBP and 7,635 calBP. It included three funerary units with two single adult burials (Burial Units 1 and 3) and one double burial with two children (Burial Unit 2) (N=4).

The later phase was dated between 3,300±90 bp and 2,910±35 bp and after calibration with mixed curve between 3,370 calBP and 3,030 calBP. It included six funerary units (4 to 9) with at least nine children and five adults (N=14 minimum). All the re-calibrated radiocarbon dates confirm that the two burial phases were very well defined chronologically at 95.4% confidence: the early burials were dated in average around 7,760 calBP and the later ones around 3,200 calBP.

Throughout the two burial phases, it appeared that Shum Laka incorporated a very rich variety of mortuary practices, which are not comparable with any other contemporary sites in West-Central Africa (Ribot *et al* 2001). The Early Holocene funerary units corresponded to: first, two single adult burials, one primary (Burial Unit 1) and the other one secondary, including human postcranial bones associated with bone artefacts (Burial Unit 3); and additionally a double primary burial with a child (Burial Unit 2). The Late Holocene funerary units provided an increasing number of skeletons with additional funerary complexity: two single primary child burials (Burial Units 4 and 5, the latter being partly disturbed), a double primary adult burial (Burial Unit 6) and a collective burial with at least seven children (Burial Unit 7). In addition, Burial Unit 6 included a small secondary deposit of burnt cranial remains of two human adults (covered with ochre) and a young chimpanzee (Burial Unit 8). A cremation that was found at the base of the Burial Unit 6 pit also suggests its association with the latter (although no ^{14}C dates were obtained on these remains).

The appearance of collective burials and the use of different mortuary practices using both fire and ochre might be related to the advent of more complex societies in the later phase (as mentioned for another Iron Age site, that of Nanda in Equatorial Guinea, where secondary burials were also found (González-Ruibal *et al* 2012)). However, no trend was visible spatially in terms of both the position and orientation of the skeletons. The primary burials in Burial Units 1, 2, 4 and 6 were laid mainly in a flexed position; while the disarticulated secondary burials were laid out in various ways (e.g., in a bone bundle (Burial Unit 3), or in a very stratified bone accumulation (Burial Unit 7)).

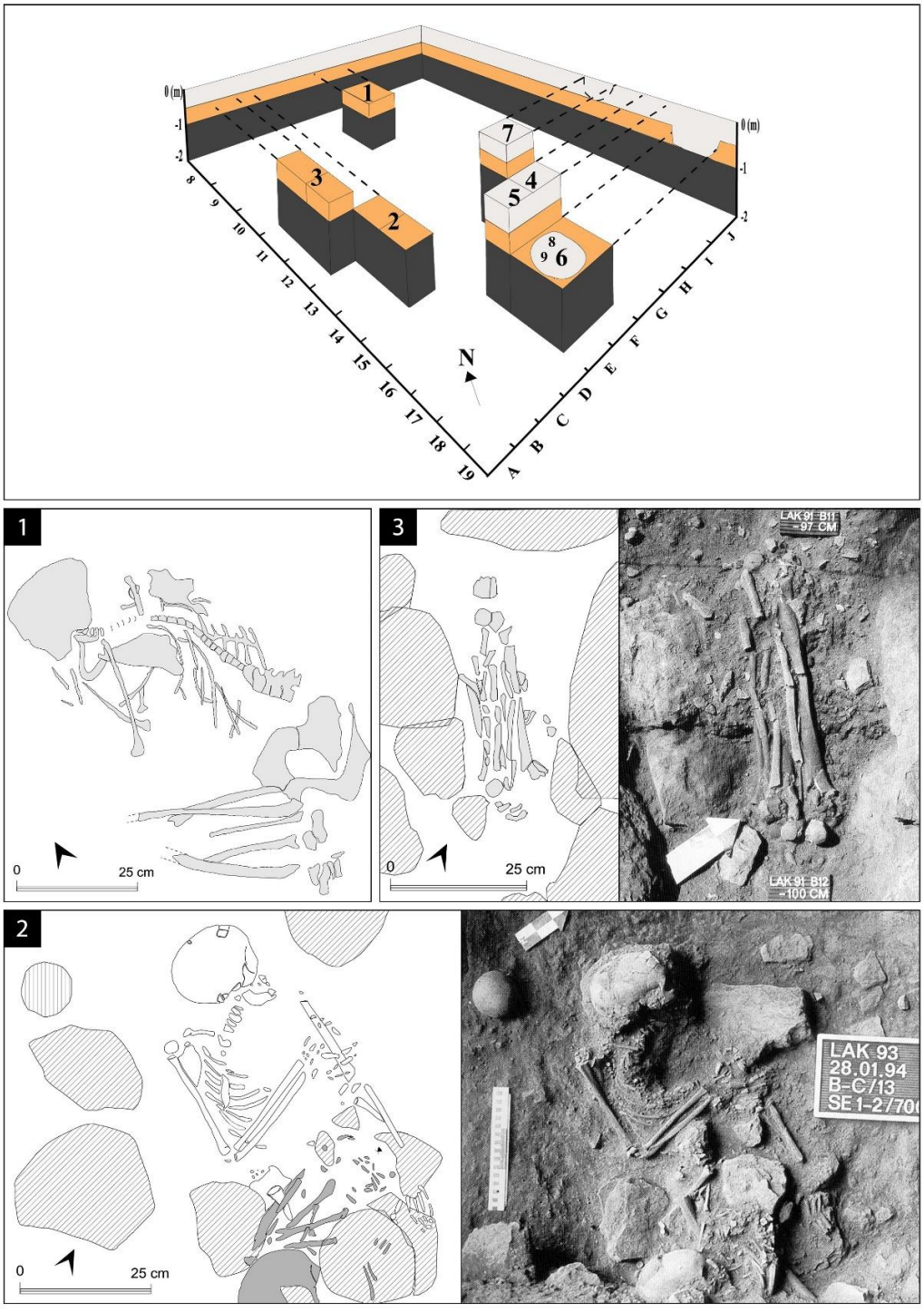

Figure S2: The Shum Laka Burials Units (1 to 9). Each one is represented by one photograph and one drawing (from Ribot *et al* 2001 and modified by O. Graf; RMCA Collection: Photographs P. de Maret © RMCA, Tervuren).

Top left: Location of burial units on a 3D excavation plan in relation to Holocene (top grey layer: Ag; middle orange layer: Ao) and Pleistocene deposits (bottom dark layer: P, S/Si).

1. Burial Unit 1 (single primary).

2. Burial Unit 2 (double primary) showing SE I overlying lower limbs of SE II (65-70cm below surface).

3. Burial Unit 3 (secondary) showing the bundle of long bones surrounded by stones (50-60cm below surface).

(Figure S2 continued)

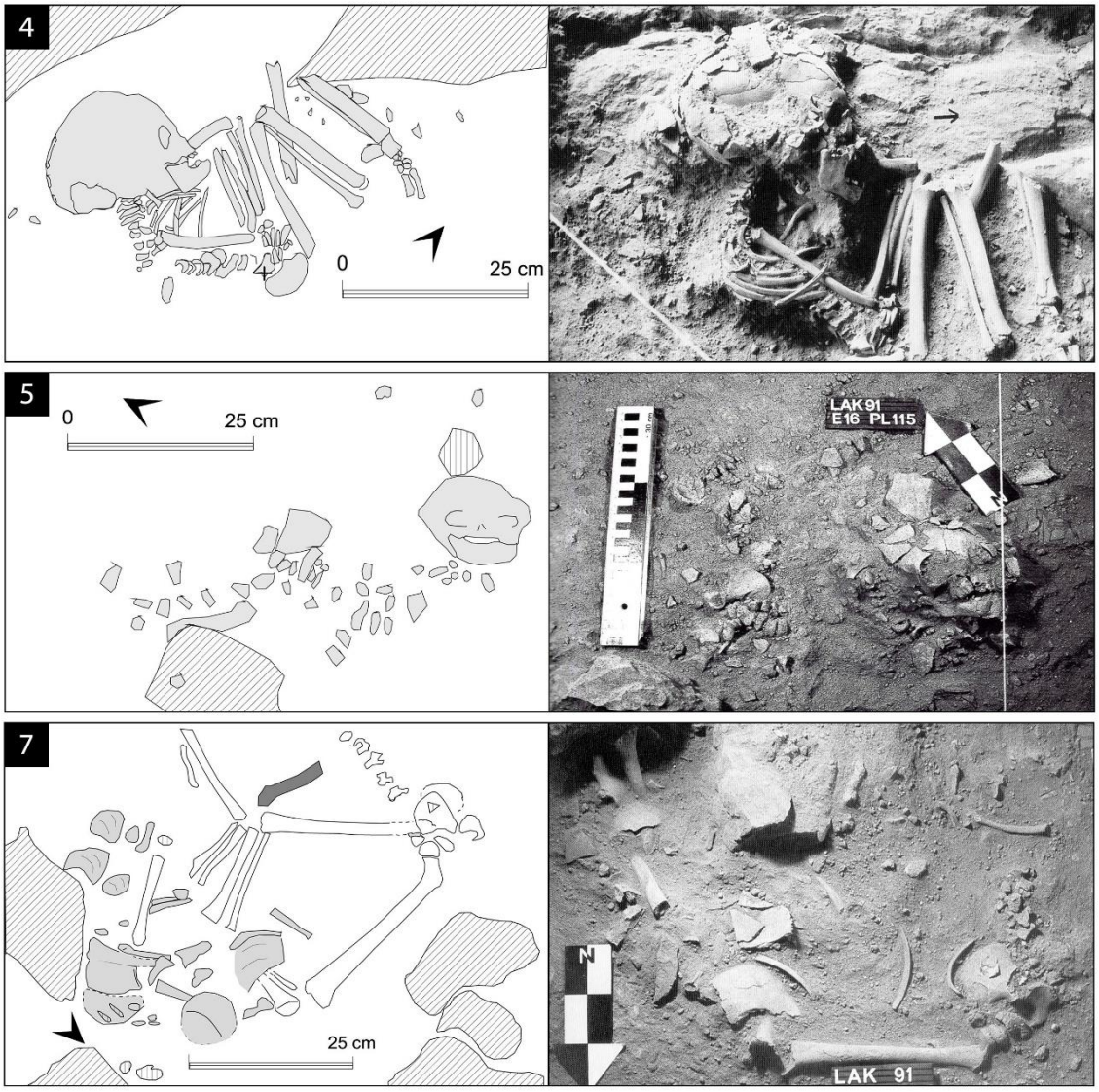

4. Burial Unit 4 (single primary) showing Skeleton A in a foetal position (20-25cm below surface).
5. Burial Unit 5 (single primary) showing Skeleton B partially articulated as disturbed (20cm below surface).
7. Burial Unit 7 (collective) showing disarticulated crania and one partially articulated post-cranial skeleton (20-30cm below surface)

(Figure S2 continued)

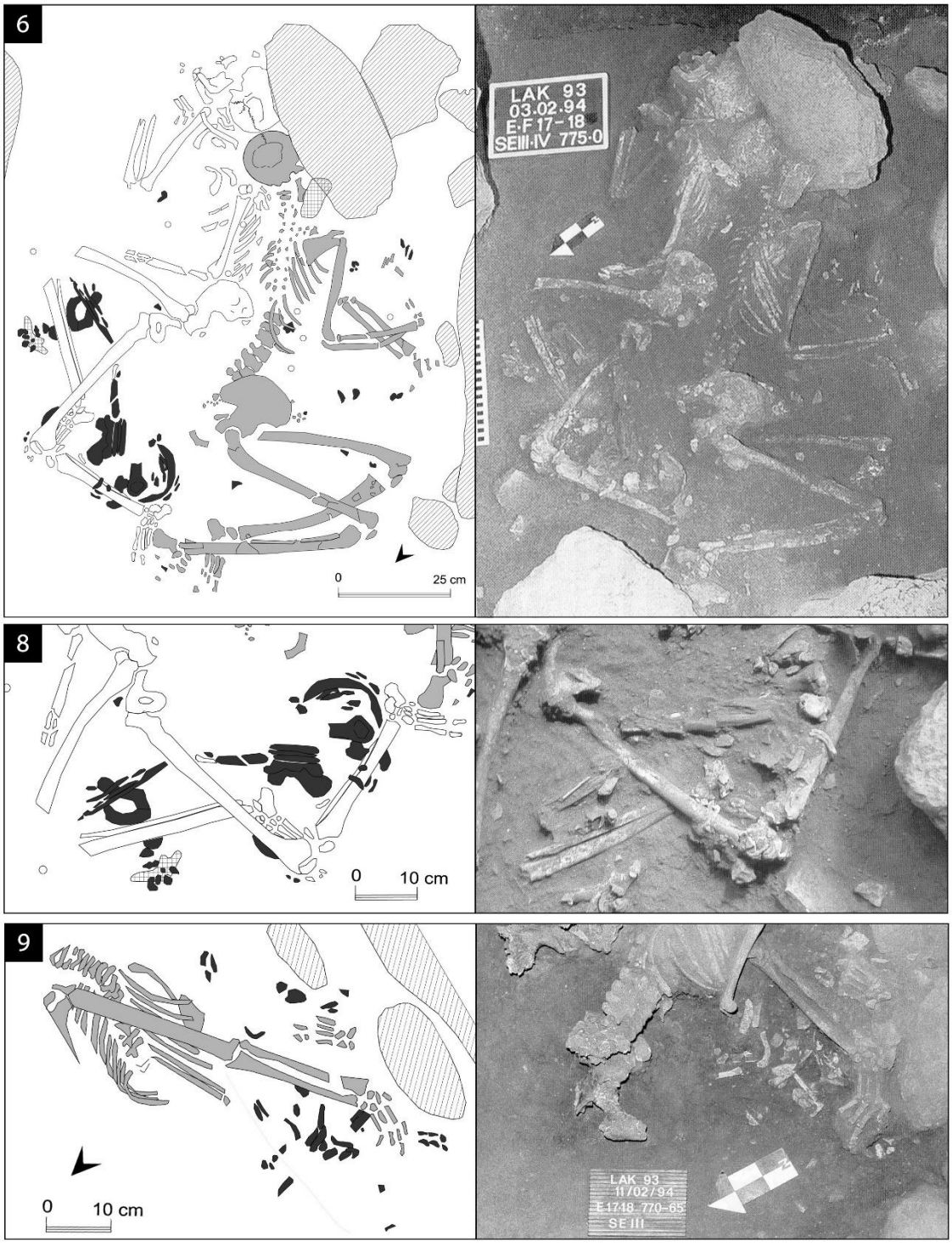

6. Burial Unit 6 (double primary) showing SE III and SE IV lying back to back (85cm below surface).

8. Burial Unit 8 (secondary) showing a deposit of disarticulated and partly burnt skeletal remains between the lower limbs of 6/SE IV (85cm below surface).

9. Burial Unit 9 (cremation) showing a concentration of very burnt and fragmented skeletal remains at the same level and just under the right upper limb of 6/SE III partially excavated and removed (85-90cm below surface).

a

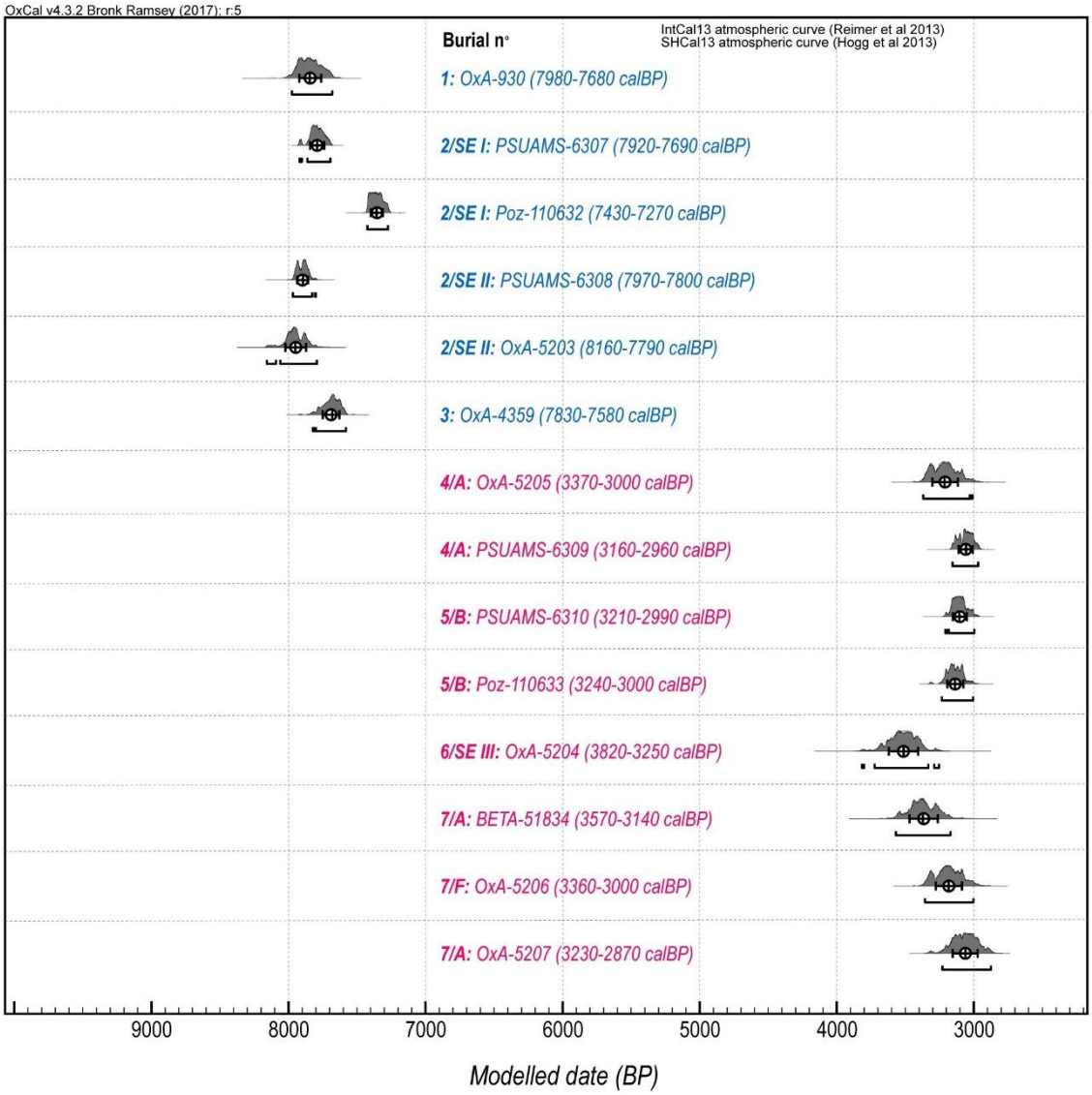

Figure S3: Calibration of ^{14}C dates from Shum Laka burials with OxCal version 4.3.2 using a mixed calibration curve (IntCal13/SHCal13) (see also Radiocarbon dates section of the main paper).

a. Multiplot showing probability distributions (95.4%) of the fourteen calibrated dates.

(Figure S3 continued)

b

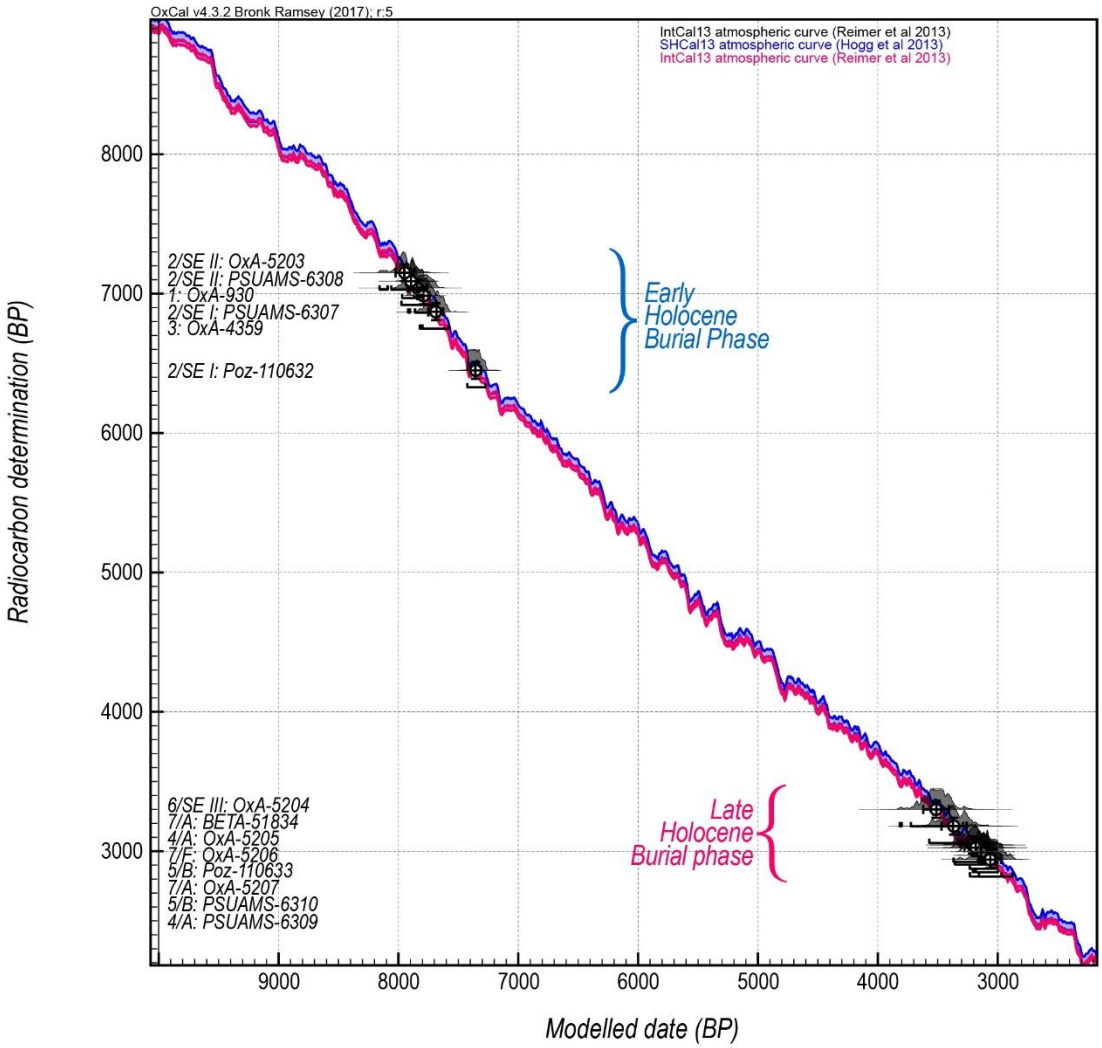

b. Calibration curve (Bronk Ramsey 2009) showing the well-defined age ranges for the two burial phases.

Basic bioarchaeological analysis

Except for Burial Unit 1, most of the human remains found at Shum Laka (Burial Units 2 to 9) are curated/deposited at the Institut Royal des Sciences Naturelles de Belgique (IRScNB). They have been analysed by Ribot *et al* (2001) with still ongoing research (e.g. 3D-morphology and reconstruction, isotopes, funerary practices). Some teeth and bones have been (micro-)CT-scanned and samples have been collected at the IRScNB for aDNA, isotopes, dental calculus and supplementary ^{14}C dating.

Standard osteological methods were used as described by Buikstra & Ubelaker (1994) and Scheuer *et al* (2010) (Table S1). Various criteria related to skeletal growth (e.g. dental development, bone fusion, diaphyseal lengths) were used to estimate the juvenile age-at-death (Moorees *et al* 1963 a/b, Scheuer & MacLaughlin-Black 1994, Steyn & Henneberg 1996), and sex estimation was performed using morphological features on the pelvis and skull (Schutkowski 1993). Other criteria related to morphological changes (auricular surface, pubic symphysis, sternal ends of ribs) as well as dental wear and cranial suture closure were assessed for the adult age-at-death estimations. Sex for the adults was also estimated with standard morphological criteria of both the pelvic bone and cranium. Each skeleton was examined for various palaeopathological conditions (e.g., enamel hypoplasia, cribra orbitalia, porotic hyperostosis, periostitis) and systematically radiographed (Ribot *et al* 2001).

In total, 18 individuals have been identified (4 for the early phase, 13 securely for the later phase, and one remains undated) (Table S1). Despite their very variable anatomical preservation indices (API: 2% to 69%) due to various factors (climate, soil composition, burial patterns), they reflected mainly the various burial patterns observed at the site (body preparation, orientation, and position) (Ribot *et al* 2001). The best preserved skeletons were discovered in the two double primary burials (Units 2 and 6) and one secondary burial including 7 incomplete individuals (Unit 7). Although the two skeletons of Burial Unit 2 provided a slightly lower level of bone preservation (API: 56% for SE I; 48% for SE II) than for the other two found in Burial Unit 6 (API: 68% for SE III; 51% for SE IV), their remains were less brittle and less fragile than the latter. This might be explained by the fact that skeletons SE III and SE IV were deposited close to the Pleistocene layers (90 cm deep burial pit intruding into S/Si deposits), which were more acidic than the ashy Holocene layers (Moeyersons 1996 a, 1996b; Moeyersons *et al* 1996). The very fragmented skeletal remains of Burial Unit 9 (246 bone fragments weighing 300g, of which 45% were anatomically identified) appeared to have been heated at a very high temperature (at least 800°C) according to both bone appearance (whitish, chalky, fragmentary) and composition (absence of collagen according X-ray diffraction analysis). They probably belonged to at least one adult individual, with less than 50% skeletal representation (Owsley 1993, McKinley 1993).

Age and sex estimations are summarized in Table S1 (Ribot *et al* 2001). Based on the minimal number of individuals (N=18), more than the half were juveniles (N=11); nine (out of 11) were buried during the later phase (Burial Unit 4, 5 and 7); and seven (out of 11) were younger than 7 years of age. Two adult females (Burial Unit 6: SE III and SE IV) and one male (Burial Unit 1) were identified, but the sex of the other four adults is less secure (Burial Units 3 and 8) and one is undetermined (Burial Unit 9).

As the population sample was in a very variable state of preservation, paleopathological interpretations are cautious. Nevertheless, some observations provided clues about individual disease histories. For example, the adults in Burial Unit 6 presented lesions related to age, occupations and/or diet on both bones (osteoarthritis and/or enthesophytes) and/or teeth (occlusal caries on molars, abscesses and diffused dental alveolar resorption).

Dental developmental defects (enamel hypoplasia, hypocalcification) were observed on four individuals (2/SE II, 4/A, 6/SE III, 7), and caries were nearly absent except for one individual (6/SE III). For the young adult female 6/SE III, the presence of numerous caries (7 out of 32 teeth) and the very small amount of calculus probably indicated a diet rich in carbohydrates and low in proteins. As her anterior superior teeth also showed marked lingual surface attrition, not only on the incisal edge but also on the lingual aspect, they suggested a wear pattern typical of a coarse diet rich in tuber roots as observed in recent agricultural populations (Irish & Turner 1987, 1997). In fact, tuber roots seem to be rather common in the hunter-gatherer diet. Ethnohistorical data on the Bayaka (Republic of Central Africa) support the presence of not only tuber roots of wild origin but also palm nuts (the latter necessitating long term masticatory activities for preparation and considered as a famine reserve during the dry season) (Heymer 1988).

Two rare paleopathological cases were observed in the Burial Unit 7: a congenital abnormality of the cranial vault (scaphocephaly); and an unhealed trauma on a pelvis due to a projectile or arrowhead (due to hunting accident or interpersonal violence) (Ribot *et al* 2001).

Preliminary isotopic analysis

Preliminary isotopic analyses were completed in 2012 by H. Bocherens (University of Tübingen) in order to understand the site's paleodietary and paleoenvironmental milieu. Human and faunal remains were both sampled (bones and/or teeth). Only bone fragments (e.g. ribs, long bones) were selected from four burial units including seven individuals (2/SE I, 2/SE II, 3, 4, 6/SE III, 6/SE IV, 7). Archaeological faunal bones and/or teeth were chosen from various species (e.g. chimpanzee, buffalo, giant forest hog, gorilla) that were found on the site.

Stable isotopic analysis (C, N, O) was performed with two different protocols. The first one consisted of the extraction of bone collagen for ^{15}N and ^{13}C analyses according to Bocherens *et al* (1997). A second protocol was used to purify the carbonate fraction of bone and tooth samples for ^{13}C and ^{18}O analysis according to Bocherens *et al* (1996). Elemental composition of the extracted collagen was measured using an elemental analyser coupled to a mass spectrometer, and the carbon and oxygen isotopic composition was analysed by mass spectrometry.

The results from the $\delta^{13}C$ analysis of collagen from human bones are fully consistent with those published together with the radiocarbon dates on collagen (Bronk Ramsey *et al* 2002, p88-90) (See Supplementary Table 1). They suggest that the Shum Laka individuals (range: -20.3 to -19.1‰), from the earlier and later period, lived in a mosaic of habitats including both the dense forest (wild pig: -27.6‰) and the savanna (buffalo: -10.5‰) and that they consumed essentially if not exclusively C_3 plants and their C_3 consumers (e.g. chimpanzee,

cercopithecine, giant forest hog) (Figure S4 a). The $\delta^{13}C$ values measured on the carbonate fraction of human bones yielded the same conclusion, indicating that the protein fraction (reflected by the collagen) as well as the carbohydrate fraction (reflected by the carbonate fraction) of the human diet were both originating from C_3 plant based food webs, therefore the savanna habitat was only marginally exploited for food procurement. This is consistent with the results obtained from the botanical and faunal analyses (de Maret *et al* 1987, Lavachery *et al* 1996), which suggest the presence of diverse resources from the forest (e.g., tuber roots, fruits, oil-producing plants, *Elais guineensis* and wild fauna typical of wooded areas, such as giant forest hog, duiker, monkey and mollusk)(Lavachery 2001).

The $\delta^{15}N$ values of two adults and two juveniles (+10.0 to +12.1‰) clearly indicated a protein fraction or a diet based on herbivore meat, such as giant forest hog (+5.2‰) and buffalo (+5.4‰). Slight differences were observed between the two periods (N=3, early phase: +11.2 to +12.1‰; N=1, late phase: +10.0‰), which could suggest a shift in food subsistence (from hunting-gathering with higher animal protein intake to proto-agriculture or arboriculture with more plant consumption).

The $\delta^{18}O$ values indicate a difference between the two burial periods: the values are higher for the later phase (+24.7 to +26.5‰) than the earlier one (+23.2 to +24.3‰) (Figure S4 b). This suggests a climatic or altitudinal shift, from cooler and/or more humid conditions and/or utilizing resources at higher altitude to a warmer and less humid and/or utilizing resources at lower altitude during the later phase. This is consistent with the paleoclimatic data that also showed a warmer and drier phase around 3000BP (Salzmann & Hoelzmann 2005).

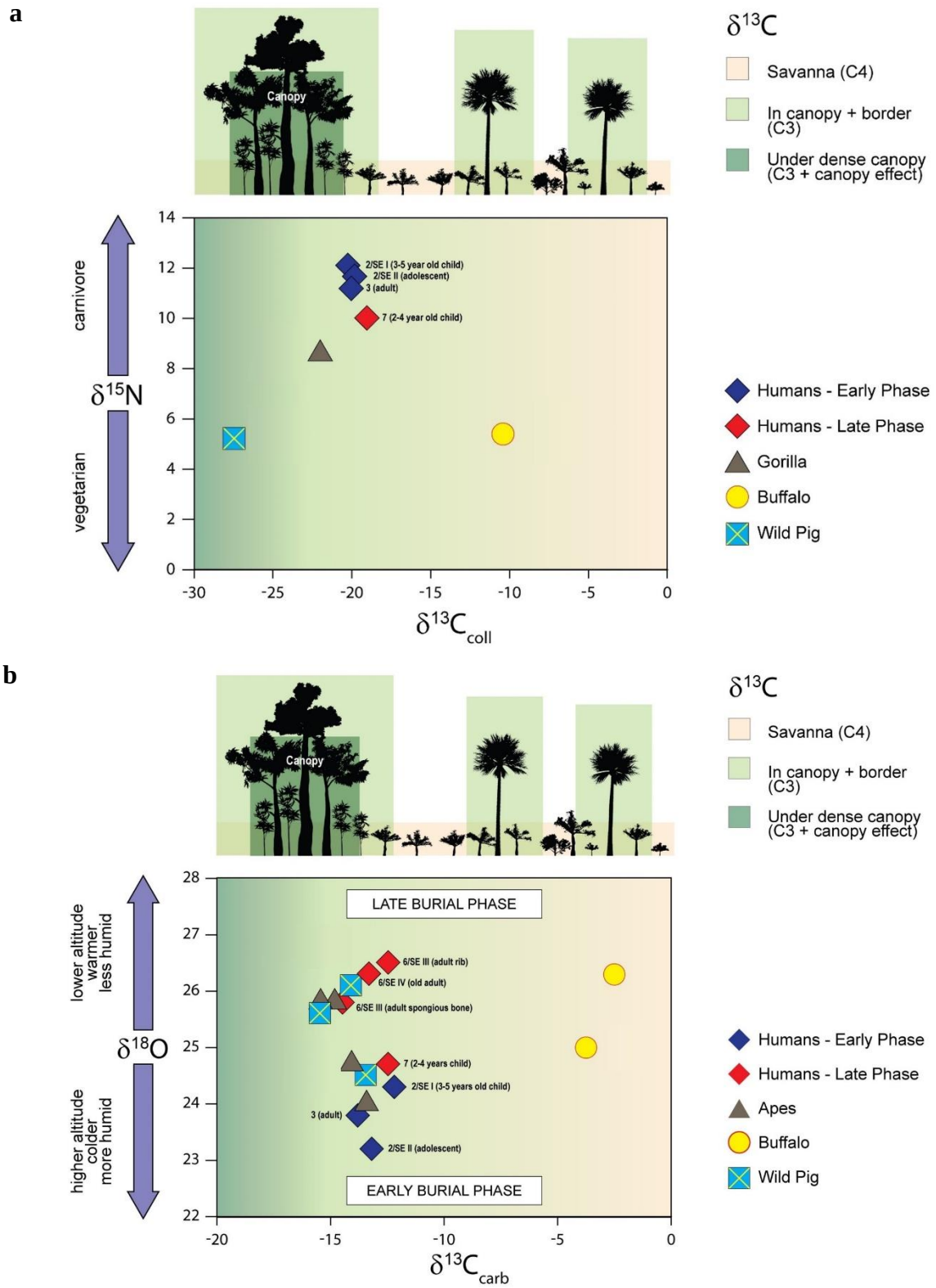

Figure S4: Preliminary results of the isotopic analyses from Shum Laka for human and faunal remains. Graph by H. Bocherens and modified by I. Ribot & O. Graf.

a. Carbon and nitrogen isotopes;

b. Carbon and oxygen isotopes.

Preliminary morphometrical analysis

Although Shum Laka's skeletal sample is relatively small and fragmentary, preliminary morphological analyses (e.g. stature, body proportions, tooth size and mandible shape) may suggest ecogeographical adaptations and population affinities. These preliminary inferences will be confirmed later by ongoing research using 3D analysis.

Using the tables of African Americans from Trotter (1970) and Trotter & Gleser (1977), who correlated long bone lengths with living stature for both sexes, the stature of four adult skeletons was estimated (Burial Units 1, 3, 6/SEIII and 6/SEIV) (Orban et al 1996; Ribot *et al* 2001). Although the results have to be taken cautiously because of various factors such as sex variation, sample size, and possible stature overestimations (Lundy & Feldesman 1987) (Table S2), they show that the individuals dated to the early phase tend to be relatively taller (range: 161-166cm) than those dated to the later phase (range for 6/SE III & SE IV: 143-155cm). In particular, the stature of the female SE IV of Burial Unit 6 (range: 143-148cm) seems closer to present-day Southern Cameroonian hunter-gatherers (Gyeli female mean: 149cm) than other neighbouring Bantu-speaking groups (Yassa female mean: 157cm) (Froment 1989). The results are less conclusive for the other female whose stature estimation (6/SE III: 153-155cm) is close to both comparative groups (Gyeli and Yassa).

Nevertheless, this slight decrease in stature through time could reflect the increasing impact of selective pressures specific to a tropical rainforest and/or the increasing genetic input of ancestry of hunter-gatherer related groups having a small body size (Bailey 1991, Perry & Dominy 2009).

Table S2: Postcranial measurements for four adult skeletons from Shum Laka.

Burial unit #	**Maximum long bone length in mm**	**Stature estimation in cm [1]**	**Body proportions**	
			RH-I[2]	**TF-I[3]**
1	452 (left femur)	166 (♂)	-	-
3	357 (right fibula)	161-165 (♂)	-	-
6/SE III	292 (left humerus) 223 (right radius) 242 (left ulna) 330 (left fibula)	154 (♀) 154 (♀) 155 (♀) 153 (♀)	76.4%	-
6/SE IV	320 (right femur) 307 (right tibia)	143 (♀) 148 (♀)	-	84.1%

[1] Stature estimation was done by comparing long bone lengths to the data from Trotter (1970) and Trotter & Gleser (1977) for African Americans for both sexes;
[2] RH-I (humero-radial index) = (maximal length of radius/maximal length of humerus) x 100 (Martin & Saller 1957).
[3] TF-I (femoro-tibial index) = (maximal length of tibia/maximal length of femur) x 100 (Martin & Saller 1957).

Body proportions were evaluated using two postcranial indices for two individuals of the later phase (Table S2). The radio-humeral index (RH-I) of the female 6/SE III (RH-I: 76.4%) appeared much lower than the mean values obtained for Late Iron Age Central Africans (Upemba Valley, Sanga & Katoto: 80.85%) (Hiernaux *et al* 1992). The femoro-tibial index of the other female 6/SE IV (TFI: 84.1%) appeared here much closer to the Late Iron Age Central Africans (TFI: 83.4%) (Hiernaux *et al* 1992). Although the upper limbs reflected a marked shortening of the distal end in contrast to the lower limbs, it is difficult here to interpret these indices in relation to any adaptation (Ruff 1994, Higgins & Ruff 2011), as the sample consists of only two individuals.

Bucco-lingual diameters for both the upper first and second permanent molars were taken from five Shum Laka individuals, two from the early phase (2/SE I and 2/SE II) and three from the later phase (4/A, 5/B and 6/SE III). They were plotted in a graph with comparative modern West-Central African (Ribot 1998, Romero *et al* 2018) and Late Iron Age Central African (Upemba Valley) data (de Maret 1979, Orban *et al* 1988) (Figure S5a & b). For both burial phases, Shum Laka upper permanent teeth appear to be very large, as their diameters are often in the highest range (M1: 12.10-12.85mm; M2: 12.25-13.05mm) in comparison to modern males (Figure S5a) and females (Figure S5b). As there is much overlap between groups, Shum Laka's teeth always fall within the 95% confidence ellipses of the variation of both modern Nigerians, Gabonese and Late Iron Age Congolese. Dental size reduction through time seems even more evident when comparing Shum Laka teeth with the Late Iron Age Central African mean sample (M1: 11.28mm; M2: 11.24mm) (Figure S5a & b). It is however interesting to note that the bucco-lingual diameters of Shum Laka upper molars exceed those observed for the modern West African Pygmies (pooled sexes mean M1: 11.73mm; mean M2: 11.70mm) (Romero *et al* 2018).

Nevertheless, Romero *et al* (2018) still observed significant tooth size differences between these modern hunter-gatherers (Baka) and various Bantu-speaking agriculturist groups (Mvae, Yassa) of Southern Cameroon (pooled sexes mean M1: 11.41mm: mean M2: 11.45mm). This suggests that not only the postcranial skeleton but also the teeth could have been under strong dietary selective pressure that induced a reduction in tooth size (Hanihara & Ishida 2005, Pilloud & Kenyhercz 2016). Therefore, Shum Laka's dental phenotype might be characteristic of some of the pre-agricultural population diversity at that time and in this region, where large teeth were selected non-randomly due to strong selective pressures linked to a hunter-gatherer lifestyle and a coarse diet.

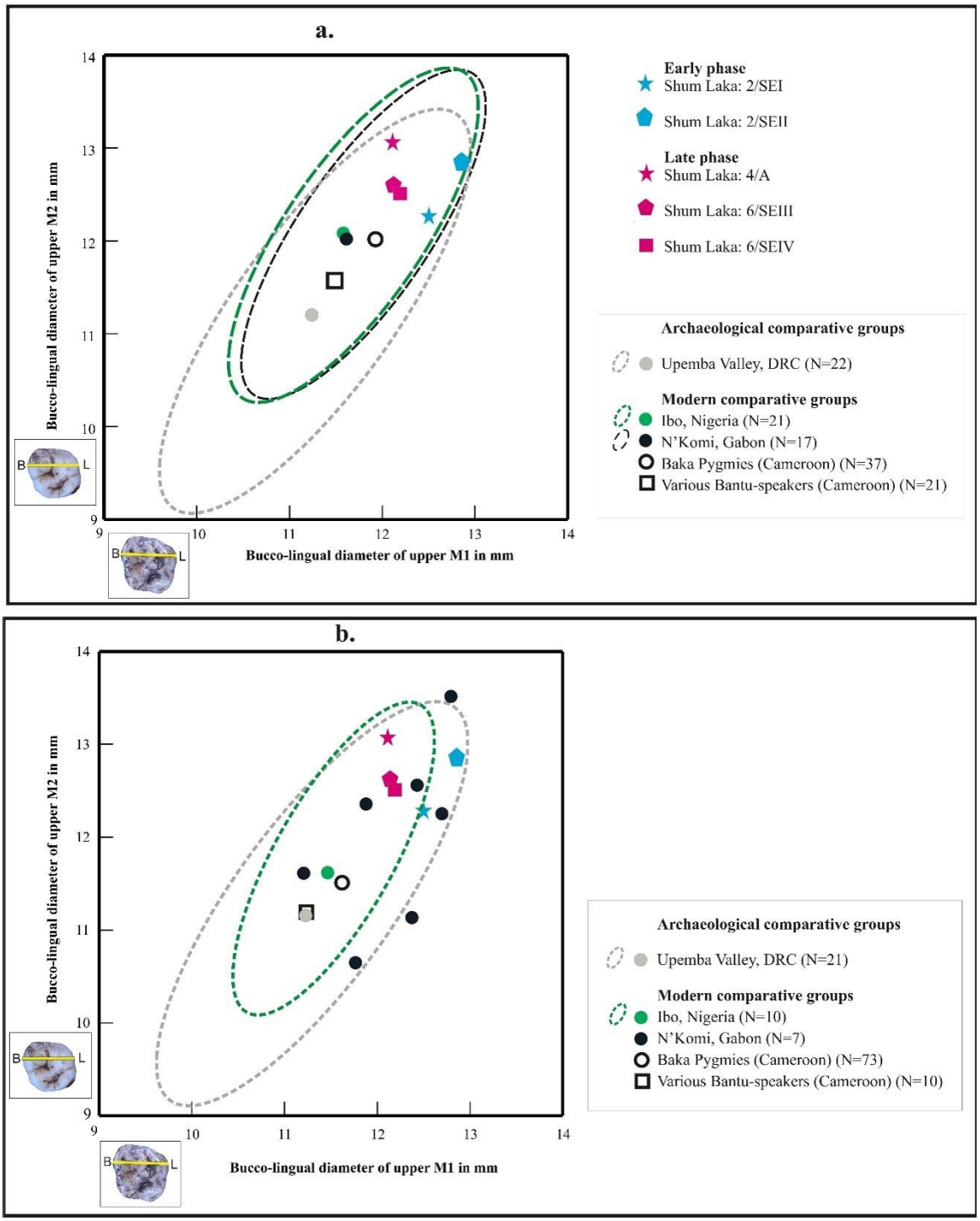

Figure S5: Scatterplot of bucco-lingual diameters of upper first permanent molars (M1) and second molars (M2) with five Shum Laka individuals and comparative groups.
The 95% confidence ellipses (with the mean) were drawn for the comparative data except for the female Gabonese sample (N<10) (Photographs: Y. Ghalem).

a. Comparison with male sample only (N=120).

b. Comparison with female sample only (N=121).

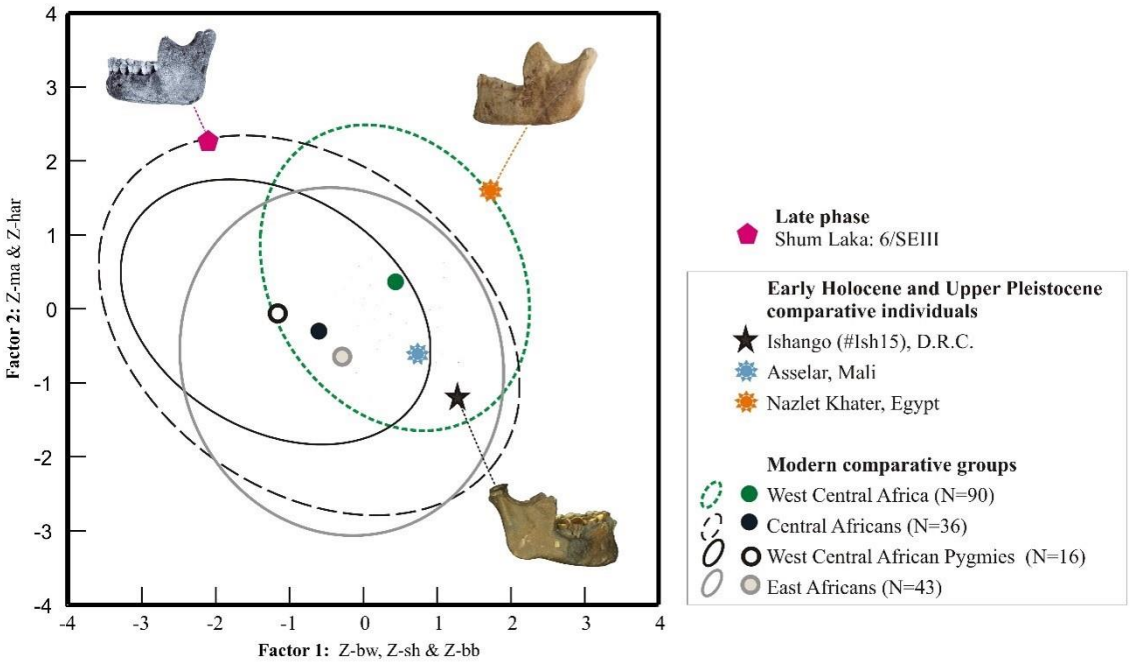

Figure S6: Scatterplot of first and second factor scores obtained from a principal component analysis using mandibular variables for 6/SE III and other comparative groups.

The 95% confidence ellipses (with the centroid) were drawn for the modern comparative data. Three variables showed the highest loadings (>0.7): the bigonial width (bw), the symphyseal height (sh) and the bicondylar breadth (bb) on factor 1, and the mandibular angle (ma) and the height of the ascending ramus on factor 2. The two factors expressed 66% of total variance. According to the squared correlation coefficient or factor loading, factor 1 accounted for 55% of the variance for variable bb, 53% for variable sh and 53% for variable bw, and factor 2 accounted for 90% of the variance for variable ma and for 41% for the height of the ascending ramus (har). Photographs: Ribot et al. 2001 (top-left) & I. Crevecoeur (top-right, bottom-right).

As individual 6/SE III provided a complete mandible, a multivariate analysis was performed using a series of mandibular measurements, in order to capture through morphology its affinities with other African groups. The comparative data (compiled and collected by Ribot *et al* 2011) were subdivided into four modern groups (West Central Africans, N=90; Central Africans, N=36; West-Central African Pygmies, N=16; East Africans, N=43) and included two Late Stone Age individuals, from Asselar in Mali (6,390 BP; Oakley & Campbell 1967, Villiers & Patti 1982), Ishango (#Ish15 dated between 19,540 BP and 24,145 BP) (Brooks *et al* 1995, Crevecoeur *et al* 2016) and Nazlet Khater (n°2 dated by ESR on tooth enamel fragments to 38 ± 6 ka) (Crevecoeur 2008, Crevecoeur *et al* 2009). To maximize sample size, five variables were selected: bicondylar width (bb or M. 65), bigonial width (bw or M.66), height of ascending ramus (har or M.70), minimal width of ascending ramus (war or M.71a) and mandibular angle (ma or M.79) (Martin & Saller 1957). After a Z-score standardization of the variables for the whole sample (pooled sexes), a principal component analysis (PCA) with varimax rotation was performed (with IBM SPSS Statistics v.25) and the two factor scores plotted into a graph (with SYSTAT v.11.5) (Figure S6). Although Shum Laka's mandible still appears to fall within the 95%

confidence ellipses of modern variation (e.g. Central Africans), its position is slightly marginal within the general variation. In fact, its morphology is rather unusual with a small mandibular angle (ma: 101°) and a high ascending ramus (har: 60.63mm). Despite a relatively small size in breadth (e.g. bb: 110.50mm), it presents robust features such as a very wide ascending ramus (war: 39.42mm) that is comparable to the mandible from Ishango (war: 39mm), but not as large as that from Nazlet Khater (war: 51mm). Nevertheless, the general shape of mandible of 6/SE III seems to be clearly different from the early Holocene (Asselar and Ishango) and Upper Pleistocene (Nazlet Khater) mandibles, which all fall at the opposite end of the range of variation (right half of the graph): despite its smaller size, the ascending ramus is very high (har: 60.63mm) and only slightly higher than that of Ishango (har: 59mm).

As suggested above for tooth size, Shum Laka's mandibular morphology is also unique with a mosaic of features. It might have developed under strong selective pressures very locally within various groups and/or through gene flow from other non-local groups. Ongoing morphometrical research might resolve these issues.

References

Asombang, R. & De Maret, P. Reinvestigating Shum Laka, *Nsi* **10/11**, 13-16 (1992).

Asombang, R. *Bamenda in prehistory, the evidence from Tiye Nkwi, Mbi Crater and Shum Laka rockshelters.* Unpublished Ph.D. Thesis, London University (1988).

Bailey, R.C. The comparative growth of Efe pygmies and African farmers from birth to age 5 years. *Ann. Hum. Biol.* **18**, 113–120 (1991).

Bello, S. & Andrews, P. The intrinsic pattern of preservation of human skeletons and its influence on the interpretation of funerary behaviours. In Knüsel, C. & Gowland, R. (eds.) *Social archaeology of funerary remains*, 1-13 (Oxbow, Oxford, 2006).

Bocherens, H., Billiou, D., Patou-Mathis, M., Bonjean, D., Otte, M., Mariotti, A. Paleobiological implications of the isotopic signature (^{13}C, ^{15}N) of fossil mammal collagen in Scladina cave (Sclayn, Belgium). *Quaternary Research* **48**, 370–380 (1997).

Bocherens, H., Koch, P.L., Mariotti, A., Geraads, D., Jaeger, J.-J. Isotopic biogeochemistry (^{13}C, ^{18}O) of mammal enamel from African Pleistocene hominid sites: implications for the preservation of paleoclimatic isotopic signals. *Palaios* **11**, 306-318 (1996).

Bronk Ramsey C. Bayesian analysis of radiocarbon dates. *Radiocarbon* **51**, 337–360 (2009).

Bronk Ramsey, C., Higham, T.F.G., Owen, D.C., Pike, A.W.G., Hedges, R.E.M. Radiocarbon dates from the Oxford AMS system : Archaeometry datelist 31. *Archaeometry* **44 supp.1**, 1-149 (2002).

Brooks, A.S., Helgren, D., Cramer, J.S., Franklin, A., Hornyak, W., Keating, J.M., Klein, R.G., Rink, W.J., Schwarcz, H., Smith, J.N.L., Stewart, K., Todd, N.E., Verniers, J. & Yellen, J.E. Dating and context of three Middle Stone Age Sites with bone points in the Upper Semliki Valley, Zaire. *Science* **268**, 548-553 (1995).

Brothwell, D.R. & Shaw, T. A late upper Pleistocene proto-West African Negro from Nigeria. *Man* **6**, 221-229 (1971).

Buikstra, J.E. & Ubelaker, D.H. *Standards for Data Collection from Human Skeletal Remains.* Arkansas Archaeological Survey Research Series, Fayetteville (1994).

Cornelissen, E. Shum Laka (Cameroon): Late Pleistocene deposits and early Holocene deposits. In Pwiti, G. & Soper, R. (eds.) *Aspects of African archaeology, Papers from 10th Congress of the Panafrican Association for Prehistory and Related Studies, Harare (June 1995)*, 257-264 (1996).

Crevecoeur, I. *Étude anthropologique du squelette du Paléolithique supérieur de Nazlet Khater 2 (Egypte). Apport à la compréhension de la variabilité passé des hommes modernes*. Leuven University Press, Leuven (2008).

Crevecoeur, I., Rougier, H., Grine, F., Froment, A. Modern human cranial diversity in the Late Pleistocene of Africa and Eurasia: Evidence from Nazlet Khater, Peştera cu Oase, and Hofmeyr. *American Journal of Physical Anthropology* **140**, 347-358 (2009).

Crevecoeur, I., Brooks, A., Ribot, I., Cornelissen, E. & Semal, P. Late Stone Age human remains from Ishango (Democratic Republic of Congo): New insights on Late Pleistocene modern human diversity in Africa. *Journal of Human Evolution* **96**, 35-57 (2016).

de Maret, P. Luba roots: the first complete iron age sequence in Zaïre. *Current Anthropology* **20**, 233-235 (1979).

de Maret, P. Preliminary report on 1980 fieldwork in the Grassfields and Yaounde, Cameroon. *Nyame Akuma* **17**, 10-12 (1980).

de Maret, P., Asombang, R., Cornelissen, E., Lavachery, P. & Moeyersons, J. Continuing research at Shum Laka rockshelter, Cameroon (1993-1994 field season). *Nyame Akuma* **43**, 2-3 (1995).

de Maret, P., Asombang, R., Cornelissen, E., Lavachery, P., Moeyersons, J. & Van Neer, W. Preliminary results of the 1991-1992 field season at Shum Laka, Northwestern Province, Cameroon. *Nyame Akuma*, **39**, 13-15 (1993).

Duday, H. Archeoethnoanatology or the Archeology of Death. In Knüsel, C. & Gowland, R. (eds.) *Social archeology of funerary remains*, 30–56 (Oxbow, Oxford, 2006).

Duday, H. L'archéothanatologie ou l'archéologie de la Mort. In Dutour, O., Hublin, J.-J. & Vandermeersch, B. (eds.) *Objets et méthodes en Paléoanthropologie*, 153–215 (Comité des Travaux Historiques et Scientifiques, Paris, 2005).

Duday, H., Courtaud, P., Crubézy, E., Sellier, P., Tillier, A.-M. L'anthropologie "de terrain", reconnaissance et interprétation des gestes funéraires. *Bulletins et Mémoires de la Société d'Anthropologie de Paris, n.s.* **2(3-4)**, 29 50 (1990).

Dutour, O. *Hommes fossiles du Sahara: peuplements holocènes du Mali septentrionnal*. CNRS publication, Marseille (1989).

Fardon, R. *Between god, the dead and the wild. Chamba interpretations of religion and ritual.* University Press of Edinburgh (1990).

Froment, A. Body morphology and the savanna - forest transition: a West African example. *International Journal of Anthropology* **4(1-2)**, 61-74 (1989).

González-Ruibal, A., Sánchez-Elipe, M., Otero-Vilariño, C. An Ancient and Common Tradition: Funerary Rituals and Society in Equatorial Guinea (First–Twelfth Centuries AD). *African Archaeological Review* **30(2)**, 115-143 (2012).

Hanihara, T. & Ishida, H. Metric dental variation of major human populations. *American Journal of Physical Anthropology* **128**, 287– 298 (2005).

Harvati, K., Stringer, C., Grün, R., Aubert, M., Allsworth-Jones, P. & Folorunso, C.A. The Later Stone Age calvaria from Iwo Eleru, Nigeria: morphology and chronology. *PLoS One* **6 (9)**, 1-8 (2011).

Heymer, A. L'abrasion dentaire chez les Pygmées Bayaka en fonction des conditions écologiques, alimentaires et d'une mastication accrue. *Homo* **XXXVII(3)**, 160-188 (1988).

Hiernaux, J., Plantier, M. & De Buyst, J. Etude ostéométrique des restes humains de Sanga et Katoto (Âge du fer, Zaïre). *Anthropologie et Préhistoire* **103**, 9-44 (1992).

Higgins, R.W. & Ruff, C.B. The Effects of Distal Limb Segment Shortening on Locomotor Efficiency in Sloped Terrain: Implications for Neandertal Locomotor Behavior. American *Journal of Physical Anthropology* **146**, 336–345 (2011).

Irish, J.D. & Turner, C.G. Brief communication: first evidence of LSAMAT in non-native Americans: Historic Senegalese from West Africa. *American Journal of Physical Anthropology* **10**, 141-146 (1997).

Irish, J.D. & Turner, C.G. More lingual surface attrition of the maxillary anterior teeth in American Indians: Prehistoric Panamanians. *American Journal of Physical Anthropology* **7**, 209-213 (1987).

Johnson, J.S. Consolidation of archaeological bone: a conservation perspective. *Journal Field Archaeology* **21**, 221-233 (1994).

Lavachery, P. Shum Laka rockshelter Late Holocene deposits: from stone to metal (Northwestern Cameroon). In Pwiti, G. & Soper, R. (eds.) *Aspects of African archaeology, Papers from 10th Congress of the Panafrican Association for Prehistory and Related Studies, Harare (June 1995)*, 265-273 (1996).

Lavachery, P., Cornelissen, E., Moeyersons, J. & de Maret, P. Trente mille ans d'occupation, six mois de fouilles: Shum Laka, un site exceptionnel en Afrique Centrale. *Anthropologie et Préhistoire* **107**, 197-212 (1996).

Lembezat, B. Kirdi, les populations païennes du Nord-Cameroun. *Mémoires de l'Institut d'Afrique Noire (Centre Cameroun)* **2** (1950).

Lundy, J.K. & Feldesman, M.R. Revised equations for estimating living stature from the long bones of the South African Negro. *South African Journal of Science* **83**, 54-55 (1987).

Martin, R. & Saller, K. *Lehrbuch der Anthropologie*. G. Fischer, Stuttgart (1957).

McKinley, J. Bone fragment size and weights of bone from modem British cremations and its implications for the interpretation of archaeological cremations. *International Journal of Osteoarchaeology* **3**, 283-287 (1993).

Moeyersons, J. Evolution of the Shum Laka rockshelter (Northwestern Cameroon) since Late Stone Age times. In Pwiti, G. & Soper, R. (eds.) *Aspects of African archaeology, Papers from 10th Congress of the Panafrican Association for Prehistory and Related Studies, Harare (June 1995)*, 245-255 (1996a).

Moeyersons, J. Rockshelter as a possible reason for waterfall retreat in the Bafochu Mbu caldeira, Western Cameroon. *Zeitschrift Geomorphologie Neue Folge* **103**, 345-358 (1996b).

Moeyersons, J., Cornelissen, E., Lavachery, P. & Doutrelepont, H. L'abri sous roche de Shum Laka (Cameroun occidental): données climatologiques et occupation humaine depuis 30,000 ans. *Geo-Eco-Trap* **20 (1-4)**, 39-60 (1996).

Moorrees, C.F.A., Fanning, E.A., Hunt, E.E. Age variation of formation stages for ten permanent teeth. *Journal of Dental Research* **42**, 1490-1502 (1963a).

Moorrees, C.F.A., Fanning, E.A., Hunt, E.E. Formation and resorption of three deciduous teeth in children. *American Journal of Physical Anthropology* **21**, 205-213 (1963b).

Ngomanda, A., Neumann, K., Schweizer, A. & Maley, J. Seasonality change and the third millennium BP rainforest crisis in southern Cameroon (Central Africa). *Quaternary Res*. **71**, 307–318 (2009).

Oakley, K.P. & Campbell, B.G. *Catalogue of fossil hominids. Part I: Africa.* Trustees of the British Museum, London (1967).

Okpoko, A.I. Traditional methods of disposal of the dead in parts of Nigeria. *West African Journal of Archaeology* **23**, 104-121 (1993).

Orban, R., Procureur, F., Semal, P. & de Maret, P. Observations sur les dents de squelettes protohistoriques provenant de l'Upemba (Zaïre). *Bulletins et Mémoires de la Société Royale Belge d'Anthropologie et Préhistoire* **99**, 61-80 (1988).

Orban, R., Ribot, I., Fenaux, S. & de Maret. P. Les restes humains de Shum Laka (Cameroun, LSA - Âge du fer). *Anthropologie et Préhistoire* **107**, 213-225 (1996).

Owsley, D.W. Identification of the fragmentary, burned remains of two U.S. journalists even years after their disappearance in Guatemala. *Journal of Forensic Science* **38(6)**, 1372-1382 (1993).

Perry, G.H. & Dominy, N.J. Evolution of the human pygmy Phenotype. *Trends in Ecology and Evolution* **24(4)**, 218-225 (2009).

Pilloud, M.A., Kenyhercz, M.W. Dental metrics in biodistance analysis. In Pilloud, M.A. & Hefner J.T. (eds.) *Biological distance analysis. Forensic and bioarchaeological perspectives*, 135-155 (Elsevier Academic Press, London, 2016).

Ribot, I. A Study through Skull Morphology on the Diversity of Holocene African Populations in a Historical Perspective. *BAR International Series S2215,* Oxford (2011).

Ribot, I. *Cranial variation in Equatorial Africa*. Unpublished Master dissertation, University of Cambridge (1998).

Romero, A., Ramirez-Rozzi, F.V. & Pérez-Pérez, A. Dental size variability in Central African Pygmy hunter-gatherers and Bantu-speaking farmers. *American Journal of Physical Anthropology*, 1–11 (2018).

Ruff, C.B. Morphological adaptation to climate in modern and fossil hominids. *Yearbook of Physical Anthropology* 37:65–107 (1994).

Salzmann, U. & Hoelzmann, P. The Dahomey Gap: an abrupt climatically induced rain forest fragmentation in West Africa during the Late Holocene. *The Holocene* **15**, 190–199 (2005).

Scheuer, L., & Maclaughlin-Black, S. Age estimation from the pars basilaris of the fetal and juvenile occipital bone. *International Journal of Osteoarchaeology* **4**, 377-380 (1994).

Scheuer, L., Black, S. & Schaefer, M.C. *Juvenile Osteology: A Laboratory and Field Manual.* Academic Press, Cambridge US (2010).

Schutkowski, H. Sex determination of infant and juvenile skeletons: I. Morphognostic features. *American Journal of Physical Anthropology* **90**, 199-205 (1993).

Steyn, M. & Henneberg, M. Skeletal growth of children from the Iron Age site at K2 (South Africa). *American Journal of Physical Anthropology* **100**, 389-396 (1996).

Trotter, M. & Gleser, G. G. Corrigenda to Estimation of stature from long bones of American Whites and Negroes, AJPA (1952). *American Journal of Physical Anthropology* **47(2)**, 355-356 (1977).

Trotter, M. Estimation of stature from intact long bone limbs. In Stewart, T.D. (ed.) *Personal identification in mass disasters*, 71-84 (Natural History Museum, Smithsonian Institution, Washington, 1970).

Van Neer, W. & Lanfranchi, R. Etude de la faune découverte dans l'abri Tshitolien de Ntadi Yomba (République Populaire du Congo). *L 'Anthropologie* **89(3)**, 351-364 (1985).

Villiers, H. & Patti, L.P. The antiquity of the Negro. *South African Journal of Sciences* **78**, 321-332 (1982).

Warnier, J.P. Histoire du peuplement et genèse des paysages dans l'ouest camerounais. *Journal of African History* **25(4)**, 395-410 (1984).

Supplementary Information section 2:
Kinship analysis for windows across the genome

In this section, we display allelic mismatch rates for each pair of individuals, as well as intra-individual comparisons, computed in overlapping 10 Mb windows at intervals of 1 Mb across the entire genome. We selected one read per individual at random at each targeted SNP. Segments where both chromosomes are shared IBD (including intra-individual comparisons) are expected to have a value one-half as large as segments with no sharing (bottom and top dashed lines, respectively); segments with one chromosome shared IBD are expected to be halfway in between (middle dashed line). Perfect matching (mismatch value of zero) occurs when an individual's two chromosomes are themselves shared IBD through inbreeding (which can also induce additional inter-individual matching). For a given pair of individuals, transitions along a chromosome from one of these levels to another are indicative of recent recombination events. Lab codes correspond to sample IDs as follows: I10871 = 2/SE II; I10872 = 2/SE I; I10873 = 4/A; and I10874 = 5/B.

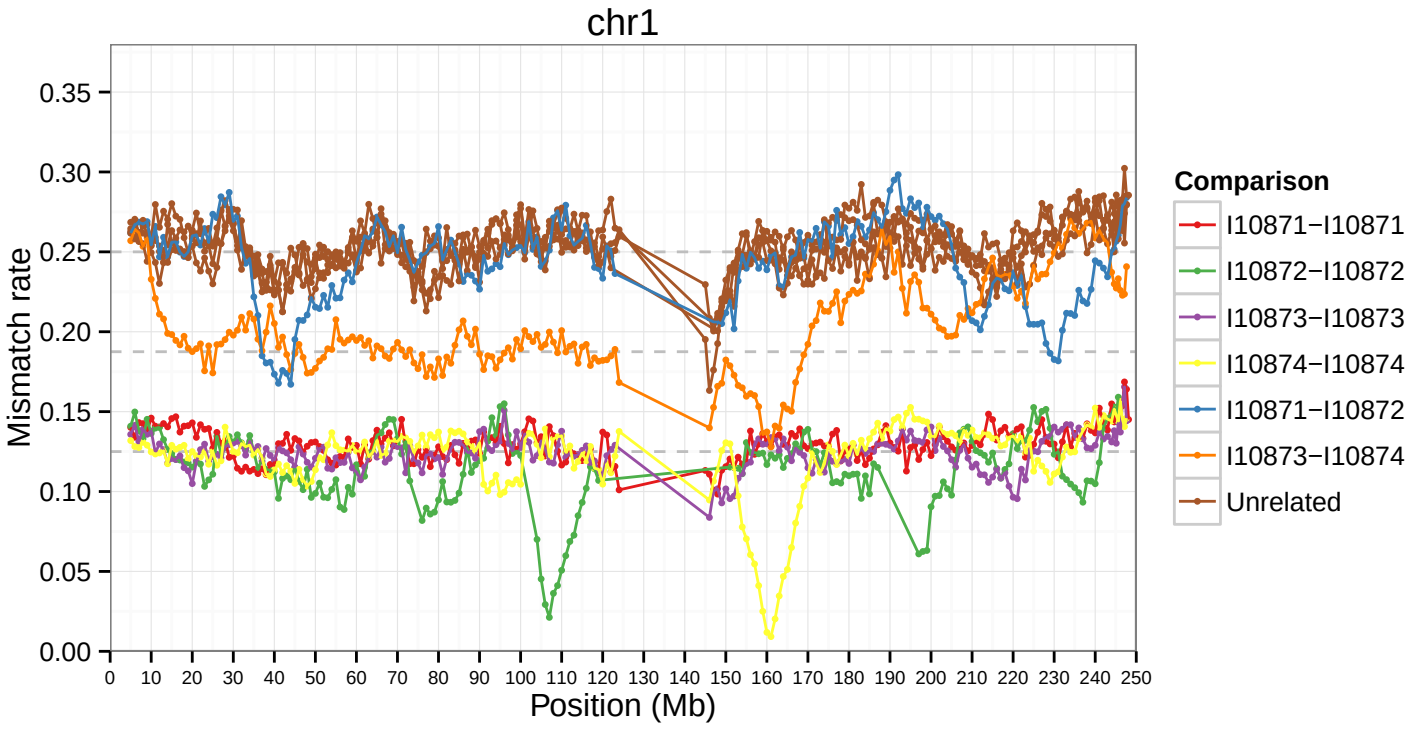
chr1
Mismatch rate
0.35
0.30
0.25
0.20
0.15
0.10
0.05
0.00
0 10 20 30 40 50 60 70 80 90 100 110 120 130 140 150 160 170 180 190 200 210 220 230 240 250
Position (Mb)
Comparison
I10871−I10871
I10872−I10872
I10873−I10873
I10874−I10874
I10871−I10872
I10873−I10874
Unrelated

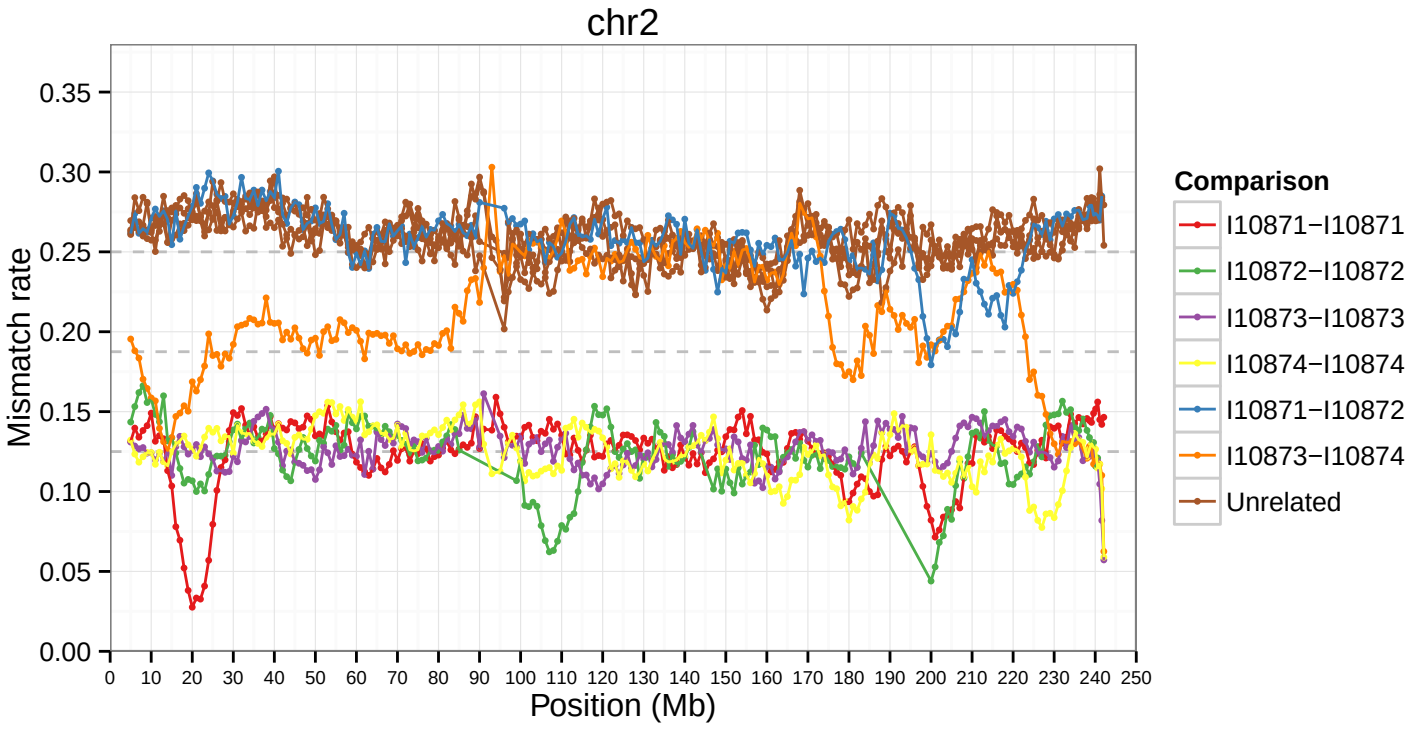
chr2
Mismatch rate
0.35
0.30
0.25
0.20
0.15
0.10
0.05
0.00
0 10 20 30 40 50 60 70 80 90 100 110 120 130 140 150 160 170 180 190 200 210 220 230 240 250
Position (Mb)
Comparison
I10871−I10871
I10872−I10872
I10873−I10873
I10874−I10874
I10871−I10872
I10873−I10874
Unrelated

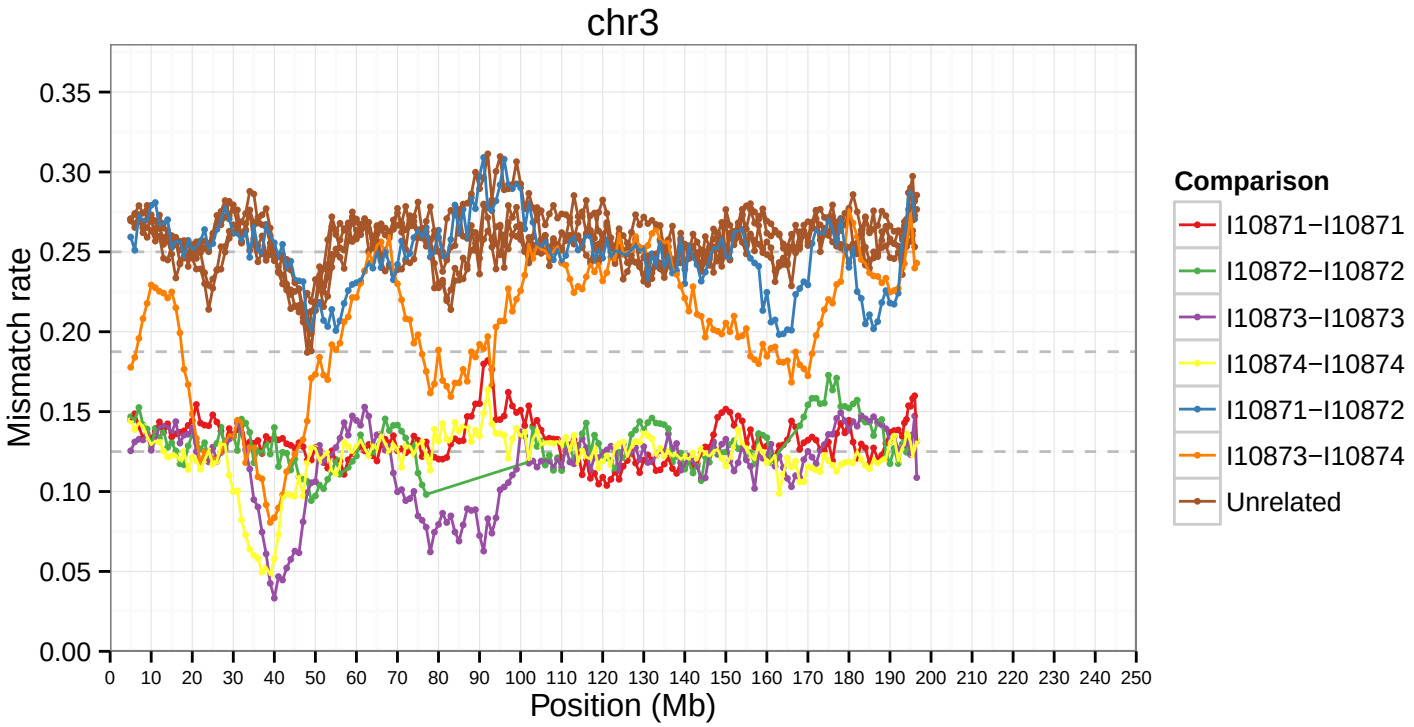
chr3
Mismatch rate
0.35
0.30
0.25
0.20
0.15
0.10
0.05
0.00
0 10 20 30 40 50 60 70 80 90 100 110 120 130 140 150 160 170 180 190 200 210 220 230 240 250
Position (Mb)
Comparison
I10871−I10871
I10872−I10872
I10873−I10873
I10874−I10874
I10871−I10872
I10873−I10874
Unrelated

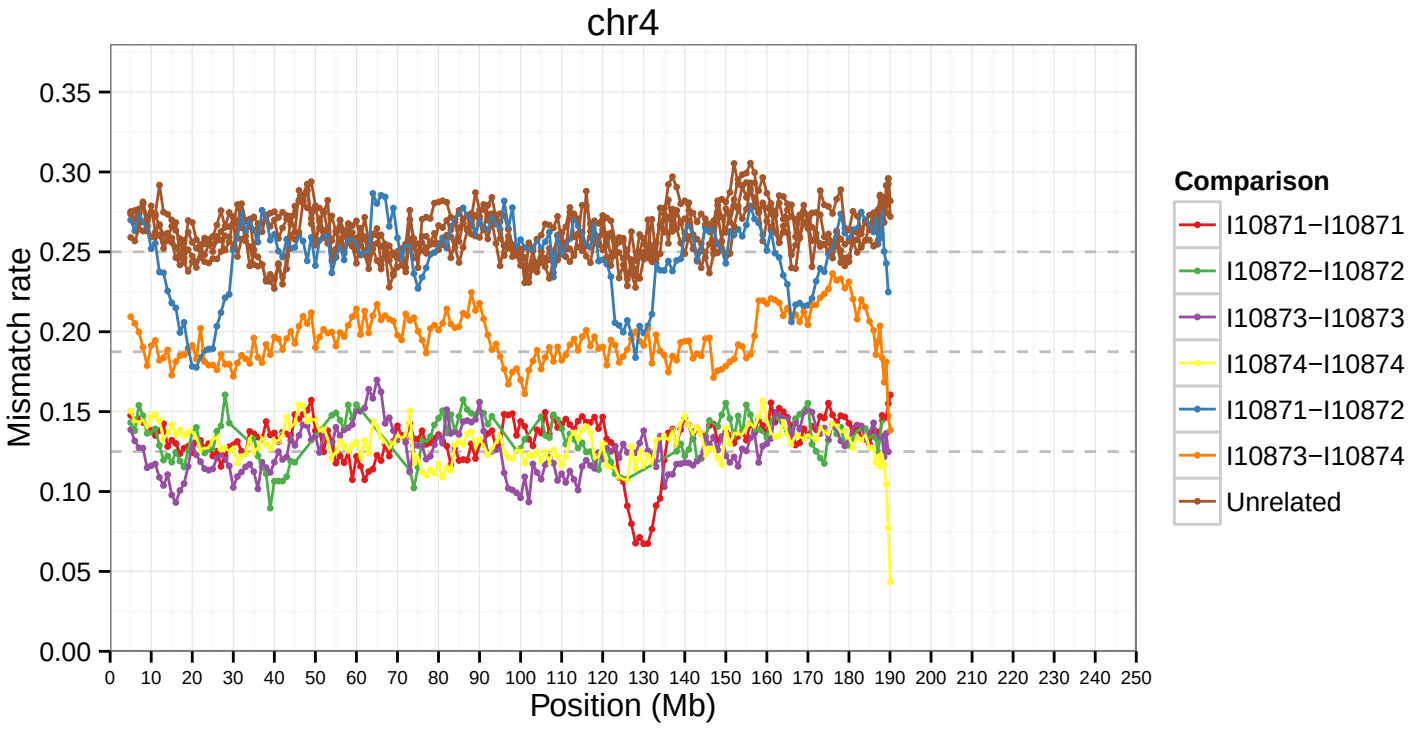
chr4
Mismatch rate
0.35
0.30
0.25
0.20
0.15
0.10
0.05
0.00
0 10 20 30 40 50 60 70 80 90 100 110 120 130 140 150 160 170 180 190 200 210 220 230 240 250
Position (Mb)
Comparison
I10871−I10871
I10872−I10872
I10873−I10873
I10874−I10874
I10871−I10872
I10873−I10874
Unrelated

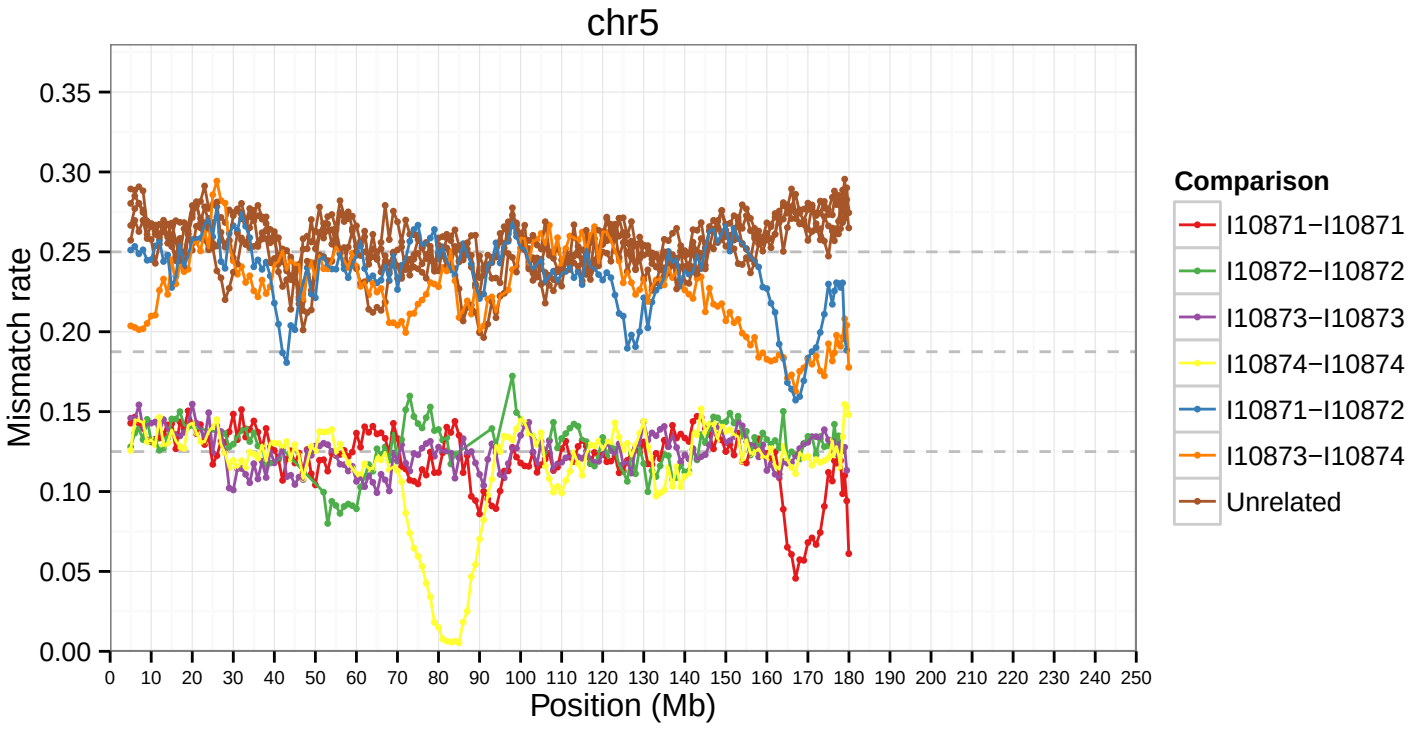
chr5
Mismatch rate
0.35
0.30
0.25
0.20
0.15
0.10
0.05
0.00
0 10 20 30 40 50 60 70 80 90 100 110 120 130 140 150 160 170 180 190 200 210 220 230 240 250
Position (Mb)
Comparison
I10871−I10871
I10872−I10872
I10873−I10873
I10874−I10874
I10871−I10872
I10873−I10874
Unrelated

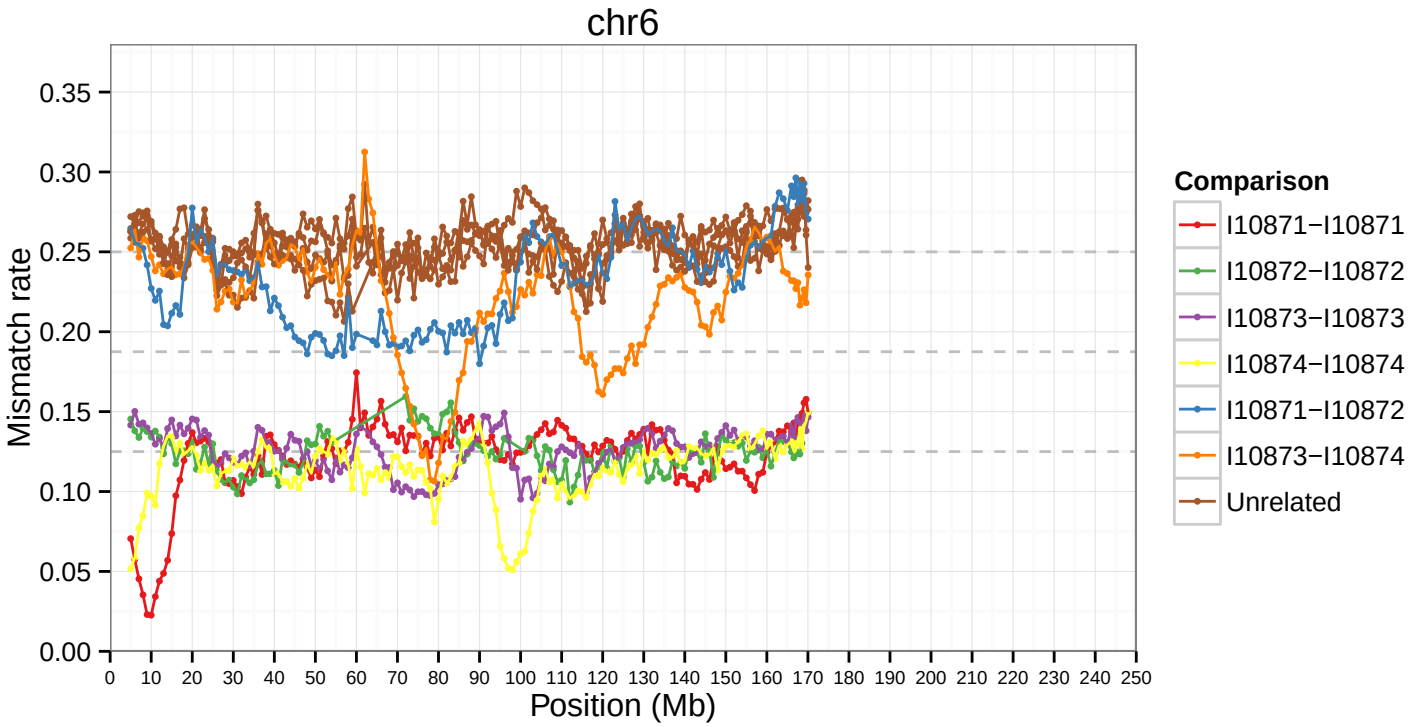
chr6
Mismatch rate
0.35
0.30
0.25
0.20
0.15
0.10
0.05
0.00
0 10 20 30 40 50 60 70 80 90 100 110 120 130 140 150 160 170 180 190 200 210 220 230 240 250
Position (Mb)
Comparison
I10871−I10871
I10872−I10872
I10873−I10873
I10874−I10874
I10871−I10872
I10873−I10874
Unrelated

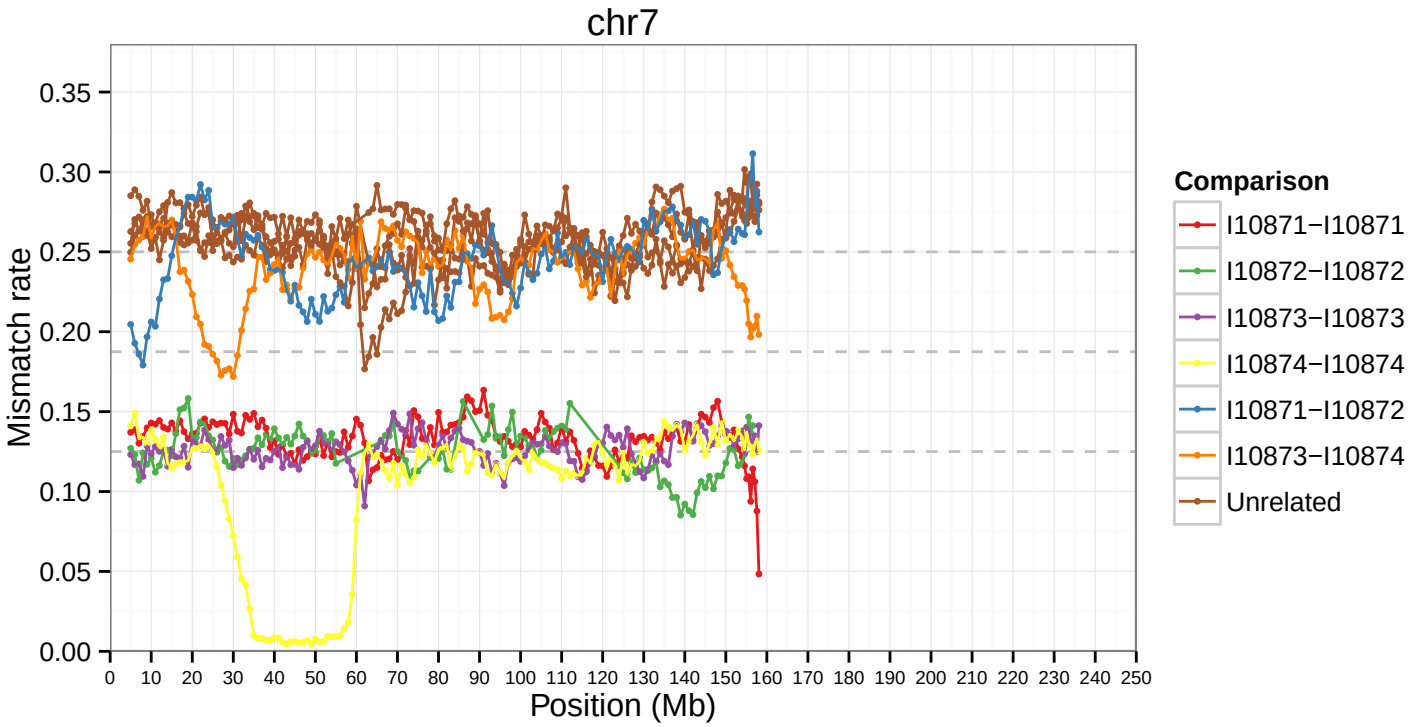
chr7
Mismatch rate
0.35
0.30
0.25
0.20
0.15
0.10
0.05
0.00
0 10 20 30 40 50 60 70 80 90 100 110 120 130 140 150 160 170 180 190 200 210 220 230 240 250
Position (Mb)
Comparison
I10871−I10871
I10872−I10872
I10873−I10873
I10874−I10874
I10871−I10872
I10873−I10874
Unrelated

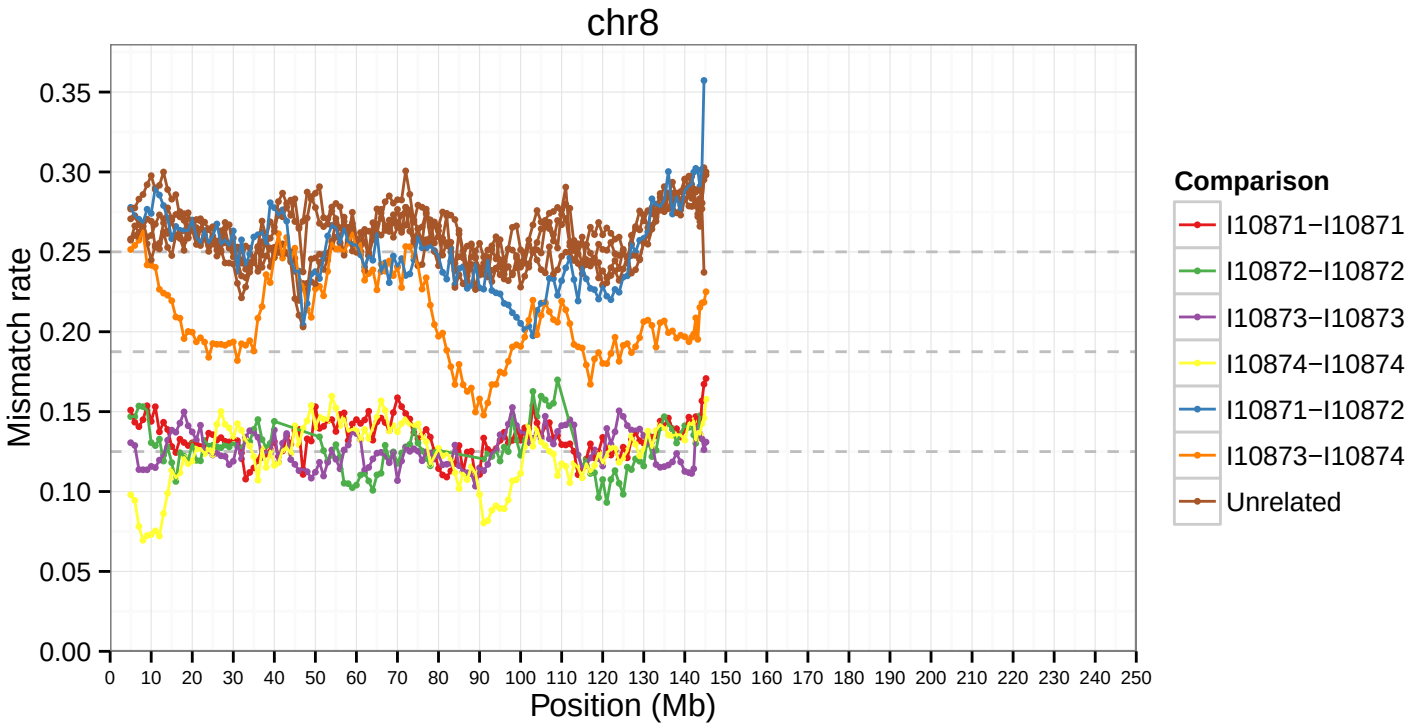
chr8
Mismatch rate
0.35
0.30
0.25
0.20
0.15
0.10
0.05
0.00
0 10 20 30 40 50 60 70 80 90 100 110 120 130 140 150 160 170 180 190 200 210 220 230 240 250
Position (Mb)
Comparison
I10871−I10871
I10872−I10872
I10873−I10873
I10874−I10874
I10871−I10872
I10873−I10874
Unrelated

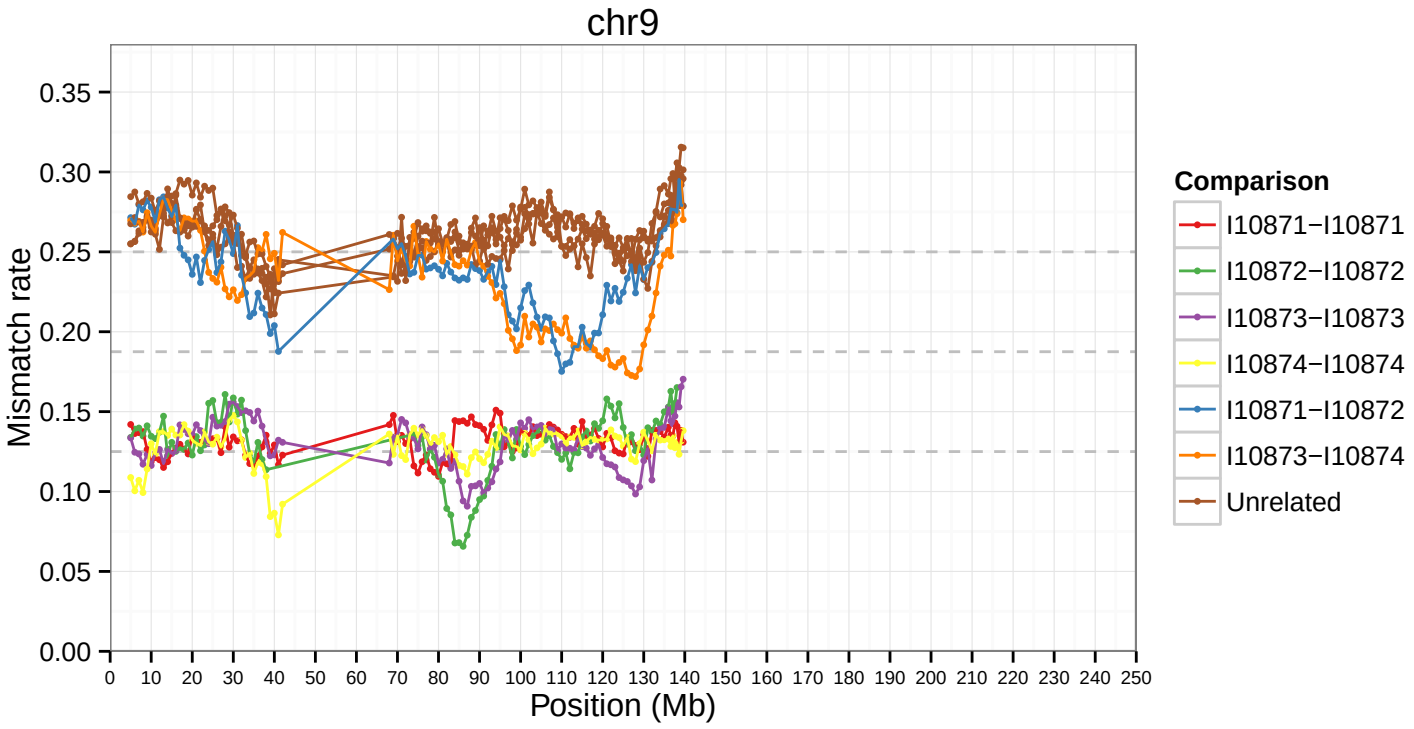
chr9
Mismatch rate
0.35
0.30
0.25
0.20
0.15
0.10
0.05
0.00
0 10 20 30 40 50 60 70 80 90 100 110 120 130 140 150 160 170 180 190 200 210 220 230 240 250
Position (Mb)
Comparison
I10871−I10871
I10872−I10872
I10873−I10873
I10874−I10874
I10871−I10872
I10873−I10874
Unrelated

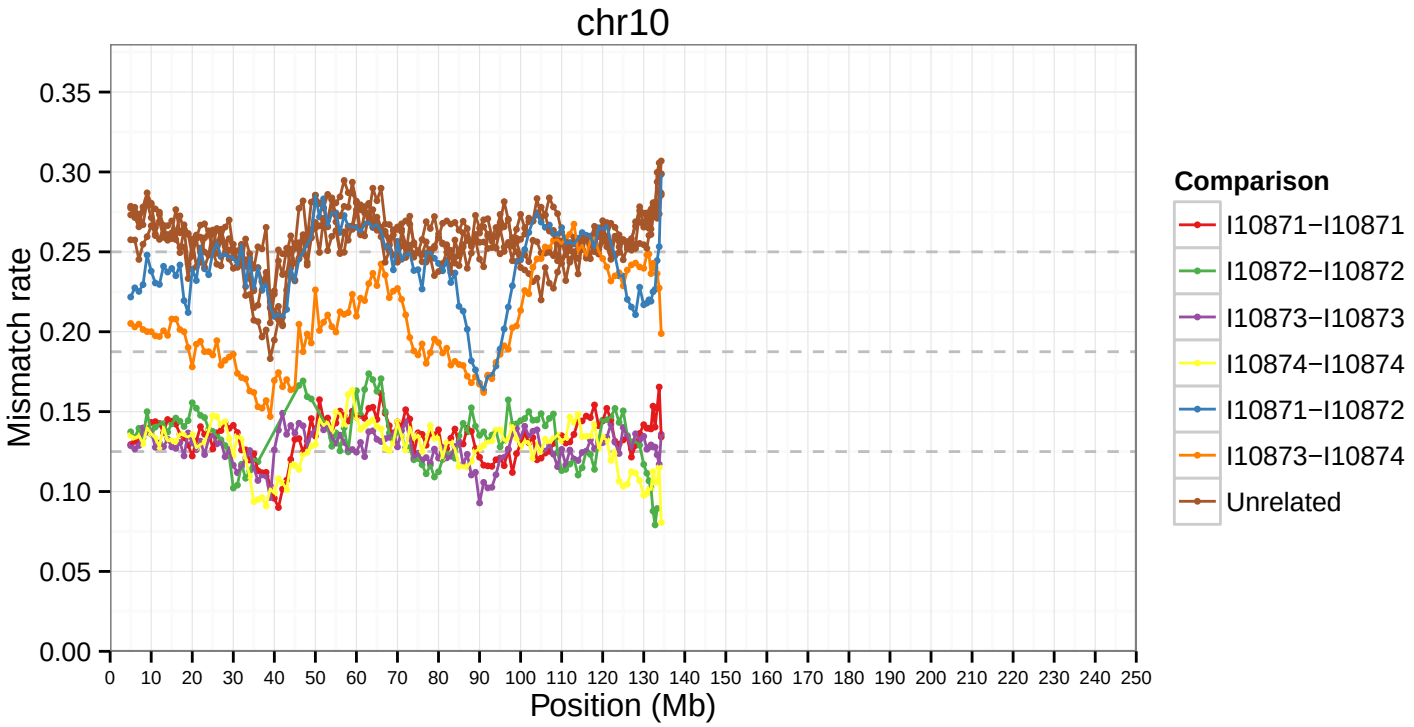
chr10
Mismatch rate
0.35
0.30
0.25
0.20
0.15
0.10
0.05
0.00
0 10 20 30 40 50 60 70 80 90 100 110 120 130 140 150 160 170 180 190 200 210 220 230 240 250
Position (Mb)
Comparison
I10871−I10871
I10872−I10872
I10873−I10873
I10874−I10874
I10871−I10872
I10873−I10874
Unrelated

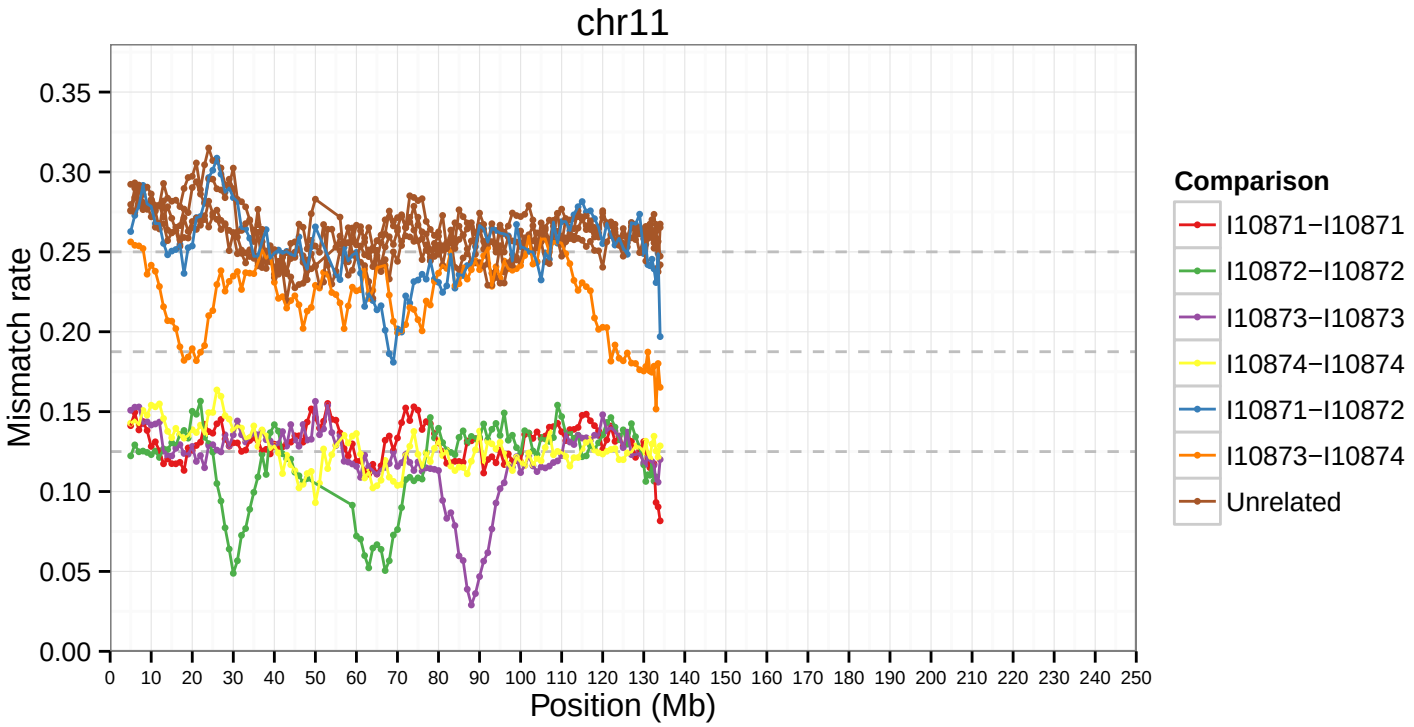
chr11
Mismatch rate
0.35
0.30
0.25
0.20
0.15
0.10
0.05
0.00
0 10 20 30 40 50 60 70 80 90 100 110 120 130 140 150 160 170 180 190 200 210 220 230 240 250
Position (Mb)
Comparison
I10871−I10871
I10872−I10872
I10873−I10873
I10874−I10874
I10871−I10872
I10873−I10874
Unrelated

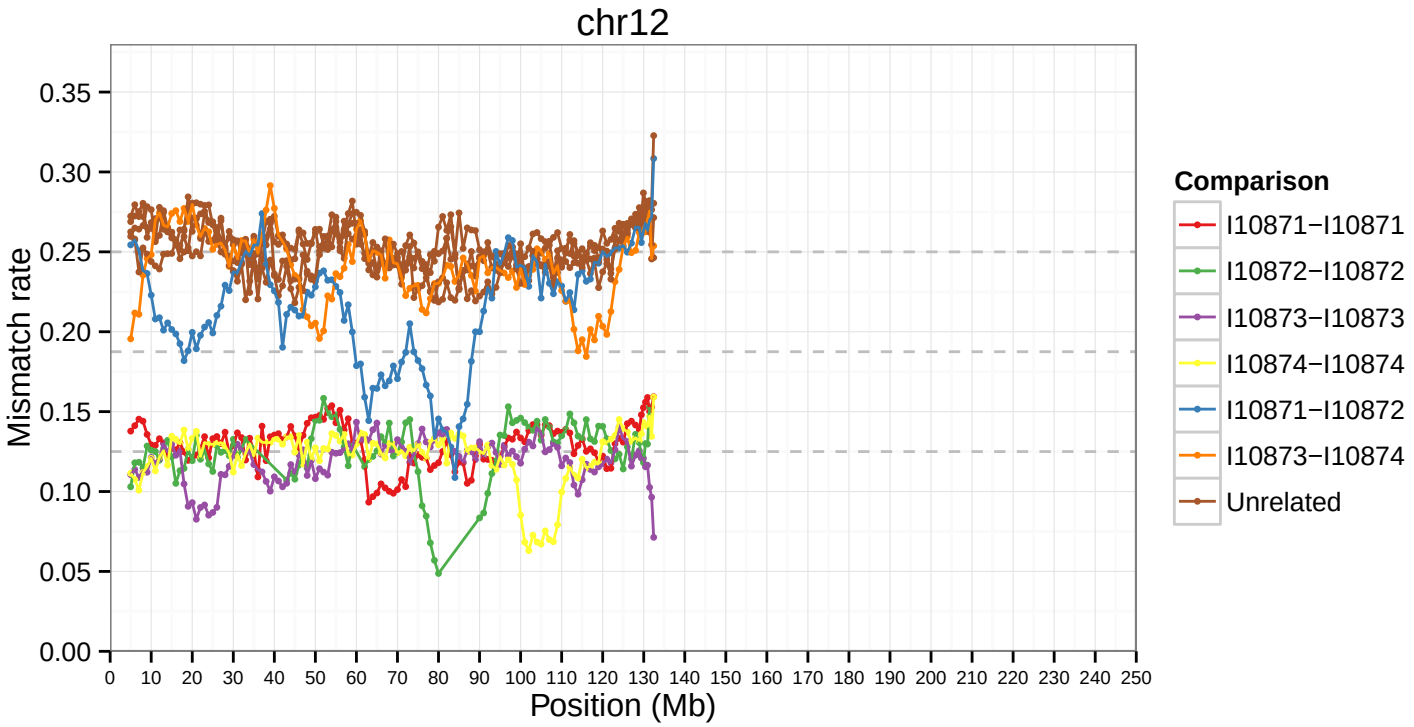
chr12
Mismatch rate
0.35
0.30
0.25
0.20
0.15
0.10
0.05
0.00
0 10 20 30 40 50 60 70 80 90 100 110 120 130 140 150 160 170 180 190 200 210 220 230 240 250
Position (Mb)
Comparison
I10871−I10871
I10872−I10872
I10873−I10873
I10874−I10874
I10871−I10872
I10873−I10874
Unrelated

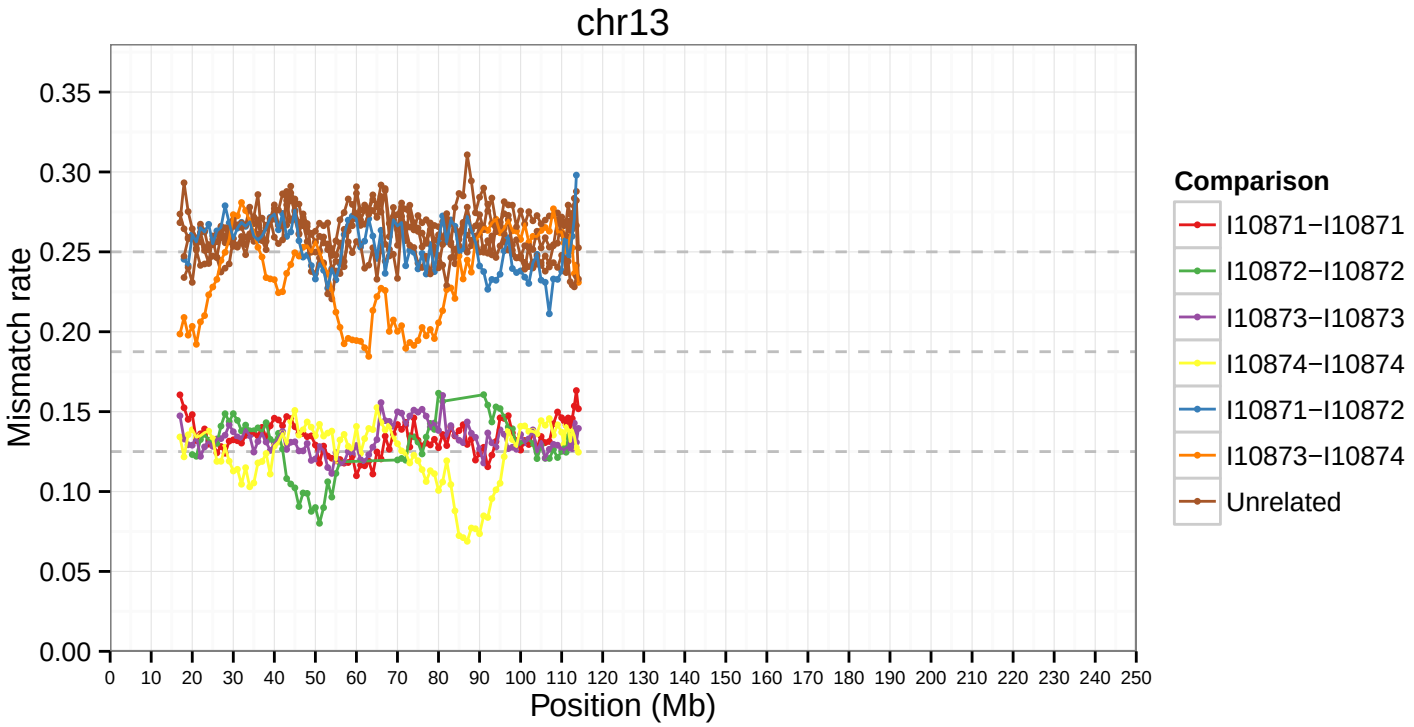
chr13
Mismatch rate
0.35
0.30
0.25
0.20
0.15
0.10
0.05
0.00
0 10 20 30 40 50 60 70 80 90 100 110 120 130 140 150 160 170 180 190 200 210 220 230 240 250
Position (Mb)
Comparison
I10871−I10871
I10872−I10872
I10873−I10873
I10874−I10874
I10871−I10872
I10873−I10874
Unrelated

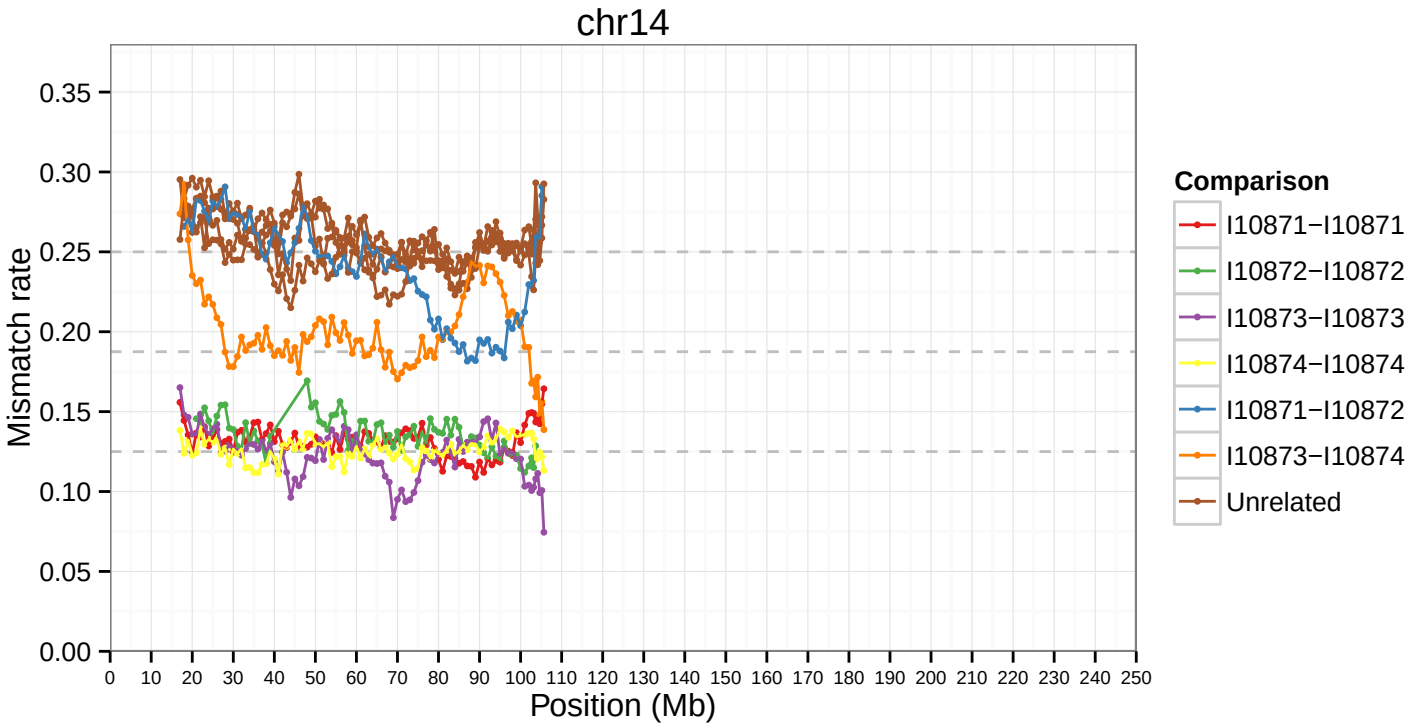
chr14
Mismatch rate
0.35
0.30
0.25
0.20
0.15
0.10
0.05
0.00
0 10 20 30 40 50 60 70 80 90 100 110 120 130 140 150 160 170 180 190 200 210 220 230 240 250
Position (Mb)
Comparison
I10871−I10871
I10872−I10872
I10873−I10873
I10874−I10874
I10871−I10872
I10873−I10874
Unrelated

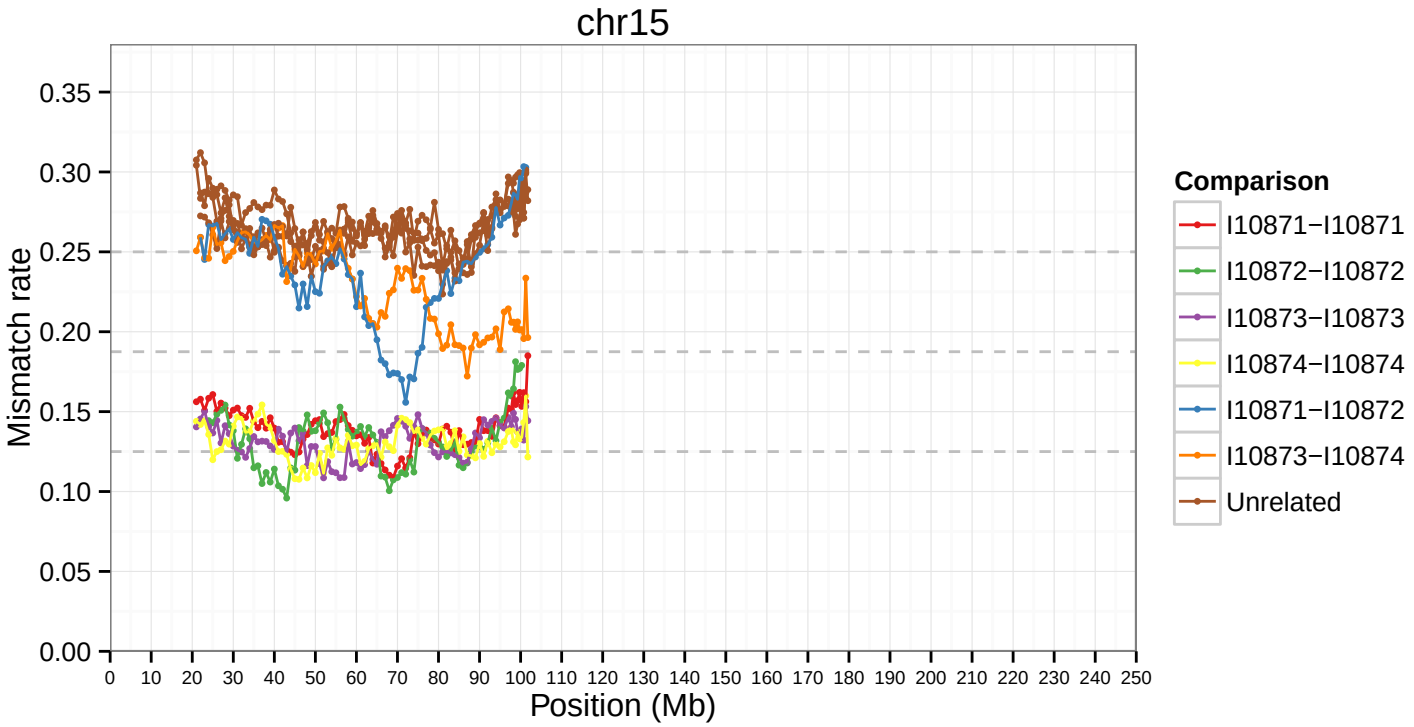
chr15
Mismatch rate
0.35
0.30
0.25
0.20
0.15
0.10
0.05
0.00
0 10 20 30 40 50 60 70 80 90 100 110 120 130 140 150 160 170 180 190 200 210 220 230 240 250
Position (Mb)
Comparison
I10871−I10871
I10872−I10872
I10873−I10873
I10874−I10874
I10871−I10872
I10873−I10874
Unrelated

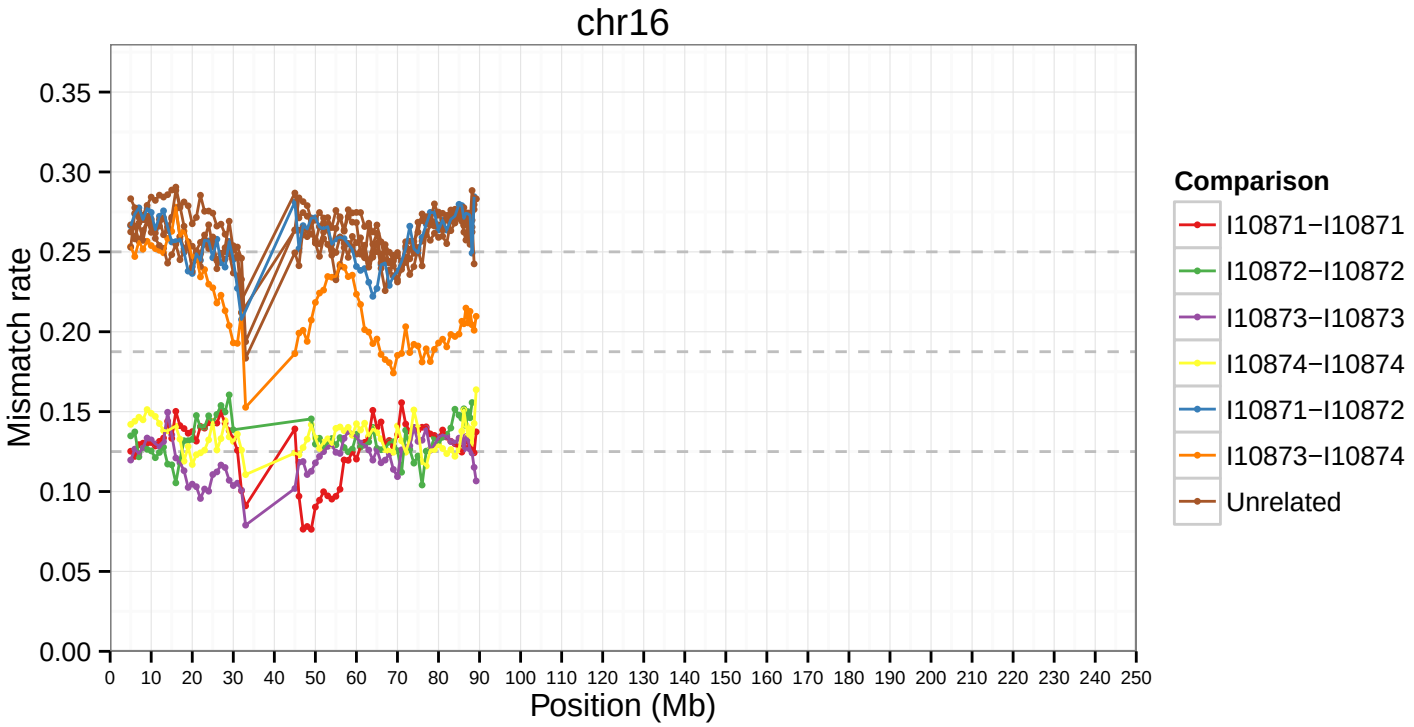
chr16
Mismatch rate
0.35
0.30
0.25
0.20
0.15
0.10
0.05
0.00
0 10 20 30 40 50 60 70 80 90 100 110 120 130 140 150 160 170 180 190 200 210 220 230 240 250
Position (Mb)
Comparison
I10871−I10871
I10872−I10872
I10873−I10873
I10874−I10874
I10871−I10872
I10873−I10874
Unrelated

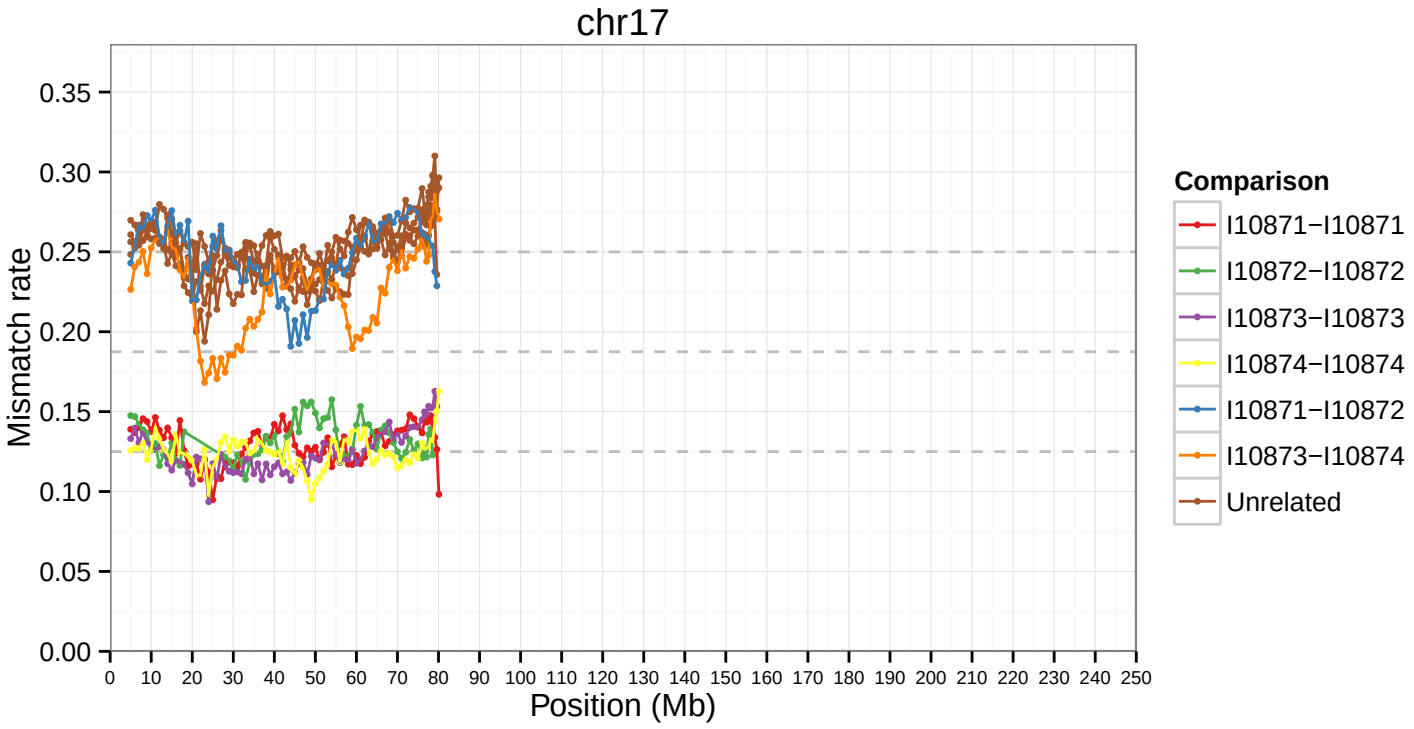
chr17
Mismatch rate
0.35
0.30
0.25
0.20
0.15
0.10
0.05
0.00
0 10 20 30 40 50 60 70 80 90 100 110 120 130 140 150 160 170 180 190 200 210 220 230 240 250
Position (Mb)
Comparison
I10871−I10871
I10872−I10872
I10873−I10873
I10874−I10874
I10871−I10872
I10873−I10874
Unrelated

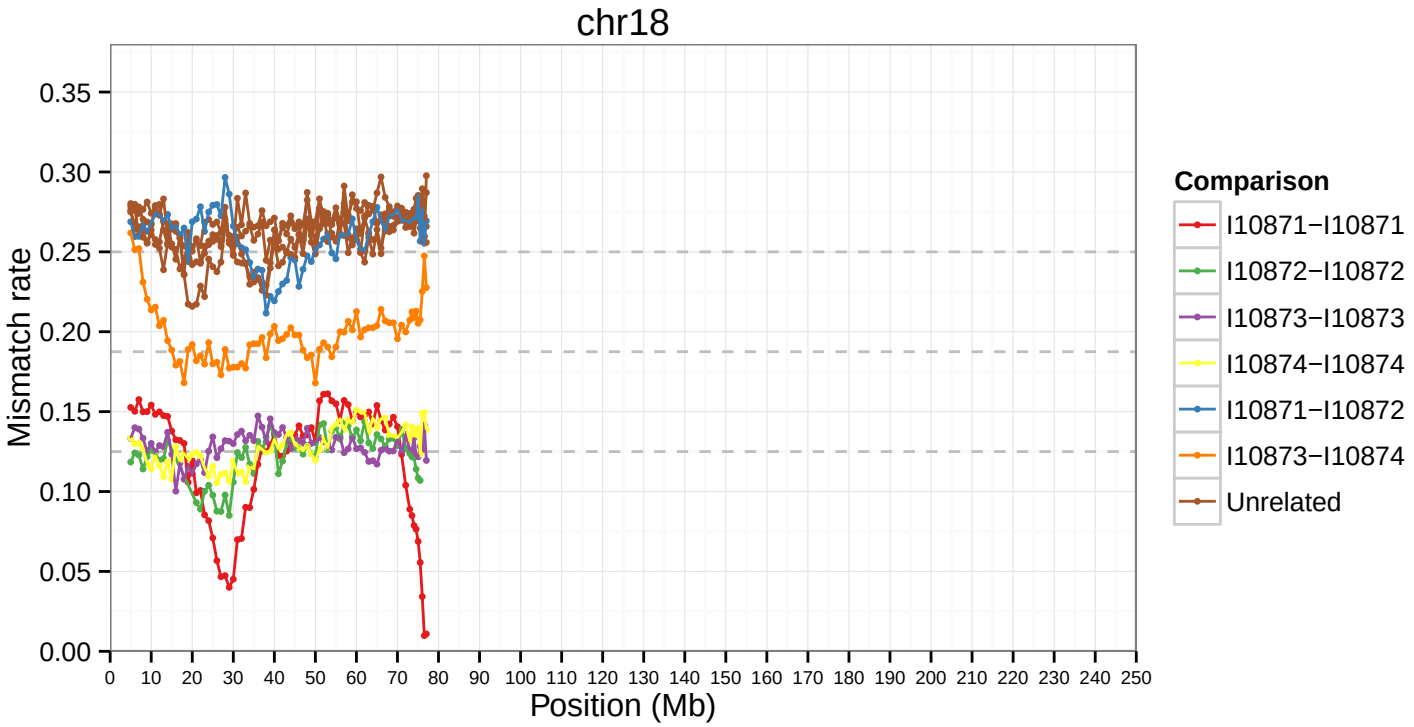
chr18
Mismatch rate
0.35
0.30
0.25
0.20
0.15
0.10
0.05
0.00
0 10 20 30 40 50 60 70 80 90 100 110 120 130 140 150 160 170 180 190 200 210 220 230 240 250
Position (Mb)
Comparison
I10871−I10871
I10872−I10872
I10873−I10873
I10874−I10874
I10871−I10872
I10873−I10874
Unrelated

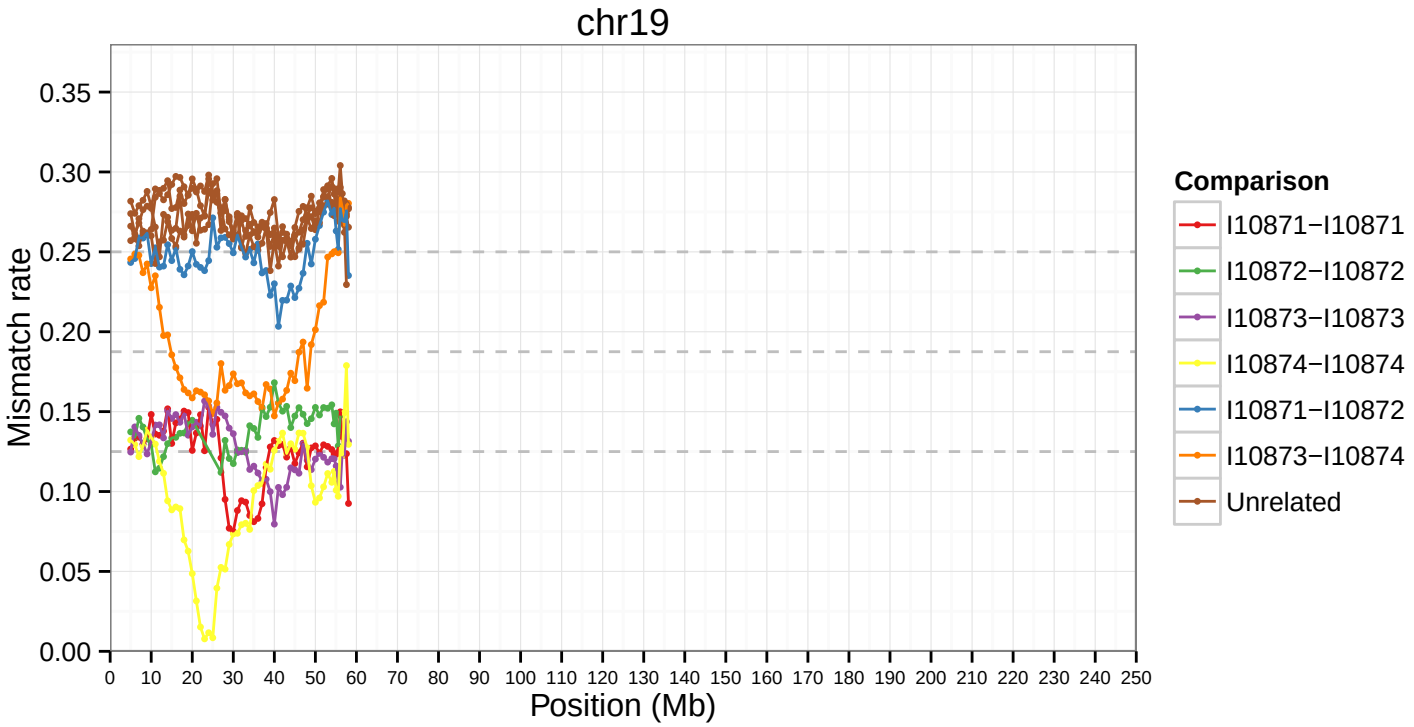
chr19
Mismatch rate
0.35
0.30
0.25
0.20
0.15
0.10
0.05
0.00
0 10 20 30 40 50 60 70 80 90 100 110 120 130 140 150 160 170 180 190 200 210 220 230 240 250
Position (Mb)
Comparison
I10871−I10871
I10872−I10872
I10873−I10873
I10874−I10874
I10871−I10872
I10873−I10874
Unrelated

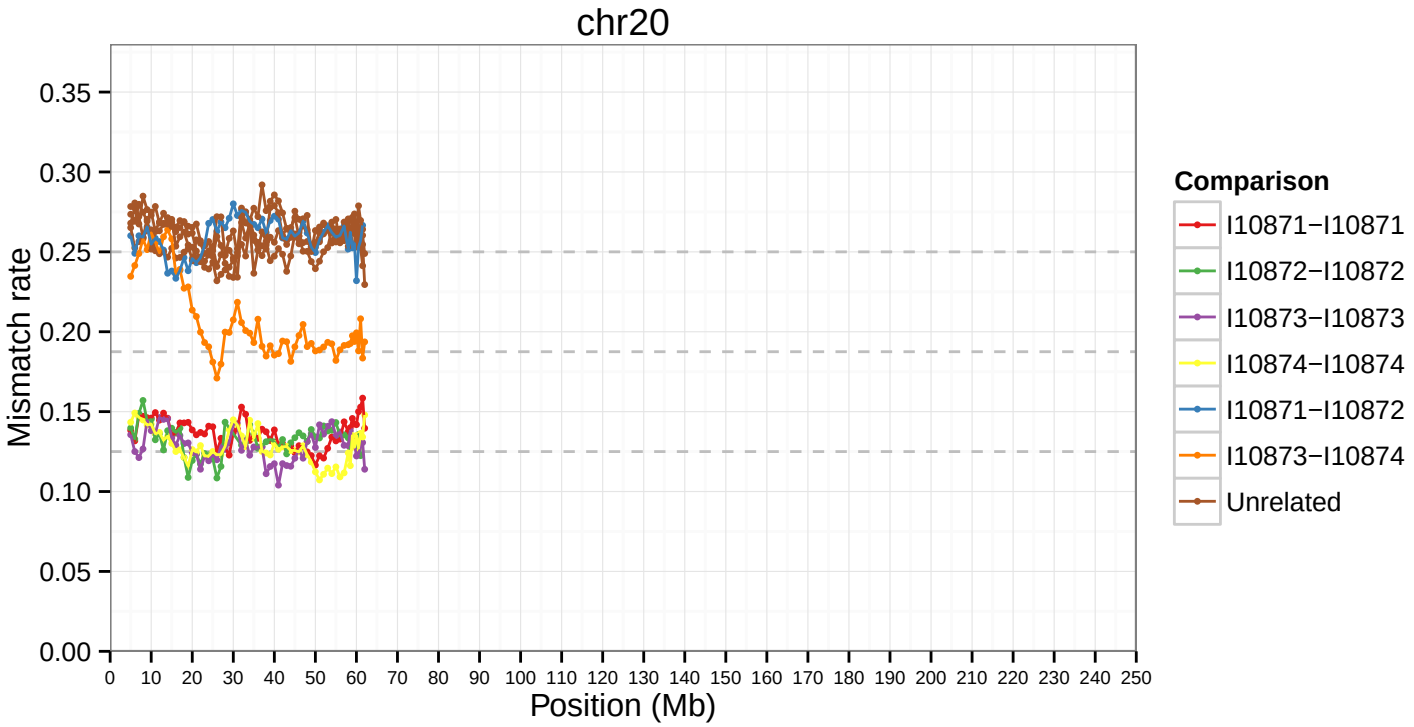
chr20
Mismatch rate
0.35
0.30
0.25
0.20
0.15
0.10
0.05
0.00
0 10 20 30 40 50 60 70 80 90 100 110 120 130 140 150 160 170 180 190 200 210 220 230 240 250
Position (Mb)
Comparison
I10871−I10871
I10872−I10872
I10873−I10873
I10874−I10874
I10871−I10872
I10873−I10874
Unrelated

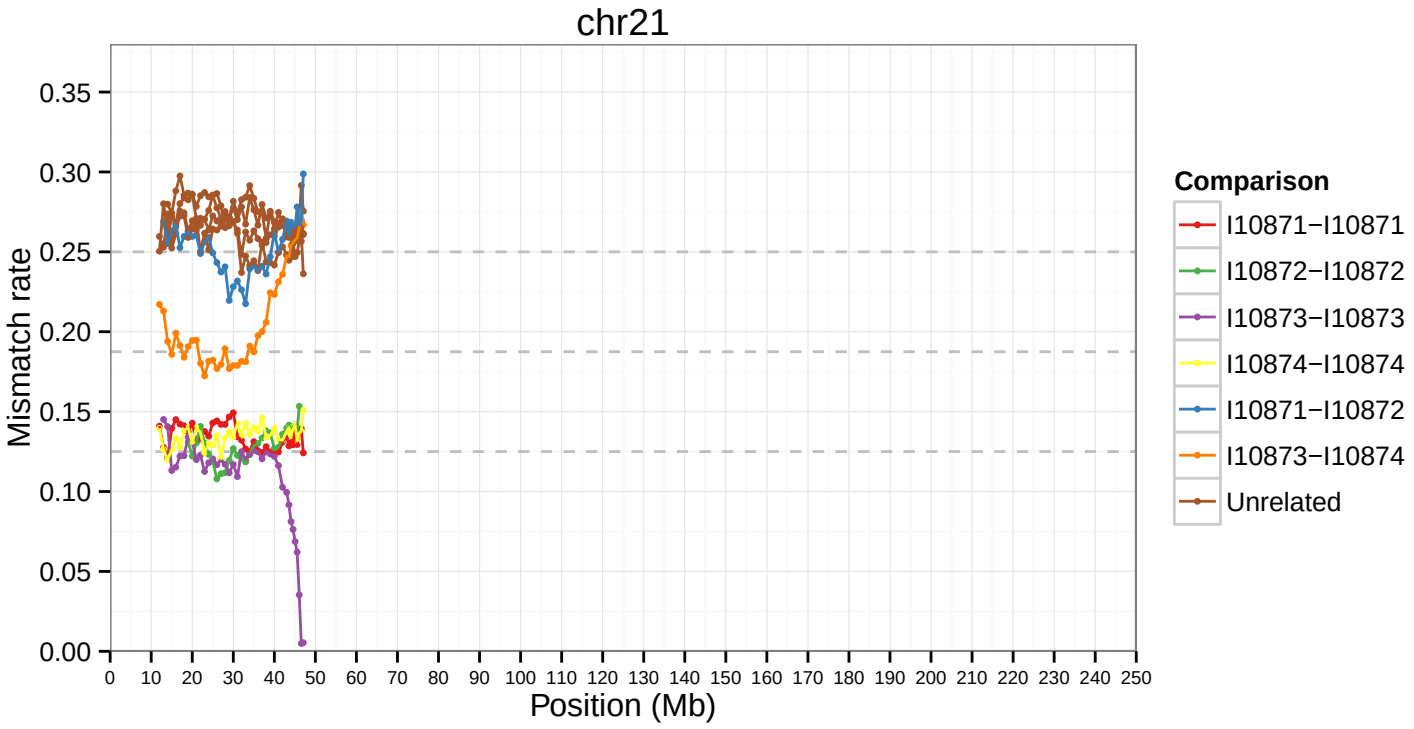
chr21
Mismatch rate
0.35
0.30
0.25
0.20
0.15
0.10
0.05
0.00
0 10 20 30 40 50 60 70 80 90 100 110 120 130 140 150 160 170 180 190 200 210 220 230 240 250
Position (Mb)
Comparison
I10871−I10871
I10872−I10872
I10873−I10873
I10874−I10874
I10871−I10872
I10873−I10874
Unrelated

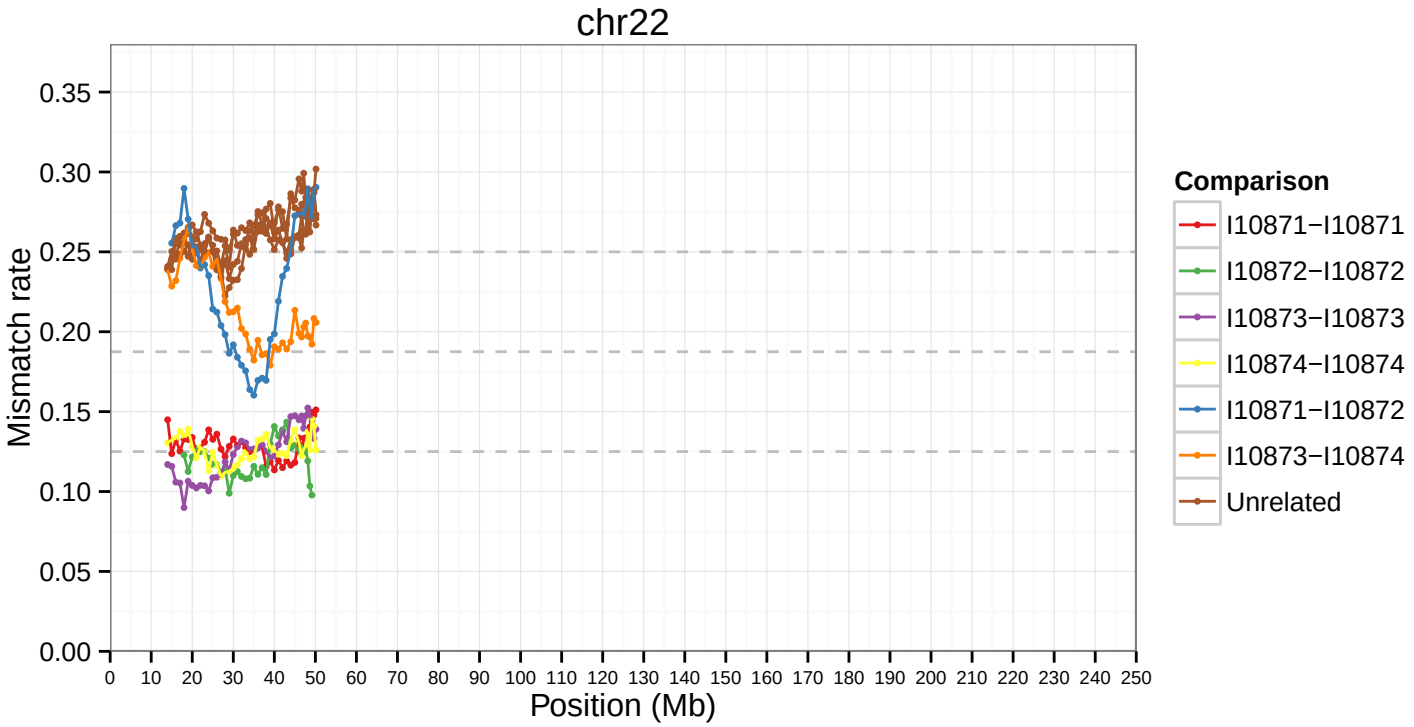
chr22
Mismatch rate
0.35
0.30
0.25
0.20
0.15
0.10
0.05
0.00
0 10 20 30 40 50 60 70 80 90 100 110 120 130 140 150 160 170 180 190 200 210 220 230 240 250
Position (Mb)
Comparison
I10871−I10871
I10872−I10872
I10873−I10873
I10874−I10874
I10871−I10872
I10873−I10874
Unrelated

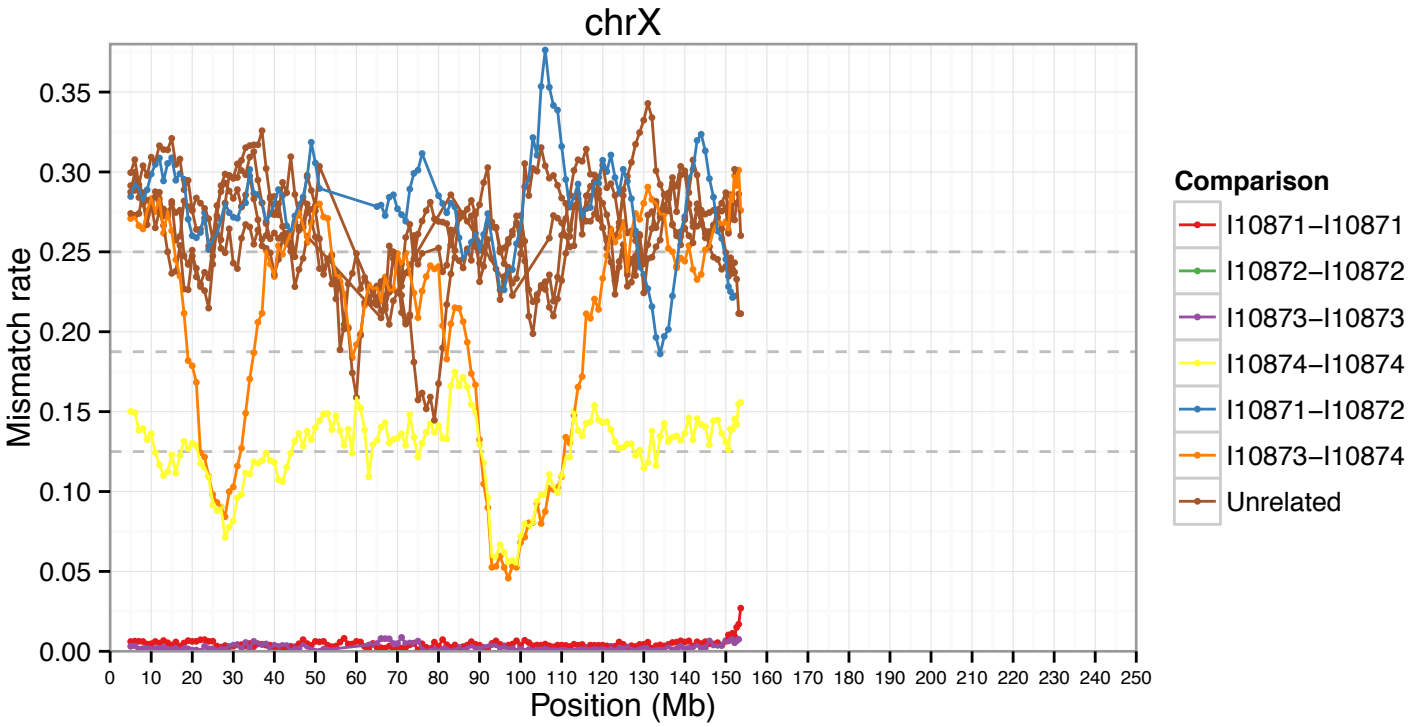
chrX
Mismatch rate
0.35
0.30
0.25
0.20
0.15
0.10
0.05
0.00
0 10 20 30 40 50 60 70 80 90 100 110 120 130 140 150 160 170 180 190 200 210 220 230 240 250
Position (Mb)
Comparison
I10871–I10871
I10872–I10872
I10873–I10873
I10874–I10874
I10871–I10872
I10873–I10874
Unrelated

Supplementary Information section 3: Alternative admixture graph model versions

Here we present the full results of all versions of our admixture graph model, differing in the exact set of populations included, the set of SNPs used, or both. Fitting the extra models serves two purposes: first, we can learn about the relationships among more populations without needing to fit an impractical number simultaneously, and second, we can evaluate the robustness and stability of our results. Inferred values of key parameters across the model versions are also summarized in Extended Data Table 3.

As discussed in Methods, the ADMIXTUREGRAPH (qpGraph) software optimizes admixture graph parameters given a user-specified model topology. In other words, the input for each run contains the tree topology (including positions of admixture events), and the output provides best-fitting branch lengths and mixture proportions. Not all possible split orders need to be tested separately, however, because the results can be used iteratively to determine optimal arrangements. For example, if populations A and B form a (true) clade with C as an outgroup, and the program is run with A and C specified as a clade instead, then the branch separating B from (A, C) will collapse to length zero, indicating that the order should be changed.

In cases where three or more populations diverge (truly) in short succession, internal branches will be short, with the consequence that the inferred split patterns can sometimes be uncertain. The two key radiation points we highlight in our model (labels 1 and 2 in Fig. 4A) are examples of this phenomenon. As an illustration, we determined the optimal ordering among the early modern human splits in each of our alternative model versions, but for simplicity, we retained a constant order for the splits of East African-related lineages. We note that in the alternative (three-component) admixture model for Shum Laka, the topology of the West African clade is in fact not optimal, as the fit is improved by placing the Shum Laka source outside the main portion of the clade, but the improvement is minimal (as compared to a $Z = 7.1$ residual in our primary two-component model).

For mixture proportions, the resolution of our inferences varies depending on the level of constraint present in the model. As a general rule, in order to estimate the value of a mixture proportion parameter, it is necessary to have four other populations present in the graph with different phylogenetic positions relative to the admixture event in question, as in an f_4-ratio test [*73*]. With only three such populations available, it is possible to see the evidence of the admixture in the model fit, but the mixture proportion is not well constrained and is confounded with a specific branch length parameter. We also note that this rule is not binary; if two of the four references occupy only slightly different positions, or if one or more of the four are themselves admixed, then the level of constraint can be intermediate. In our model, the proportions that are relatively weakly constrained are marked with asterisks in Fig. 4A (see also Extended Data Table 3).

Our model was constructed in practice by combining results from smaller admixture graphs with external evidence of admixture (e.g., PCA, f-statistics, and results from previous studies). Two examples of sub-graphs can be seen in Figs. S3.24 and S3.25. At each stage, after opti-

mizing the population split order, we examine the list of residual statistics in the model (i.e., pairs, triples, or quartets of populations whose relationships are not well captured by the current graph) to evaluate any possible additional signals of admixture. Ultimately, of course, much of the value of the admixture graph framework comes from the ability to test proposed admixture events simultaneously in the context of a multi-population model, and simpler models that fit successfully can sometimes be rejected when new populations are incorporated. Thus, the fitting process is not a simple linear progression of adding one population at a time, and the final evaluation of the fit is the most important step.

The majority of the admixture events in our model involve a combination of ancestry derived from the early modern human split cluster (point 1 in Fig. 4A) and ancestry related to East or West Africans. The justification for these events can be seen most clearly in the statistics shown in Fig. 3A and Extended Data Table 2, which provide evidence for different proportions of deep ancestry in different populations. In our admixture graph, we can model ancient South African hunter-gatherers as unadmixed, Mbuti and Aka with admixture from a Bantu-associated source (and Mbuti as well from an East African-related source), and Shum Laka with admixture from a basal West African source. (We note that we computed f_3-statistics for Shum Laka as the test population and did not observe any negative values, which is likely due to the lack of an unadmixed reference population from the Central African hunter-gatherer lineage and/or post-admixture drift in the Shum Laka ancestral population.) As discussed in the main text, we also infer the presence of "ghost" deep modern human ancestry in Mota and in all West African-related populations, the latter with a small proportion of archaic ancestry as well in our primary model. All of these signals of differential deep ancestry would cause significant deviations between the model and the data if not accounted for (i.e., they are associated with significantly nonzero f_4-statistics, as in Fig. 3A), and the model presented (along with the alternative deep source version for West Africans) provides a parsimonious set of admixture events to explain them. Together with Neanderthal admixture into non-Africans and non-African-related and Mota-related ancestry in Agaw, these admixture events comprise a sufficient collection to explain all observed two-, three-, and four-way population relationships (to within 2.3 standard errors in our primary model).

Lastly, we note that when comparing different models built for the same set of populations and SNPs (e.g., the alternative deep source for West Africans), we can evaluate their relative support through the fit score (an approximate log-likelihood) provided by the qpGraph program. Broadly speaking, models with higher likelihood are preferable, and more complex models (for example, with an additional admixture event) need even higher likelihoods given their extra free parameters. These comparisons can in principle be thought of within an AIC/BIC framework, but we treat exact model score differences with caution, as the number of free parameters or implicit hypothesis tests between two models can be difficult to define. Taking the example of adding a new admixture event, in some situations the source could be allowed to range over the entire graph, whereas in others it might be determined *a priori* to be derived from a particular lineage already present in the model. Using AIC, a model with two additional degrees of freedom (here, one new source position parameter and one mixture proportion) would be preferred

if its log-likelihood is at least 2 units superior (with the strength of preference determined by the exact score difference), but in light of the above caveat, our qualitative approach is to consider models to be roughly equivalent if their fit scores are within a few units of each other and neither has highly significant residual f-statistics.

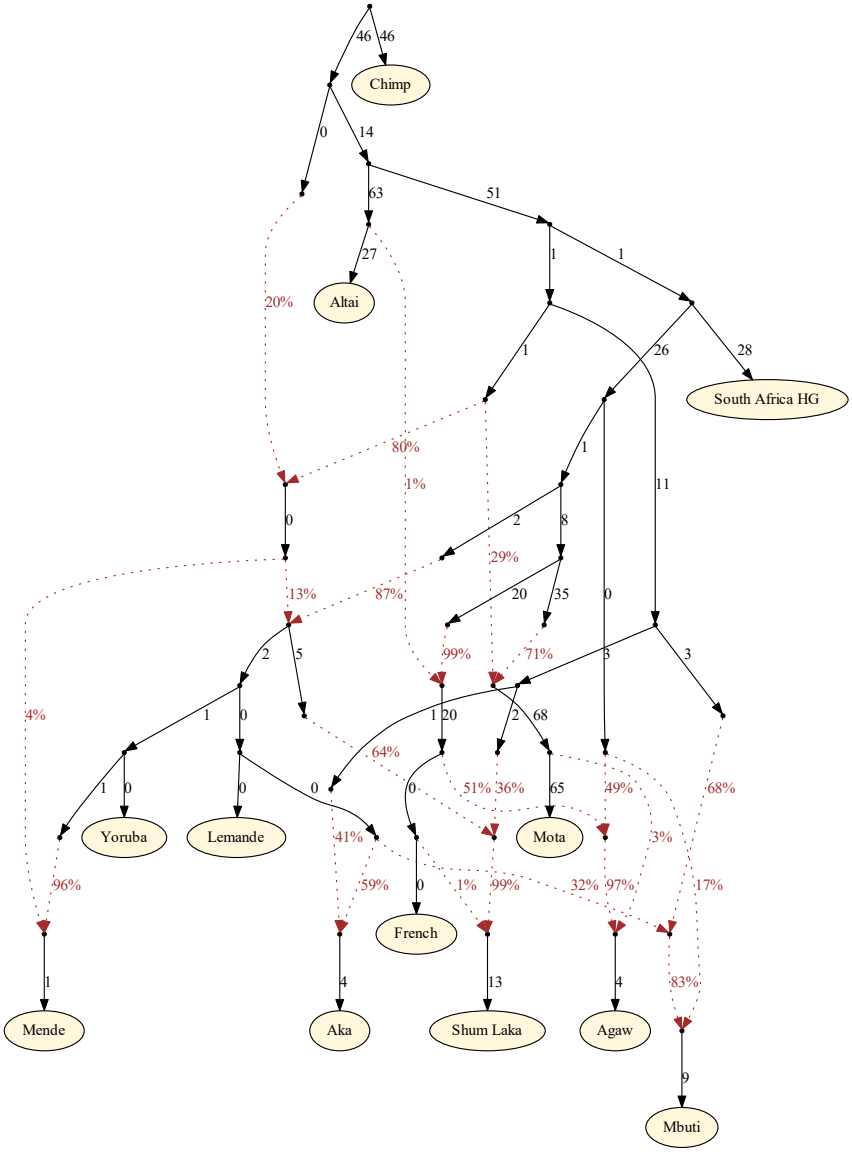

Figure S3.1. Primary inferred admixture graph with full parameters shown (same as Extended Data Fig. 4). Of the ∼1.2M targeted SNPs, 932k are used for fitting (i.e., are covered by all populations in the model). Branch lengths (in units of squared allele frequency divergence) are rounded to the nearest integer. All f-statistics relating the populations are predicted to within 2.3 standard errors of their observed values.

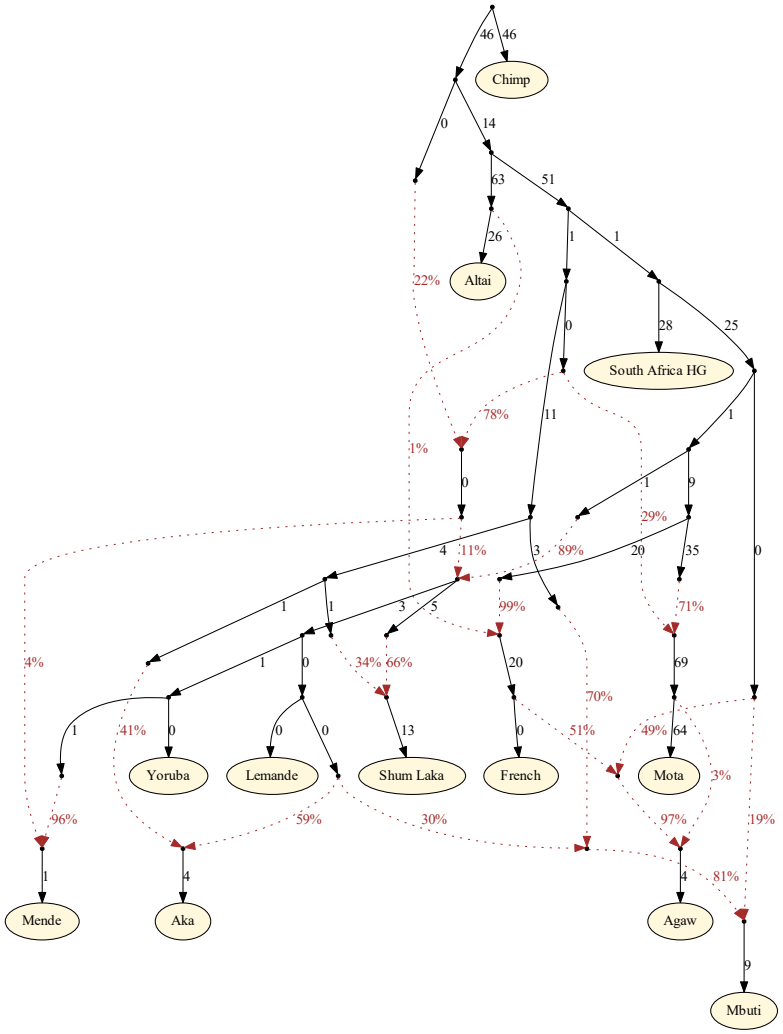

Figure S3.2. Admixture graph with no "dummy" non-African-related admixture into Shum Laka (932k SNPs covered). Branch lengths (in units of squared allele frequency divergence) are rounded to the nearest integer. All f-statistics relating the populations are predicted to within 2.5 standard errors of their observed values, and to within 2.3 standard errors for statistics not involving Shum Laka and French together (four such statistics having $2.2 \leq Z \leq 2.5$). Parameter estimates are almost identical to the primary version with non-African-related admixture into Shum Laka (intended to account for $\sim$1% contamination).

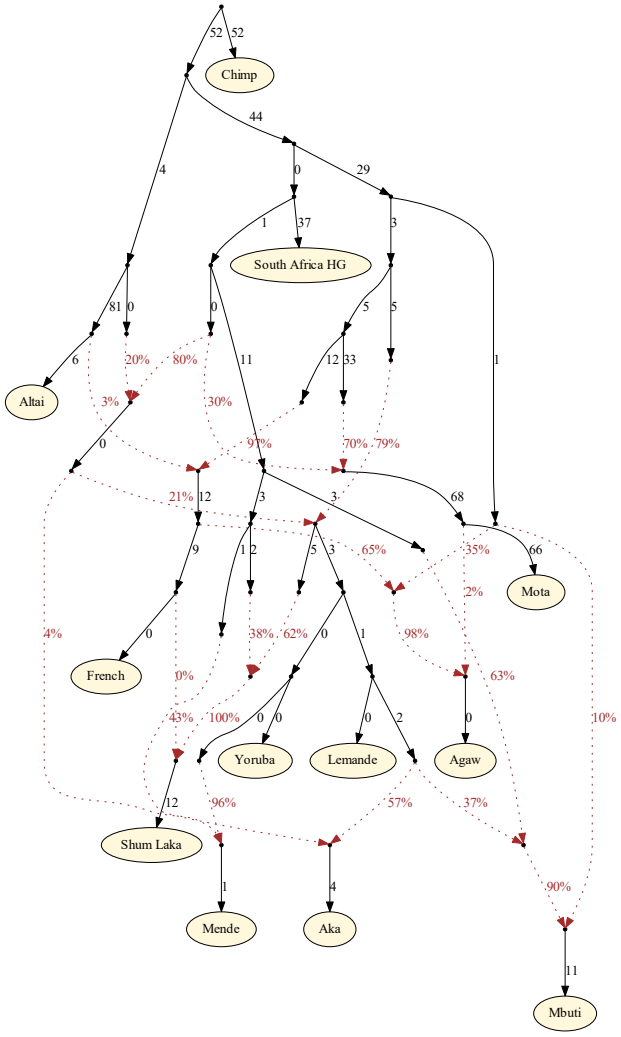

Figure S3.3. Admixture graph fit using only panels 4 and 5 of the Human Origins array (SNPs ascertained as heterozygous in Yoruba and Khoesan individuals; 211k SNPs covered). Branch lengths (in units of squared allele frequency divergence) are rounded to the nearest integer. All f-statistics relating the populations are predicted to within 2.5 standard errors of their observed values. The archaic source contributing to West Africans is inferred to be (slightly) on the Neanderthal lineage, and the southern African and Central African hunter-gatherer lineages are inferred to split almost simultaneously.

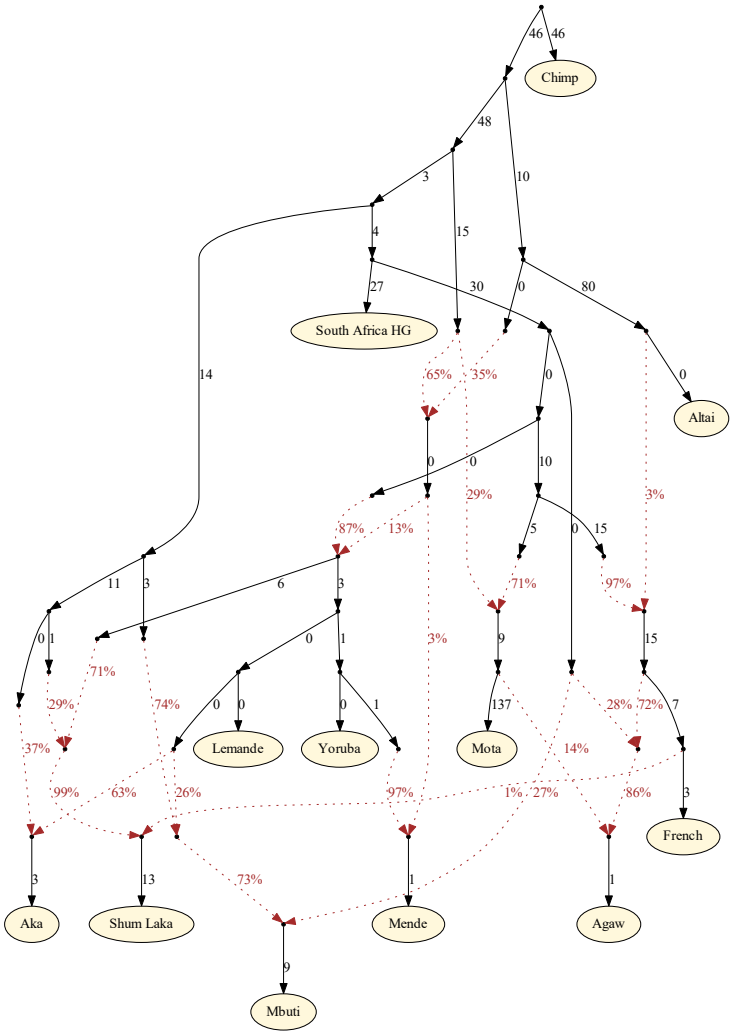

Figure S3.4. Admixture graph fit using only transversions (181 SNPs covered). Branch lengths (in units of squared allele frequency divergence) are rounded to the nearest integer. All f-statistics relating the populations are predicted to within 2.4 standard errors of their observed values. The archaic source contributing to West Africans is inferred to be (slightly) on the Neanderthal lineage, and the deep modern human admixture source is inferred to split (slightly) before the Central African hunter-gatherer lineage.

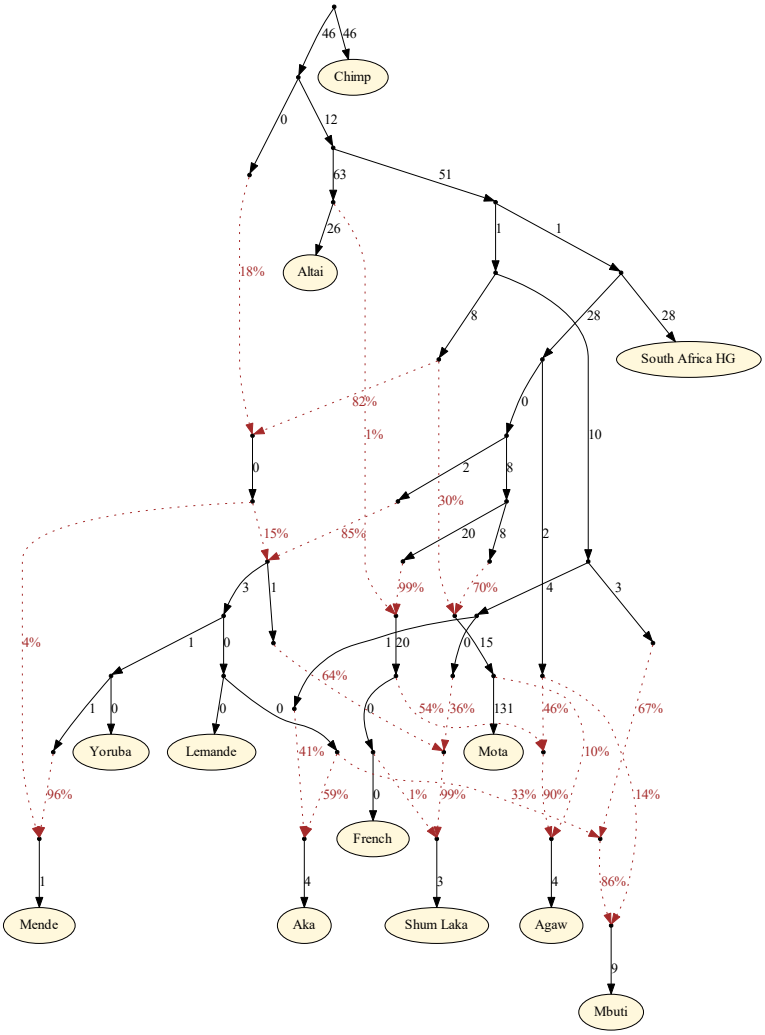

Figure S3.5. Admixture graph with whole-genome sequence data for individuals 2/SE II and 4/A to represent Shum Laka. Of the ∼1.2M targeted SNPs, 986k are covered. Branch lengths (in units of squared allele frequency divergence) are rounded to the nearest integer. All f-statistics relating the populations are predicted to within 2.5 standard errors of their observed values.

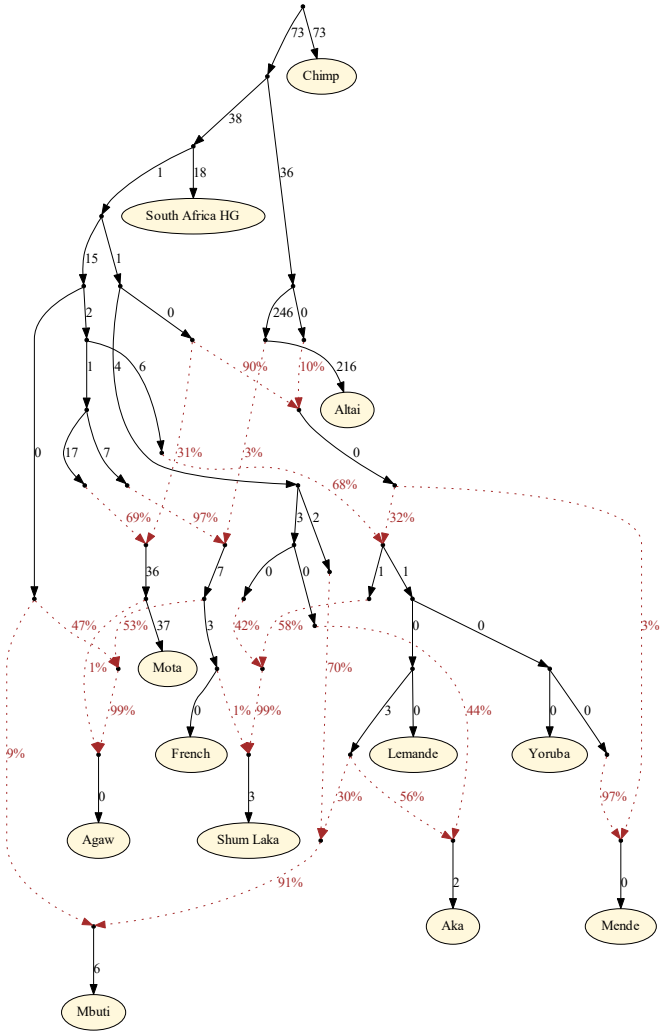

Figure S3.6. Admixture graph fit using a set of transversions ascertained as having one derived and one ancestral allele when sampling one allele at random from each of Altai Neanderthal and Denisova (336k SNPs covered). Shum Laka is represented by shotgun data for individuals 2/SE II and 4/A. Branch lengths (in units of squared allele frequency divergence) are rounded to the nearest integer. All f-statistics relating the populations are predicted to within 2.6 standard errors of their observed values. The archaic source contributing to West Africans is inferred to be on the Neanderthal lineage, and the southern African hunter-gatherer lineage is inferred to split (slightly) before the Central African hunter-gatherer lineage.

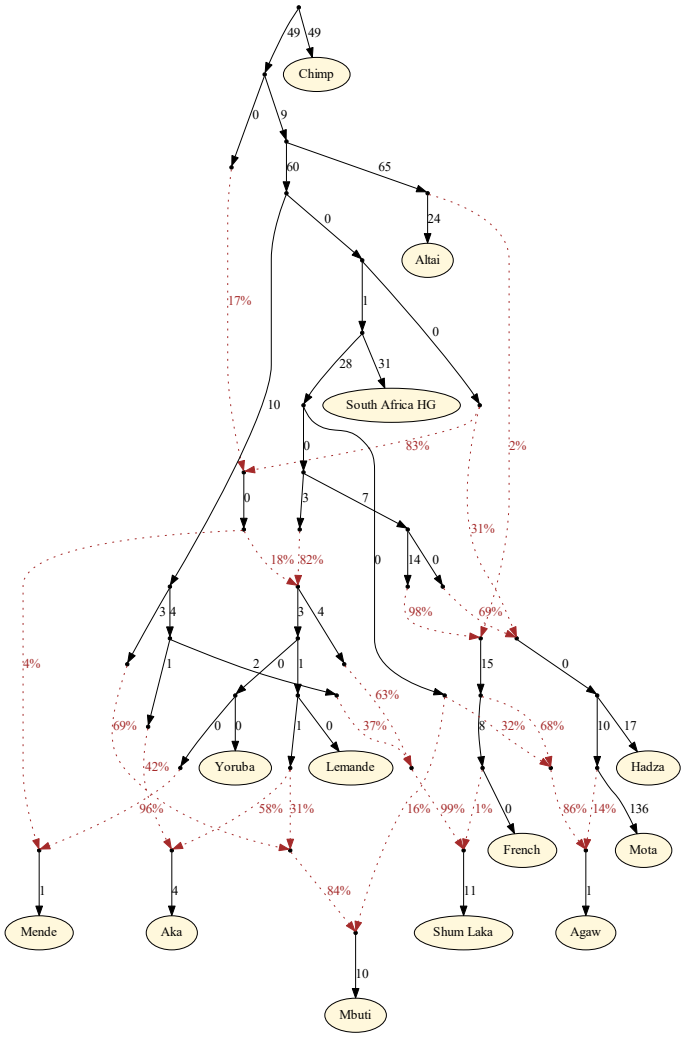

Figure S3.7. Admixture graph with Hadza added, using SNPs from the Human Origins array (497k covered). Branch lengths (in units of squared allele frequency divergence) are rounded to the nearest integer. All f-statistics relating the populations are predicted to within 2.9 standard errors of their observed values. Hadza is inferred to fit well as a clade with Mota, sharing the same deep admixture ($\sim$30%). The deep modern human admixture source is inferred to split (slightly) before the Central African hunter-gatherer lineage.

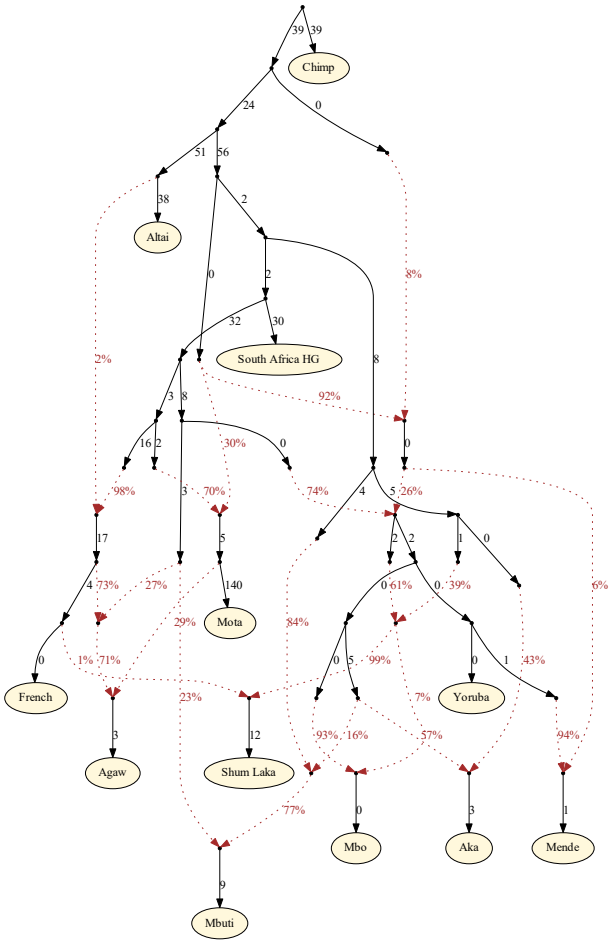

Figure S3.8. Admixture graph with Mbo in place of Lemande, using SNPs from the Human Origins array (493k covered). Branch lengths (in units of squared allele frequency divergence) are rounded to the nearest integer. All f-statistics relating the populations are predicted to within 2.8 standard errors of their observed values. Mbo is inferred to have predominantly "Bantu-associated" ancestry, plus 7.3% related to Shum Laka. The deep modern human admixture source is inferred to split (slightly) before the Central African hunter-gatherer lineage. When we fit other present-day Cameroonian populations in place of Mbo, we obtain estimates of 7.6% Shum laka-related ancestry for Aghem (max $Z = 2.8$), 6.8% for Bafut ($Z = 3.0$), 3.6% for Bangwa ($Z = 3.2$), 3.6% for Bakoko ($Z = 3.0$), and 4.2% for Lemande ($Z = 2.7$).

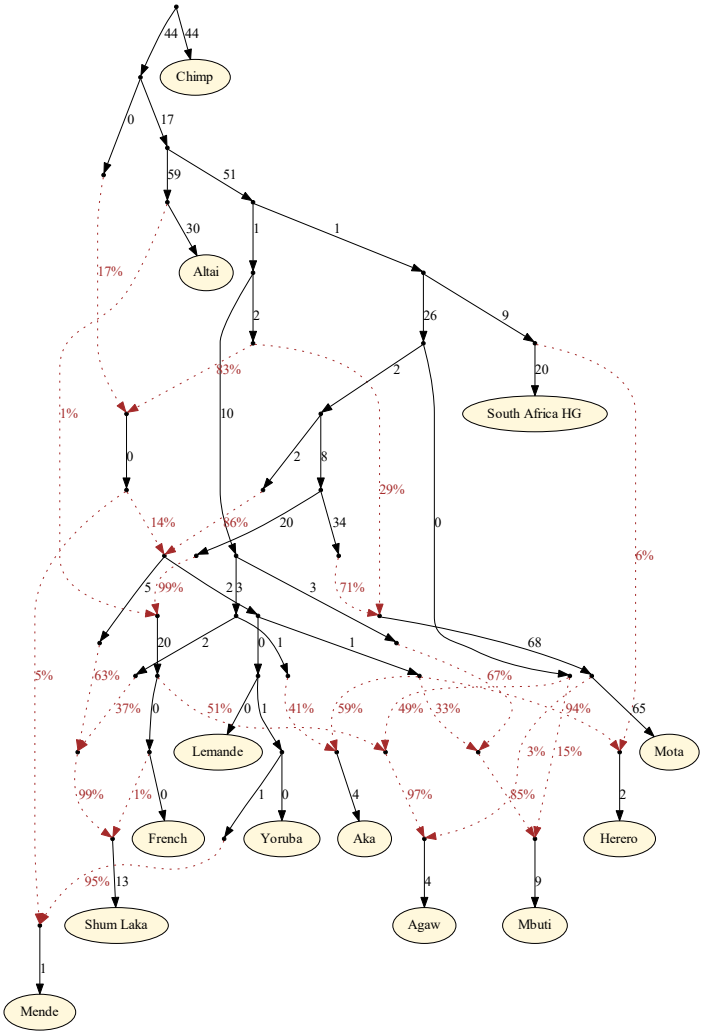

Figure S3.9. Admixture graph with Herero added (936k SNPs covered). Branch lengths (in units of squared allele frequency divergence) are rounded to the nearest integer. All f-statistics relating the populations are predicted to within 2.7 standard errors of their observed values. Herero is modeled as a mixture of Bantu-associated (94%) and southern African hunter-gatherer-related ancestry. The Bantu-associated source is inferred to split (slightly) before the Yoruba/Lemande divergence.

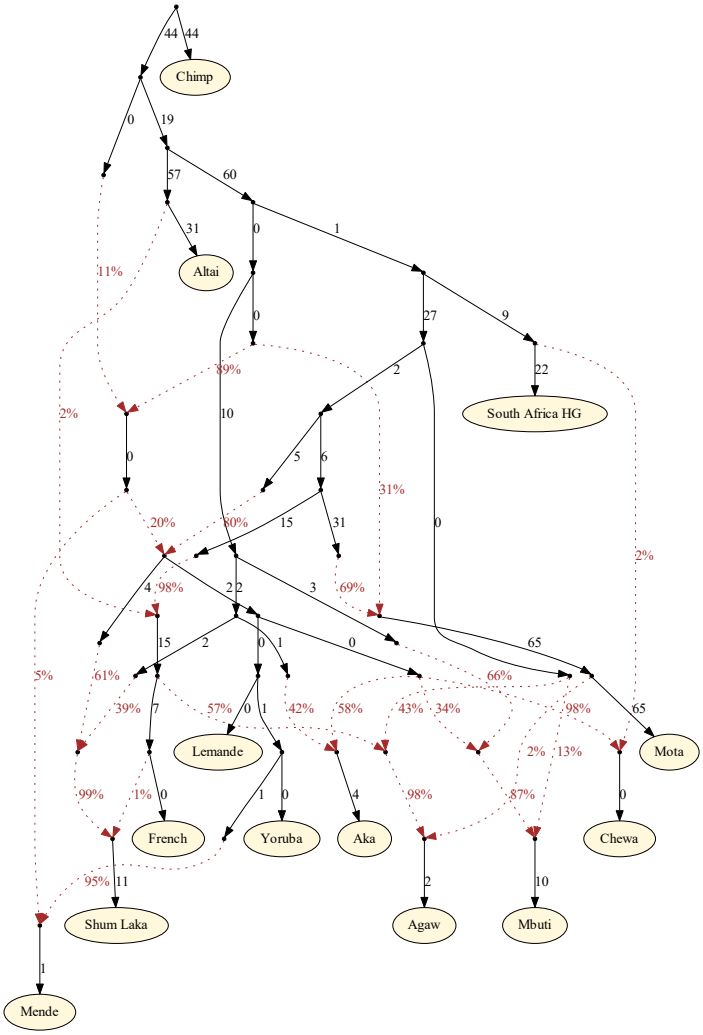

Figure S3.10. Admixture graph with Chewa added, using SNPs from the Human Origins array (500k SNPs covered). Branch lengths (in units of squared allele frequency divergence) are rounded to the nearest integer. All f-statistics relating the populations are predicted to within 2.6 standard errors of their observed values. Chewa is modeled as a mixture of Bantu-associated (98%) and southern African hunter-gatherer-related ancestry (maximum residual statistic of $Z = 3.8$ without admixture). The Bantu-associated source is inferred to split (slightly) before the Yoruba/Lemande divergence. We note that previous results for Malawi showed that ancient hunter-gatherers from the sites of Hora, Chencherere, and Fingira (∼8000–2500 BP) were largely continuous in their ancestry but highly differentiated from present-day populations [*22*], a pattern reminiscent of the one we observe for Cameroon and Shum Laka.

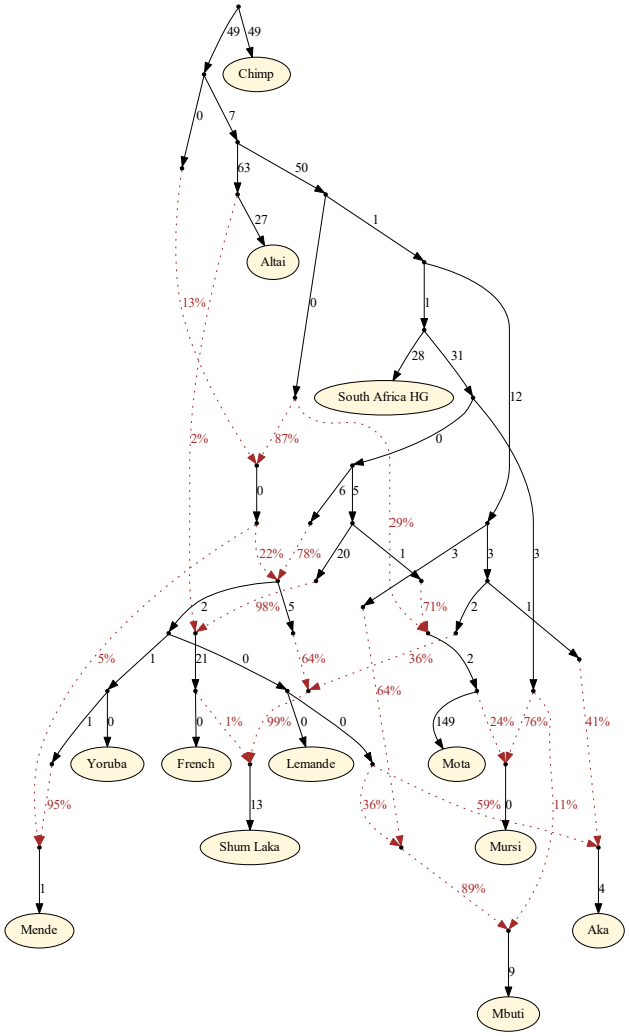

Figure S3.11. Admixture graph with Mursi in place of Agaw (930k SNPs covered). We locked the non-African-related dummy admixture into Shum Laka at 1.1% to match the value from our primary model. Branch lengths (in units of squared allele frequency divergence) are rounded to the nearest integer. All f-statistics relating the populations are predicted to within 3.2 standard errors of their observed values (2.3 excluding two statistics involving Neanderthal and chimpanzee). Mursi is modeled as admixed with 24% Mota-related ancestry. The deep modern human admixture source is inferred to split (slightly) before the Central African hunter-gatherer lineage.

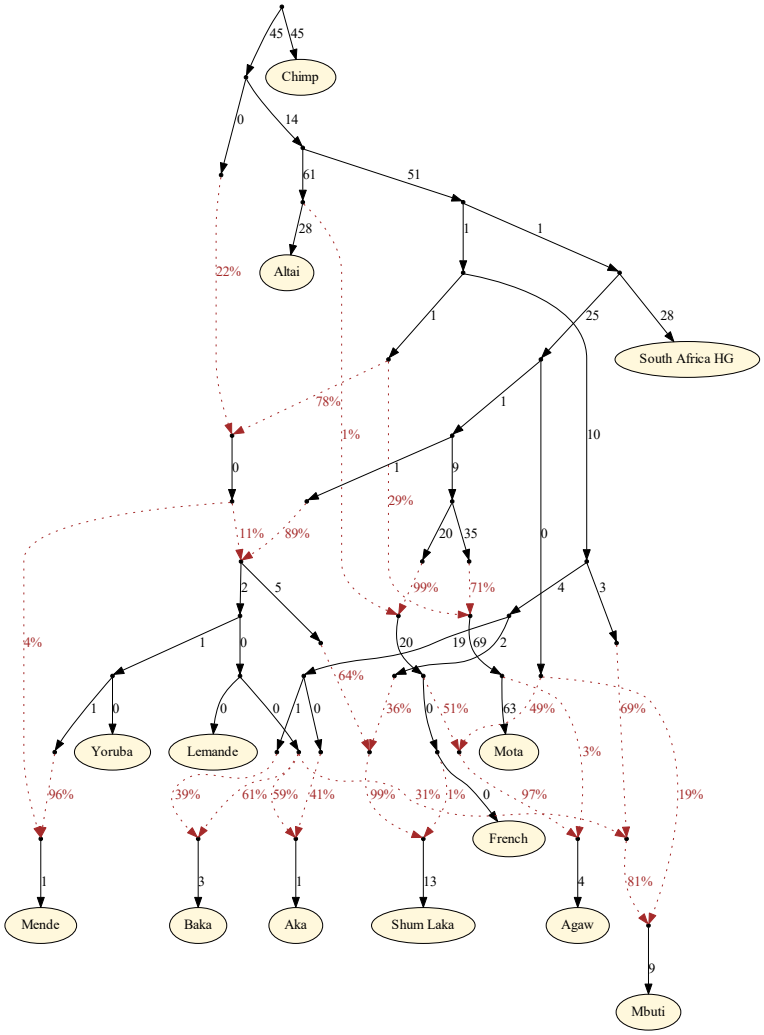

Figure S3.12. Admixture graph with Baka added (935k SNPs covered). Branch lengths (in units of squared allele frequency divergence) are rounded to the nearest integer. All f-statistics relating the populations are predicted to within 2.3 standard errors of their observed values. Baka are inferred to have 61% Bantu-associated ancestry.

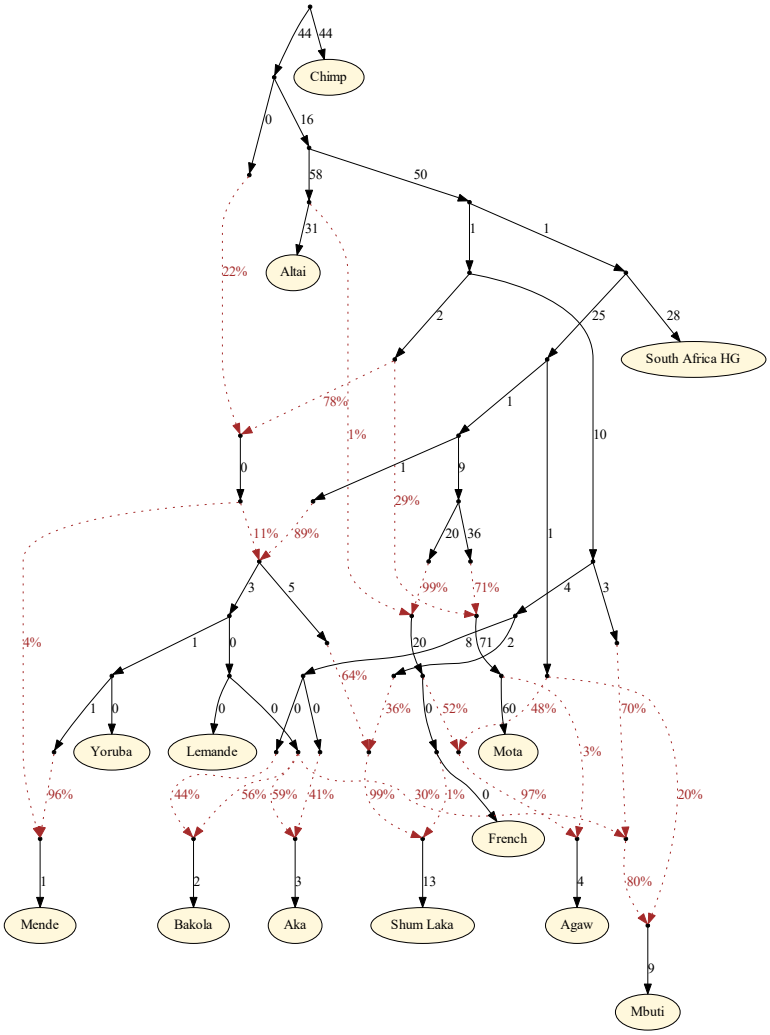

Figure S3.13. Admixture graph with Bakola added (935k SNPs covered). Branch lengths (in units of squared allele frequency divergence) are rounded to the nearest integer. All f-statistics relating the populations are predicted to within 3.5 standard errors of their observed values. Bakola are inferred to have 56% Bantu-associated ancestry, with the most extreme residual statistics pointing to a small proportion of non-African-related ancestry.

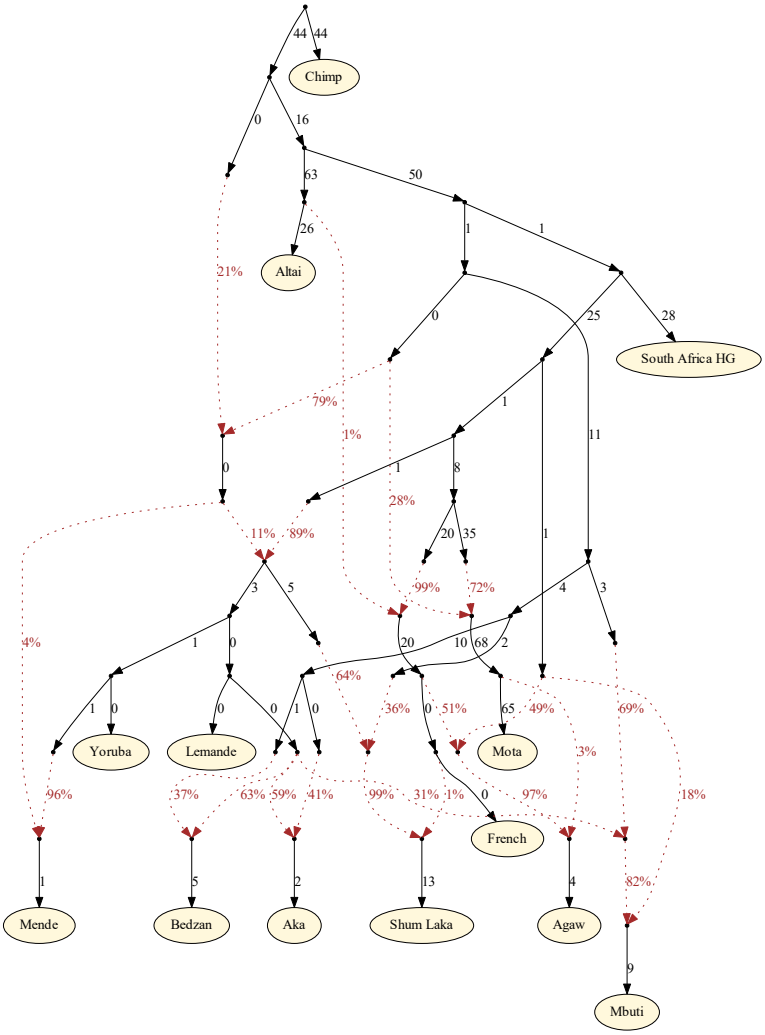

Figure S3.14. Admixture graph with Bedzan added (935k SNPs covered). Branch lengths (in units of squared allele frequency divergence) are rounded to the nearest integer. All f-statistics relating the populations are predicted to within 2.6 standard errors of their observed values. Bedzan are inferred to have 63% Bantu-associated ancestry.

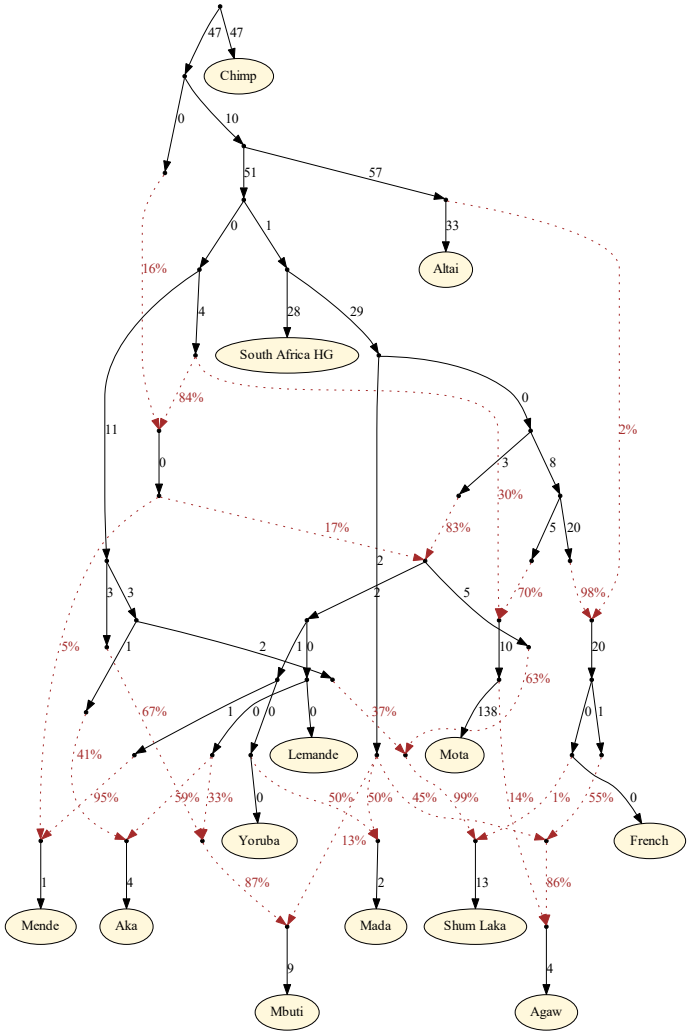

Figure S3.15. Admixture graph with Mada added (936k SNPs covered). Branch lengths (in units of squared allele frequency divergence) are rounded to the nearest integer. All f-statistics relating the populations are predicted to within 2.8 standard errors of their observed values. Mada are inferred to have 50% Yoruba-related and 50% East African-related ancestry.

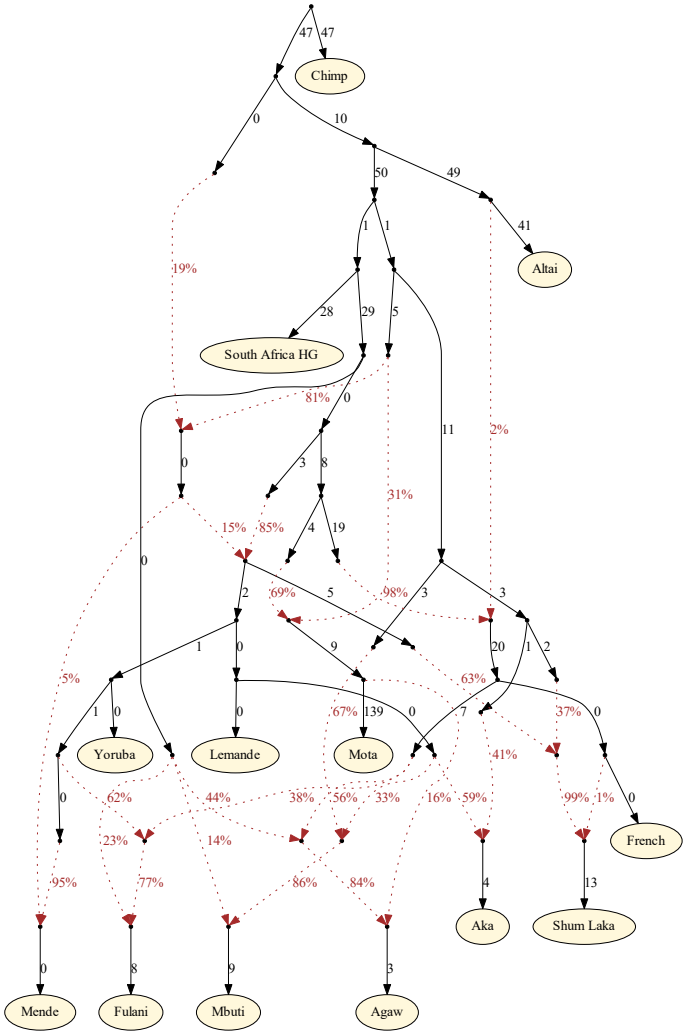

Figure S3.16. Admixture graph with Fulani added (936k SNPs covered). Branch lengths (in units of squared allele frequency divergence) are rounded to the nearest integer. All f-statistics relating the populations are predicted to within 3.7 standard errors of their observed values. Fulani are inferred to have 48% Mende-related, 23% East African-related, and 29% non-African-related ancestry.

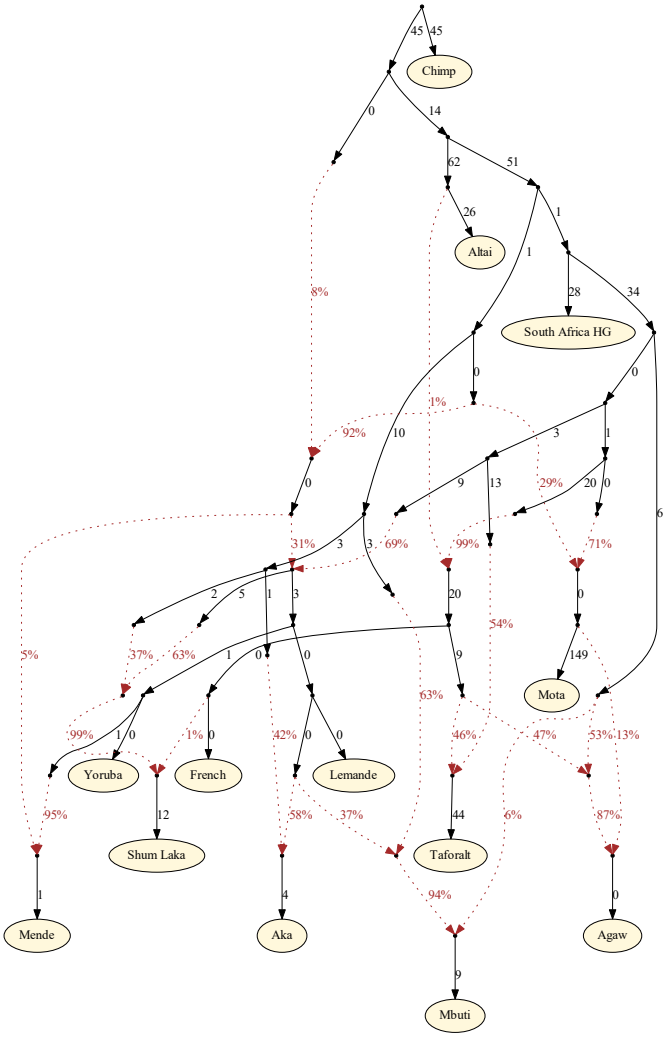

Figure S3.17. Admixture graph adding ancient individuals from Taforalt in Morocco associated with the Iberomaurusian culture (922k SNPs covered). Branch lengths (in units of squared allele frequency divergence) are rounded to the nearest integer. All f-statistics relating the populations are predicted to within 2.7 standard errors of their observed values. Taforalt is modeled as admixed with 46% ancestry from the non-African lineage (most closely related to the source for ancestry in Agaw) and 54% from a source splitting at an intermediate position between East and West Africans.

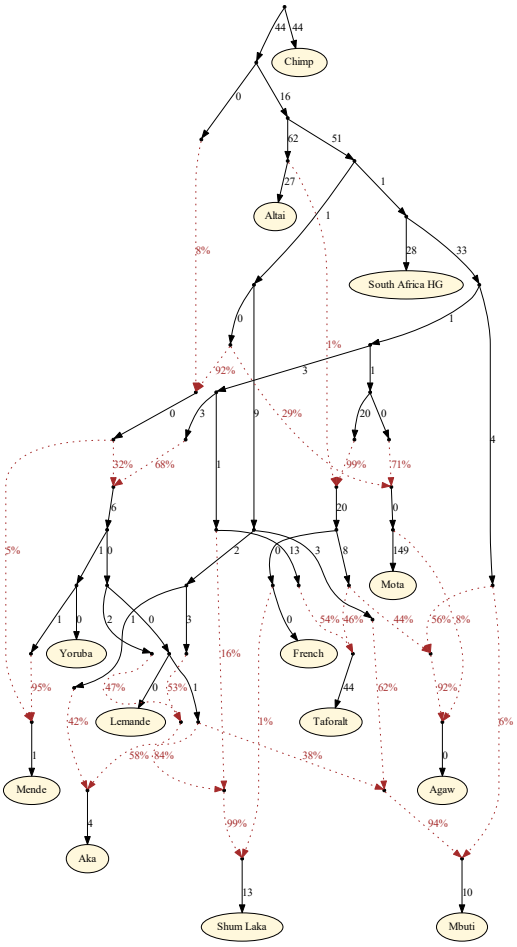

Figure S3.18. Admixture graph including ancient individuals from Taforalt in Morocco associated with the Iberomaurusian culture (922k SNPs covered), in which the Shum Laka individuals are modeled as having a mixture of hunter-gatherer-related ancestry plus two additional components: one from within the main portion of the West African clade, and one splitting at nearly the same point as the intermediate East-West African ancestry component in Taforalt. The proportions are inferred to be 44%, 40%, and 16%, respectively. Branch lengths (in units of squared allele frequency divergence) are rounded to the nearest integer. All f-statistics relating the populations are predicted to within 2.5 standard errors of their observed values. The log-likelihood score is 4.6 units superior to our primary model including Taforalt (Fig. S3.17), but with extra free parameters used for the additional admixture event (see Methods).

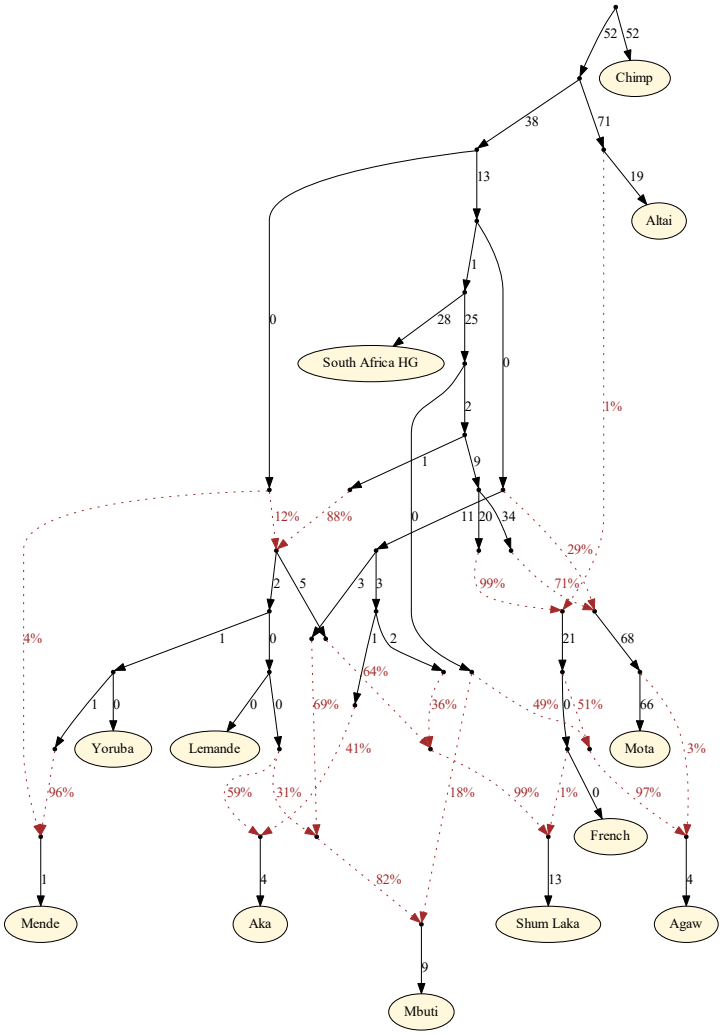

Figure S3.19. Admixture graph with alternative deep source for West Africans (932k SNPs covered). Branch lengths (in units of squared allele frequency divergence) are rounded to the nearest integer. All f-statistics relating the populations are predicted to within 3.1 standard errors of their observed values. The log-likelihood score is 7.3 units inferior to our primary model (see Methods).

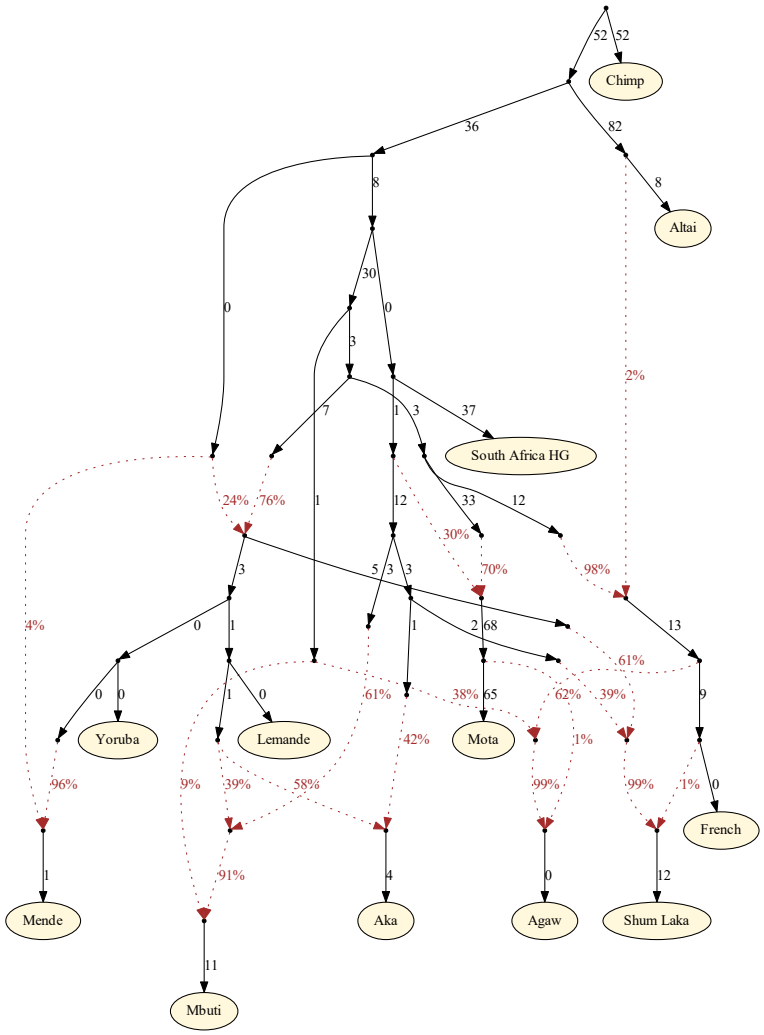

Figure S3.20. Admixture graph with alternative deep source for West Africans fit using only panels 4 and 5 of the Human Origins array (SNPs ascertained as heterozygous in Yoruba and San individuals; 211k SNPs covered). Branch lengths (in units of squared allele frequency divergence) are rounded to the nearest integer. All f-statistics relating the populations are predicted to within 2.5 standard errors of their observed values. The log-likelihood score is 1.4 units inferior to our primary model using panels 4 and 5 (Fig. S3.3; see Methods). The southern African and Central African hunter-gatherer lineages are inferred to form a (weak) clade.

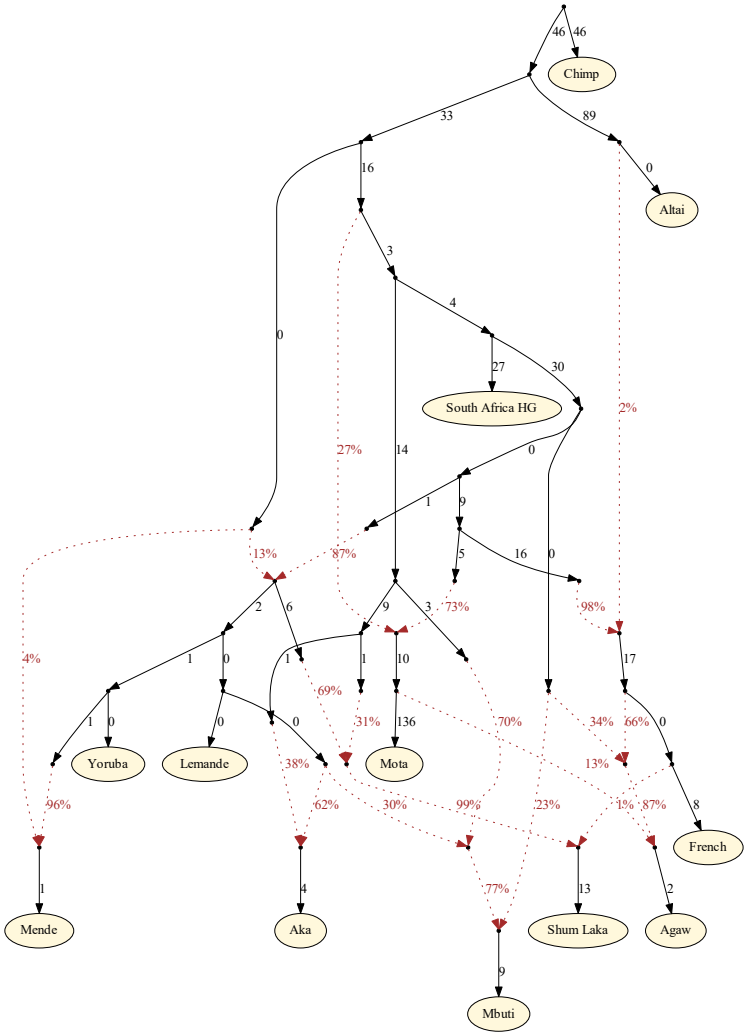

Figure S3.21. Admixture graph with alternative deep source for West Africans fit using only transversion SNPs (181k SNPs covered). Branch lengths (in units of squared allele frequency divergence) are rounded to the nearest integer. All f-statistics relating the populations are predicted to within 2.4 standard errors of their observed values. The log-likelihood score is 5.0 units inferior to our primary model using transversions (Fig. S3.4; see Methods). The deep modern human admixture source for Mota is inferred to split (slightly) before the Central African hunter-gatherer lineage.

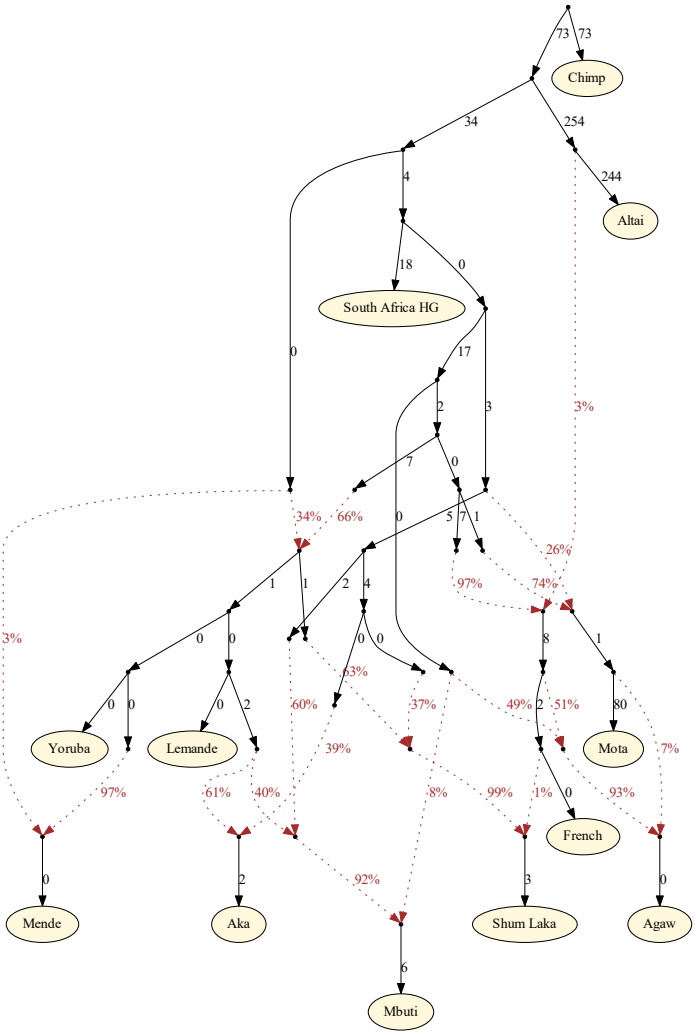

Figure S3.22. Admixture graph with alternative deep source for West Africans fit using a set of transversions ascertained as having one derived and one ancestral allele when sampling one allele at random from each of Altai Neanderthal and Denisova (336k SNPs covered). Shum Laka is represented by shotgun data for individuals 2/SE II and 4/A. Branch lengths (in units of squared allele frequency divergence) are rounded to the nearest integer. All f-statistics relating the populations are predicted to within 2.6 standard errors of their observed values. The log-likelihood score is 1.5 units inferior to our primary model using this set of SNPs (Fig. S3.6; see Methods). The southern African hunter-gatherer lineage is inferred to split (slightly) before the Central African hunter-gatherer lineage.

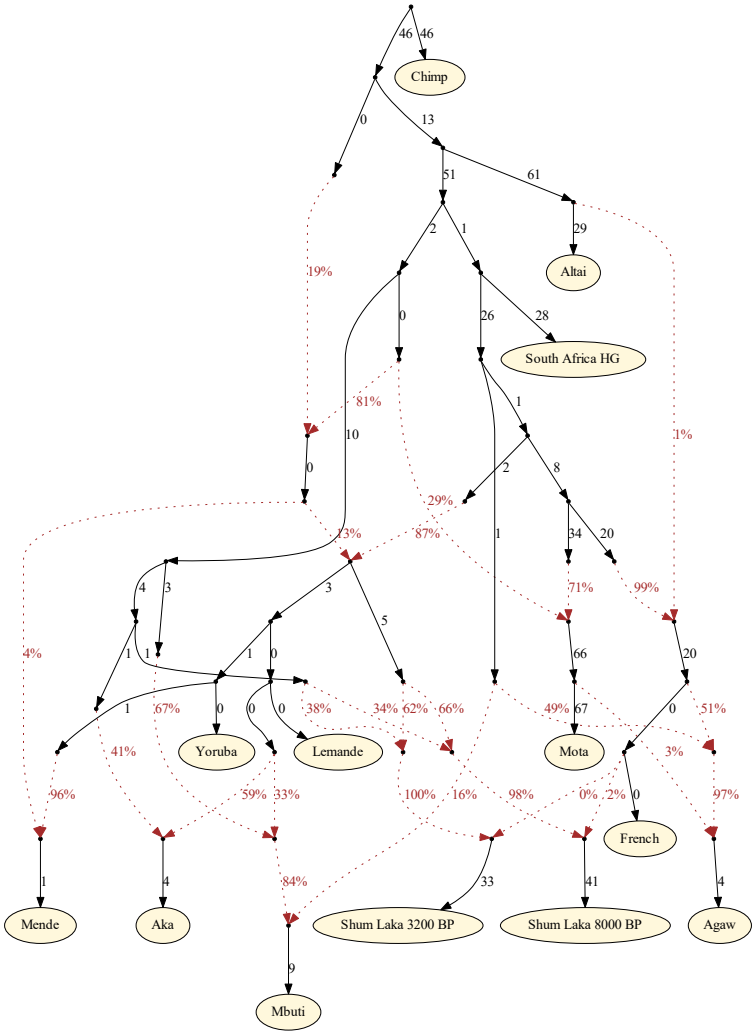

Figure S3.23. Admixture graph with the earlier and later pairs of Shum Laka individuals fit as separate populations in the model. Of the ∼1.2M targeted SNPs, 847k are covered. Branch lengths (in units of squared allele frequency divergence) are rounded to the nearest integer. All f-statistics relating the populations are predicted to within 2.2 standard errors of their observed values. The earlier pair is inferred to have 66.5% basal West African-related ancestry, and the later pair is inferred to have 61.5%.

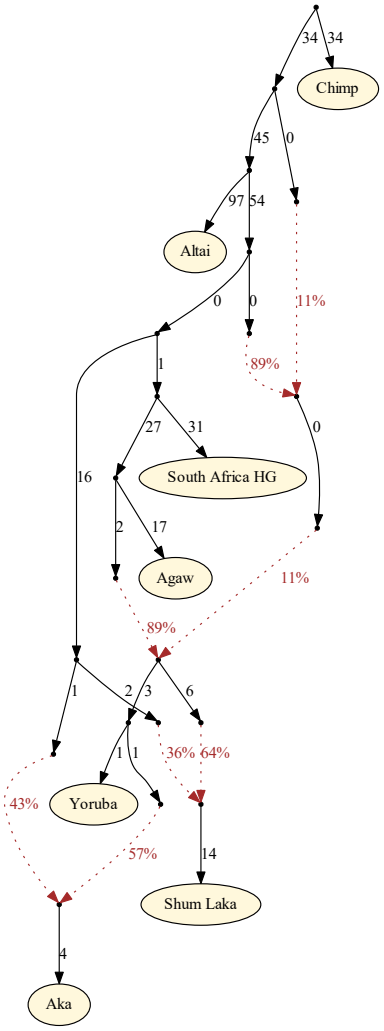

Figure S3.24. Reduced model with seven populations: Chimp, Altai Neanderthal, South African hunter-gatherers, Aka, Shum Laka, Agaw, and Yoruba (866k SNPs covered). Branch lengths (in units of squared allele frequency divergence) are rounded to the nearest integer. All f-statistics relating the populations are predicted to within 1.7 standard errors of their observed values. The modeled admixture events are deep ancestry (itself a mixture of deep modern human and archaic sources) into the West Afrian clade and West African-related ancestry into Aka and Shum Laka.

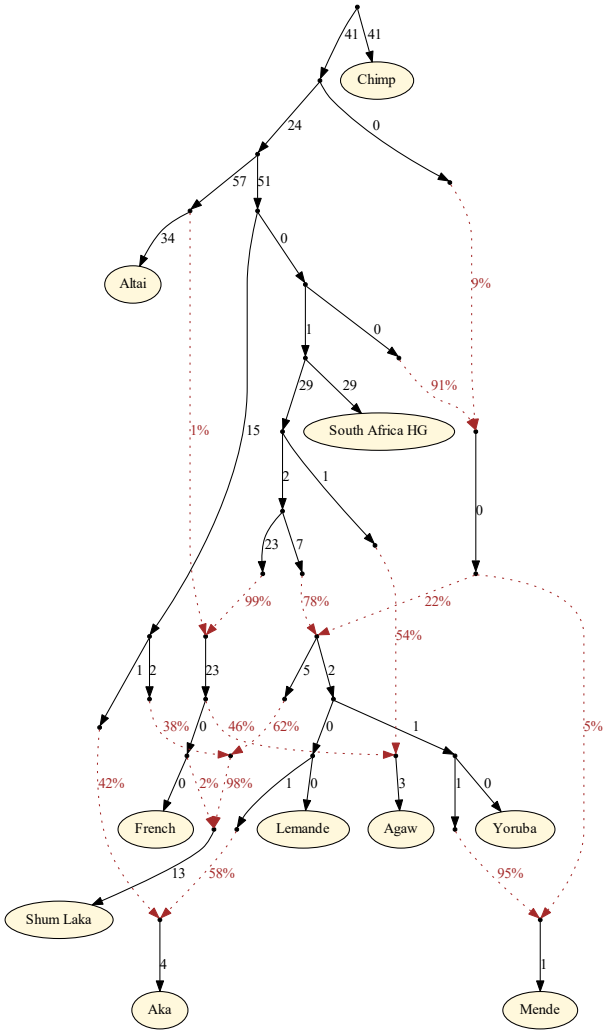

Figure S3.25. Reduced model with the same populations as the full admixture graph except for Mota and Mbuti (922k SNPs covered). Branch lengths (in units of squared allele frequency divergence) are rounded to the nearest integer. All f-statistics relating the populations are predicted to within 2.2 standard errors of their observed values. The modeled admixture events are the same as in the full admixture graph (for the populations present) except without Mota-related ancestry in Agaw.